
SIMULTANEOUS INFERENCE IN MULTIPLE MATRIX-VARIATE GRAPHS FOR HIGH-DIMENSIONAL NEURAL RECORDINGS

A PREPRINT

Zongge Liu *

Department of Statistics & Data Science
Carnegie Mellon University
Pittsburgh, PA 15213
zonggel@andrew.cmu.edu

Heejong Bong *

Department of Statistics
Purdue University
West Lafayette, IN 47907
hbong@umich.edu

Zhao Ren

Department of Statistics
University of Pittsburgh
Pittsburgh, PA 15260
zren@pitt.edu

Matthew A. Smith

Department of Biomedical Engineering
Carnegie Mellon University
Pittsburgh, PA 15213
msmith@andrew.cmu.edu

Robert E. Kass

Department of Statistics & Data Science
Carnegie Mellon University
Pittsburgh, PA 15213
kass@stat.cmu.edu

January 21, 2026

ABSTRACT

We study simultaneous inference for multiple matrix-variate Gaussian graphical models in high-dimensional settings. Such models arise when spatiotemporal data are collected across multiple sample groups or experimental sessions, where each group is characterized by its own graphical structure but shares common sparsity patterns. A central challenge is to conduct valid inference on collections of graph edges while efficiently borrowing strength across groups under both high-dimensionality and temporal dependence. We propose a unified framework that combines joint estimation via group penalized regression with a high-dimensional Gaussian approximation bootstrap to enable global testing of edge subsets of arbitrary size. The proposed procedure accommodates temporally dependent observations and avoids naive pooling across heterogeneous groups. We establish theoretical guarantees for the validity of the simultaneous tests under mild conditions on sample size, dimensionality, and non-stationary autoregressive temporal dependence, and show that the resulting tests are nearly optimal in terms of the testable region boundary. The method relies only on convex optimization and parametric bootstrap, making it computationally tractable. Simulation studies and a neural recording example illustrate the efficacy of the proposed approach.

Keywords Gaussian graphical model · Simultaneous testing · Multiple graphs · Heterogeneous learning · Bandable matrix

1 Introduction

Graphical models provide a powerful framework for characterizing dependency structures in high-dimensional data. Their matrix-variate extensions have been widely used for analyzing high-dimensional spatiotemporal data, with prominent applications including functional connectivity networks among brain regions in neuroscience (Kass et al., 2023; Bong et al., 2021) and financial stock price networks in econometrics (Chang et al., 2018). A central challenge in these settings arises from the high dimensionality of the target graph, where the prohibitive number of candidate edges leads to a severe multiple testing burden. Addressing this challenge requires not only new inferential tools but also careful and efficient use of available data. In many applications, it is necessary to combine data from multiple

*The authors contribute equally to this paper.

sample groups collected under heterogeneous conditions, such as different subjects or experimental sessions, in order to overcome the limited sample size available within each group. However, naive pooling across groups can introduce spurious dependencies due to heterogeneity, while analyzing each group separately often results in substantial loss of statistical power. In this paper, we develop a method for jointly estimating multiple matrix-variate graphical models by leveraging shared sparsity structures across sample groups, together with a unified framework for high-dimensional inference on graph edges.

The literature on inference for graphical models is extensive (Friedman et al., 2008; Allen and Tibshirani, 2010; Jankova and van de Geer, 2015; Chen and Liu, 2018; Ye et al., 2021; Liu, 2013; Ren et al., 2015), but relatively few frameworks address matrix-variate Gaussian graphical models (MGGMs; see Section 2). Existing work includes (Leng and Tang, 2012; Yin and Li, 2012; Zhou, 2014; Chen and Liu, 2018; Ye et al., 2021). For example, Chen and Liu (2018) developed a multiple testing framework for support recovery with asymptotic guarantees on normality and false discovery rate control, while Ye et al. (2021) proposed paired tests for detecting changes in matrix graph across correlated samples. Both approaches rely on multiple testing procedures with false discovery rate control. In contrast, Chang et al. (2018) derived a single global test statistic for assessing subgroups of edges simultaneously in vector-variate graphical models under temporal dependence.

Inference procedures for multiple matrix-variate graphs remain largely unexplored. In the vector-variate setting, several approaches have been proposed for joint estimation of multiple graphs, including optimization-based methods (Danaher et al., 2014; Cai et al., 2016a; Lee and Liu, 2015) and Bayesian formulations with structured priors (Peterson et al., 2015). The work most closely related to our setting is Zhu and Li (2018), who studied estimation of multiple MGGMs via nonconvex optimization with sparsity and group Lasso penalties. While their estimator exhibits some desirable properties, its convergence relies on strong assumptions and formal inference procedures are not developed.

We develop and study a multiple matrix-variate graph-based method for discovering common sparsity structures with improved sensitivity. Our approach uses group Lasso to borrow strength across sample groups, yielding more accurate partial-correlation estimates than the naive strategy of fitting models separately to each group; see Section 3 for details. We establish improved convergence rates through theoretical analysis and simulation studies in Sections 4 and 5. In particular, we provide a self-contained analysis of the convergence rates and prediction error of the group Lasso estimator under temporal dependence in Section 4.1. Although group Lasso itself dates to 2006 (Yuan and Lin, 2006), its theoretical properties under temporal correlation have not previously been studied, and may be of independent interest for high-dimensional statistics with dependent data. In Section 4.2, we develop theoretical guarantees for the proposed inference procedures using a Gaussian approximation bootstrap method based on Chernozhukov et al. (2013). This represents the first attempt to formulate a global significance test for edge groups of arbitrary size in matrix-variate graphs beyond false discovery rate based methods. Finally, we apply our method to microelectrode recordings from two brain regions, V4 and PFC, and identify distinct cross-area subgroups with differential dynamics across cognitive stages (Section 5.2). Our results reveal increased V4–PFC connectivity during visual memory retention, supporting their joint role in working memory.

Notations: For a vector \mathbf{x} , let $\|\mathbf{x}\|_p$ denote the ℓ_p -norm. For a real matrix X , we use $X_{i\cdot}$ to denote the i -th row of X and $X_{\cdot j}$ to denote the j -th column of X . Let $\|X\|_p$ denote the matrix p -norm, where $\|X\|_2$ is also referred to as the spectral or operator norm. We denote the Frobenius norm of X by $\|X\|_F$ and the entry-wise supremum norm by $\|X\|_\infty$. For a set A , its cardinality is denoted by $|A|$. We denote the zero vector, whose elements are all zero, by $\mathbf{0}$. For a positive integer d , we use $[d]$ to denote the set $\{1, 2, \dots, d\}$.

2 Matrix-variate Gaussian Graphical Model

Let $X \in \mathbb{R}^{p \times q}$ denote an observed sample of spatiotemporal data. At a given time point $t \in [p]$, the row vector $X_{t\cdot} \in \mathbb{R}^q$ represents measurements across q spatial locations. A *matrix-variate Gaussian graphical model* (MGGM, Dawid, 1981) is specified by two covariance matrices: the temporal (row) covariance $\Sigma^{(T)} \in \mathbb{R}^{p \times p}$ and the spatial (column) covariance $\Sigma^{(S)} \in \mathbb{R}^{q \times q}$. We say that X follows this model with mean μ , denoted by $X \sim \text{MN}(\mu, \Sigma^{(T)}, \Sigma^{(S)})$, if and only if the vectorized data $\text{vec}(X)$ follow a multivariate normal distribution with mean $\text{vec}(\mu)$ and covariance matrix $\Sigma^{(S)} \otimes \Sigma^{(T)}$, where \otimes denotes the Kronecker product.

Because this parametrization is not identifiable up to a scaling factor, we assume without loss of generality that $\text{tr}(\Sigma^{(T)}) = p$. Imposing the Kronecker product structure reduces the number of free covariance parameters from $pq(pq + 1)/2$ to $p(p + 1)/2 + q(q + 1)/2$. Under this model, the covariance between entries X_{ti} and X_{sj} is given by $\text{Cov}(X_{ti}, X_{sj}) = \Sigma_{ts}^{(T)} \Sigma_{ij}^{(S)}$. If we denote the corresponding precision matrices by $\Omega^{(T)} := (\Sigma^{(T)})^{-1}$ and $\Omega^{(S)} := (\Sigma^{(S)})^{-1}$, then the inverse covariance of $\text{vec}(X)$ admits a simple analytic form: $(\Sigma^{(S)} \otimes \Sigma^{(T)})^{-1} = \Omega^{(S)} \otimes \Omega^{(T)}$. In MGGM, interest primarily lies in the conditional independence graph structure among q spatial locations, where each

node represents a spatial location and the absence of an edge indicates that the corresponding nodes are conditionally independent given all remaining nodes. For Gaussian distributions, this graph structure is encoded by the precision matrix, or equivalently, by partial correlations. Thus, the target parameters in this work are the spatial partial correlations, which can be recovered from the spatial precision matrix: the partial correlation between spatial points i and j is $\rho_{ij}^{(S)} = -\frac{\Omega_{ij}^{(S)}}{\sqrt{\Omega_{ii}^{(S)}\Omega_{jj}^{(S)}}}$, which remains invariant across all time points (see Section 3.1).

3 Simultaneous Inference Framework

In this section we develop an inference framework for identifying spatial partial-correlation graphs in multiple spatiotemporal observations. The full procedure is summarized in Algorithm 1.

For each sample group $l \in [m]$, we observe n_l i.i.d. spatiotemporal measurements in $p \times q$ matrix-variate samples. At group l , we assume for $k \in [n_l]$ that the k -th sample $X^{(k,l)}$ follows matrix-variate Gaussian distribution $\text{MN}(0, \Sigma^{(\mathcal{T},l)}, \Sigma^{(\mathcal{S},l)})$, where $\Sigma^{(\mathcal{T},l)} \in \mathbb{R}^{p \times p}$ and $\Sigma^{(\mathcal{S},l)} \in \mathbb{R}^{q \times q}$ are the group-specific temporal and spatial covariance matrices, respectively. We denote the temporal and spatial precision matrices by $\Omega^{(\mathcal{T},l)} := (\Sigma^{(\mathcal{T},l)})^{-1}$ and $\Omega^{(\mathcal{S},l)} := (\Sigma^{(\mathcal{S},l)})^{-1}$, respectively.

Algorithm 1 Simultaneous Testing for Multiple Matrix-variate Gaussian Graphical Models

- 1: **Input:** Multi-group data \mathcal{D} , edge set \mathcal{S} , test level α
 - 2: **Output:** Confidence region $\mathcal{C}_E(1 - \alpha)$
 - 3: **Spatial precision matrix estimation:**
 - 4: **for** $i = 1 : q$ **do**
 - 5: Estimate the regression coefficient $\beta_{\cdot,i}^{(\mathcal{S},l)}$ and the residual $\epsilon_{\cdot,i}^{(\mathcal{S},k,l)}$ using Eq. (2).
 - 6: **end for**
 - 7: **for** $l = 1 : m, i = 1 : q, j = 1 : q$ **do**
 - 8: Estimate the de-biased residual variance $\Phi_{ij}^{(\mathcal{S},l)}$ using Eq. (3).
 - 9: Estimate the spatial precision $\Omega_{ij}^{(\mathcal{S},l)}$ and partial correlation $\rho_{ij}^{(\mathcal{S},l)}$ using Eq. (4).
 - 10: **end for**
 - 11: **Temporal precision matrix estimation:**
 - 12: **for** $l = 1 : m$ **do**
 - 13: Estimate the temporal regression coefficient $\beta^{(\mathcal{T},l)}$, residual variance $\Phi^{(\mathcal{T},l)}$ and temporal covariance $\Sigma^{(\mathcal{T},l)}$ using Eqs. (10), (11) and (13).
 - 14: **end for**
 - 15: **Hypothesis testing based on bootstrap:**
 - 16: Estimate the covariance matrix S_{EE} of the test statistic T_E using the plug-in estimator \hat{S}_{EE} in Eq. (7).
 - 17: Sample $\{\hat{Z}_i\}_{i=1,\dots,B} \sim N(0, \hat{S}_{EE})$ and calculate the confidence region in Eq. (8).
 - 18: **return** Confidence region $\mathcal{C}_E(1 - \alpha)$
-

3.1 Estimation of Spatial Covariance Matrix

Under the matrix-variate Gaussian graphical model, for a given spatial location $i \in [q]$, at each time point $t \in [p]$, the conditional distribution of the random variable $X_{ti}^{(k,l)}$ given the remaining variables in $X_{t,\cdot}^{(k,l)}$ follows a normal distribution and can be modeled as a linear regression:

$$X_{ti}^{(k,l)} = X_{t,\cdot}^{(k,l)} \beta_{\cdot,i}^{(\mathcal{S},l)} + \epsilon_{ti}^{(\mathcal{S},k,l)}, \quad (1)$$

where the regression coefficients are related to the spatial precision matrix via $\beta_{ji}^{(\mathcal{S},l)} = -\frac{\Omega_{ji}^{(\mathcal{S},l)}}{\Omega_{ii}^{(\mathcal{S},l)}} \mathbb{I}(i \neq j)$, and $\mathbb{E}[\epsilon_{ti}^{(\mathcal{S},k,l)}] = 0$. Due to the Kronecker product structure in the model, the regression coefficients are time-independent. It is common in many applications of graphical models to assume that the graph exhibits a certain sparsity structure. Consequently, sparsity in the spatial precision matrix $\Omega^{(\mathcal{S},l)}$ implies corresponding sparsity in the regression coefficients $\beta^{(\mathcal{S},l)}$. A similar sparsity appears in the covariance of the node-wise regression residuals. Specifically, for the residuals $\epsilon_{t,\cdot}^{(\mathcal{S},k,l)} := (\epsilon_{t1}^{(\mathcal{S},k,l)}, \dots, \epsilon_{tq}^{(\mathcal{S},k,l)})^\top$, the covariance is given by $\text{Cov}[\epsilon_{t,\cdot}^{(\mathcal{S},k,l)}] = \Sigma_{tt}^{(\mathcal{T},l)} \cdot \Phi^{(\mathcal{S},l)}$, where $\Phi_{ij}^{(\mathcal{S},l)} :=$

$\frac{\Omega_{ij}^{(S,l)}}{\Omega_{ii}^{(S,l)}\Omega_{jj}^{(S,l)}}$. Our target, the spatial partial correlation, is expressed as $\rho_{ij}^{(S,l)} = -\frac{\Omega_{ij}^{(S,l)}}{\sqrt{\Omega_{ii}^{(S,l)}\Omega_{jj}^{(S,l)}}} = -\frac{\Phi_{ij}^{(S,l)}}{\sqrt{\Phi_{ii}^{(S,l)}\Phi_{jj}^{(S,l)}}}$, and testing $\Phi_{ij}^{(S,l)} = 0$ is equivalent to testing $\rho_{ij}^{(S,l)} = 0$. Because $\Phi^{(S,l)}$ is invariant across t and k , $\Phi^{(S,l)} = \mathbb{E} \left[\frac{1}{n_l p} \sum_{k=1}^{n_l} \sum_{t=1}^p \epsilon_{t,\cdot}^{(S,k,l)} \epsilon_{t,\cdot}^{(S,k,l)\top} \right]$, noting that $\text{tr}(\Sigma^{(T,l)}) = p$ under the identifiability constraint. It is worth noting that the residuals corresponding to different time points $t \in [p]$ exhibit temporal dependence.

We fit all m sample groups jointly to improve the estimation accuracy of each $\rho_{ij}^{(S,l)}$. Under a mild assumption that the spatial precision matrices $\Omega_{ij}^{(S,l)}$ share the same sparsity pattern across sample groups, the corresponding regression coefficients $\beta_{\cdot,i}^{(S,l)}$ also exhibit a common support across the m sample groups, albeit with potentially distinct values. To harness this group sparsity assumption, we treat the coefficients $\beta_{ji}^{(S,1)}, \dots, \beta_{ji}^{(S,m)}$ as a group of parameters for each pair (i, j) and apply group Lasso (Yuan and Lin, 2006) to improve estimation by borrowing strength across sample groups:

$$\{\widehat{\beta}_{\cdot,i}^{(S,l)}\}_{l=1,\dots,m} := \underset{\{b^{(l)}\}_{l=1,\dots,m}}{\text{argmin}} \left\{ \frac{1}{2n_0 p} \sum_{l=1}^m \sum_{k=1}^{n_l} \|X_{\cdot,i}^{(k,l)} - X^{(k,l)} b^{(l)}\|_2^2 + \gamma_i \sum_{j:j \neq i} \sqrt{\sum_{l=1}^m \frac{\|\sum_k X_{\cdot,j}^{(k,l)}\|_2^2}{n_l p}} b_j^{(l)2} \right\}, \quad (2)$$

with respect to $b_i^{(l)} = 0$ for all l , where $n_0 = \min_{1 \leq l \leq m} n_l$. The parameter γ_i can be tuned using cross-validation or other model selection methods.

Once the regression coefficients are estimated, the residuals are computed as $\widehat{\epsilon}_{ti}^{(S,k,l)} := X_{ti}^{(k,l)} - X_{t,\cdot}^{(k,l)} \widehat{\beta}_{\cdot,i}^{(S,l)}$. Although the empirical covariance matrix of the fitted residuals provides a straightforward estimate of $\Phi_{ij}^{(S,l)}$, this estimate is biased due to the lasso-type penalty, leading to a larger error rate than the expected $1/\sqrt{n_l p}$ rate (Liu, 2013). To address this bias, we adopt a bias-correction term in the covariance estimate:

$$\widehat{\Phi}_{ij}^{(S,l)} := \begin{cases} -\frac{1}{n_l p} \sum_{k=1}^{n_l} \sum_{t=1}^p \left(\widehat{\epsilon}_{ti}^{(S,k,l)} \widehat{\epsilon}_{tj}^{(S,k,l)} + \widehat{\epsilon}_{tj}^{(S,k,l)2} \widehat{\beta}_{ji}^{(S,l)} + \widehat{\epsilon}_{ti}^{(S,k,l)2} \widehat{\beta}_{ij}^{(S,l)} \right), & \text{if } i \neq j, \\ \frac{1}{n_l p} \sum_{k=1}^{n_l} \sum_{t=1}^p \widehat{\epsilon}_{ti}^{(S,k,l)} \widehat{\epsilon}_{tj}^{(S,k,l)}, & \text{if } i = j. \end{cases} \quad (3)$$

We then estimate the spatial precision matrix $\Omega^{(S,l)}$ and the partial correlation matrix $\rho^{(S,l)}$ as follows:

$$\widehat{\Omega}_{ij}^{(S,l)} := \frac{\widehat{\Phi}_{ij}^{(S,l)}}{\widehat{\Phi}_{ii}^{(S,l)} \widehat{\Phi}_{jj}^{(S,l)}} \quad \text{and} \quad \widehat{\rho}_{ij}^{(S,l)} := -\frac{\widehat{\Phi}_{ij}^{(S,l)}}{\sqrt{\widehat{\Phi}_{ii}^{(S,l)} \widehat{\Phi}_{jj}^{(S,l)}}}. \quad (4)$$

While our partial correlation estimator is similar to the form proposed by Chen and Liu (2018) for a single matrix-variate Gaussian graphical model, our approach leverages information from multiple sample groups using the group Lasso estimate, leading to a faster convergence rate, as demonstrated in Theorem 4.1, which in turn facilitates the subsequent inference procedure.

3.2 Simultaneous Test by Parametric Bootstrap

3.2.1 Single Edge Test

By leveraging information across m sample groups using group Lasso (Eq. (2)), we not only improve the efficiency of spatial partial correlation estimates but also enhance the power of tests for detecting significant associations. We first consider testing a single edge: for a pair (i, j) , the null hypothesis is

$$H_{0,ij} : \rho_{ij}^{(S,l)} = 0, \quad \forall l = 1, \dots, m. \quad (5)$$

Given the group sparsity structure, we construct a test statistic by summing the partial correlation estimates $\widehat{\rho}_{ij}^{(S,l)}$ across all sample groups. To account for varying sample sizes across sample groups, we weight the estimates by $\sqrt{n_l p}$ and define the test statistic as $\widehat{T}_{ij} := \frac{1}{\sqrt{m}} \sum_{l=1}^m \sqrt{n_l p} \widehat{\rho}_{ij}^{(S,l)}$. In Theorem 4.2, we show that \widehat{T}_{ij} asymptotically follows a normal distribution with mean $T_{ij} := \frac{1}{\sqrt{m}} \sum_{l=1}^m \sqrt{n_l p} \rho_{ij}^{(S,l)}$. Assuming the sign of the associations remains consistent across sample groups, the mean equals zero if and only if the null hypothesis holds, so \widehat{T}_{ij} should be significantly different from zero under the alternative hypothesis. Once the asymptotic variance is consistently estimated, constructing a confidence interval for T_{ij} and the corresponding p -value for $H_{0,ij}$ is straightforward.

Remark 3.1. More generally, additional sign information on $\rho_{ij}^{(S,l)}$ may be available. With this additional knowledge, we present a test statistic based on a linear combination of those $\hat{\rho}_{ij}^{(S,l)}$ for $l \in [m]$, which is closely related to its ℓ_1 norm. More specifically, with an edge-specific sign vector $\sigma_{ij} := (\sigma_{ij}^{(1)}, \dots, \sigma_{ij}^{(m)})^\top \in \{-1, 1\}^m$, we replace \hat{T}_{ij} with the following sign-addressed test statistic $\hat{T}_{ij,\sigma} := \frac{1}{\sqrt{m}} \sum_{l=1}^m \sigma_{ij}^{(l)} \sqrt{m_l p} \hat{\rho}_{ij}^{(S,l)}$. The normal approximation we establish in Section 4 also applies to the sign-addressed test statistic.

3.2.2 Simultaneous Test

Now we shift our focus to a more challenging problem of multiple edge testing. In this scenario, we aim to test whether there are no edges at all in a user-specified edge set $E \subseteq [p] \times [p]$, regardless of its size, which corresponds to the following null hypothesis:

$$H_{0,E} : \rho_{ij}^{(S,l)} = 0, \quad \forall (i, j) \in E, \quad \forall l = 1, \dots, m.$$

When E consists of a single edge (i, j) , $H_{0,E}$ reduces to the single-edge null hypothesis $H_{0,ij}$ in Eq. (5). While multiple testing techniques, such as Bonferroni correction, can be applied to extend single-edge tests to multiple-edge tests, these methods are often overly conservative. Moreover, in neuroscience applications, the edge set E typically represents connections between different brain areas, and its cardinality can grow on the order of q^2 . As a result, even if we establish the asymptotic normality of a single \hat{T}_{ij} , traditional multiple testing methods may not be valid in high-dimensional settings where $|E|$ grows rapidly.

To address this challenge, we propose a simultaneous testing approach based on the supremum norm of $\hat{T}_E := (\hat{T}_{ij} : (i, j) \in E)$, defined as:

$$\|\hat{T}_E\|_\infty := \max_{(i,j) \in E} |\hat{T}_{ij}|. \quad (6)$$

The key idea leverages on high-dimensional central limit theorems (e.g., Chernozhukov et al., 2013): Although the full vector \hat{T}_E may not be asymptotically jointly normal as $|E|$ increases, the supremum norm $\|\hat{T}_E - T_E\|_\infty$ exhibits the same limiting behavior as $\|Z\|_\infty$, where Z is a centered normal random vector with the same covariance as the asymptotic covariance of \hat{T}_E . Specifically, this covariance is given by the matrix of asymptotic covariances between $\hat{T}_{i_1 j_1}$ and $\hat{T}_{i_2 j_2}$ for $(i_1, j_1), (i_2, j_2) \in E$, expressed as (see Section E for the derivation):

$$S_{(i_1, j_1), (i_2, j_2)} := \sum_{l=1}^m \frac{\|\Sigma^{(\mathcal{T}, l)}\|_F^2}{mp} \begin{bmatrix} \rho_{i_1 i_2}^{(S,l)} \rho_{j_1 j_2}^{(S,l)} + \rho_{i_1 j_2}^{(S,l)} \rho_{i_2 j_1}^{(S,l)} + \frac{1}{2} \rho_{i_1 j_1}^{(S,l)} \rho_{i_2 j_2}^{(S,l)} \left(\rho_{i_1 i_2}^{(S,l)2} + \rho_{j_1 j_2}^{(S,l)2} + \rho_{i_1 j_2}^{(S,l)2} + \rho_{i_2 j_1}^{(S,l)2} \right) \\ - \rho_{i_1 i_2}^{(S,l)} \rho_{i_2 j_2}^{(S,l)} \rho_{i_2 j_1}^{(S,l)} - \rho_{i_1 i_2}^{(S,l)} \rho_{i_1 j_1}^{(S,l)} \rho_{i_1 j_2}^{(S,l)} - \rho_{j_1 j_2}^{(S,l)} \rho_{i_2 j_2}^{(S,l)} \rho_{i_1 j_2}^{(S,l)} - \rho_{j_1 j_2}^{(S,l)} \rho_{i_2 j_1}^{(S,l)} \rho_{i_1 j_1}^{(S,l)} \end{bmatrix}. \quad (7)$$

We approximate the distribution of $\|Z\|_\infty$ using a parametric bootstrap based on the plug-in estimator \hat{S}_{EE} of the asymptotic covariance. Generating bootstrap samples $\{\hat{Z}^{(1)}, \dots, \hat{Z}^{(B)}\}$ from $N(0, \hat{S}_{EE})$, we construct a $(1 - \alpha)$ -confidence region for T_E :

$$\mathcal{C}_E(1 - \alpha) := \{t \in \mathbb{R}^{|E|} : \|t - \hat{T}_E\|_\infty \leq \hat{q}_{1-\alpha}\}, \quad (8)$$

where $\hat{q}_{1-\alpha}$ is the empirical $(1 - \alpha)$ -quantiles of $\{\|\hat{Z}^{(1)}\|_\infty, \dots, \|\hat{Z}^{(B)}\|_\infty\}$. The null hypothesis $H_{0,E}$ is rejected if $\mathbf{0} \notin \mathcal{C}_E(1 - \alpha)$. The coverage of this confidence region is studied in Theorem 4.3, with a power analysis provided in Theorem 4.4. We further discuss how borrowing information across sample groups enhances testing power in Theorem 4.5.

3.3 Estimation of Temporal Covariance Matrix

The plug-in estimator \hat{S}_{EE} of the asymptotic covariance (Eq. (7)) requires the Frobenius norm of the temporal covariance matrix, $\Sigma^{(\mathcal{T}, l)}$ for each sample group. We propose to estimate $\Sigma^{(\mathcal{T}, l)}$ based on a modified Cholesky decomposition of its inverse, the temporal precision matrix $\Omega^{(\mathcal{T}, l)}$ (Bickel and Levina, 2008; Liu and Ren, 2020). The Cholesky decomposition characterizes the autoregressive dependence of the signal at each time point on its past values. Specifically, suppose for each sample group $l \in [m]$ that the modified Cholesky decomposition of $\Omega^{(\mathcal{T}, l)}$ is $\Omega^{(\mathcal{T}, l)} = L^{(\mathcal{T}, l)} D^{(\mathcal{T}, l)} L^{(\mathcal{T}, l)\top}$, where $D^{(\mathcal{T}, l)}$ is a diagonal matrix, and $L^{(\mathcal{T}, l)}$ is a lower triangular matrix with diagonal entries equal to 1. Let $\beta^{(\mathcal{T}, l)} := I - L^{(\mathcal{T}, l)\top}$. Then the first $(t - 1)$ entries of $\beta^{(\mathcal{T}, l)}$'s t -th row, $\beta_{\cdot t}^{(\mathcal{T}, l)}$, correspond to the regression coefficients of $X_{it}^{(k,l)}$ on its past values, $X_{1i}^{(k,l)}, X_{2i}^{(k,l)}, \dots, X_{(t-1)i}^{(k,l)}$ at each spatial location $i \in [q]$. That is,

$X_{ti}^{(k,l)} = X_{\cdot,i}^{(k,l)\top} \beta_{\cdot,t}^{(\mathcal{T},l)} + \epsilon_{ti}^{(\mathcal{T},k,l)}$ for each time t . Due to the Kronecker product structure, the regression coefficients are invariant across spatial points $i \in [q]$, whereas the residuals exhibit spatial dependence characterized by $\Sigma^{(\mathcal{S},l)}$. To accommodate the matrix-variate data and the identifiability constraint $\text{tr}(\Sigma^{(\mathcal{T},l)}) = p$, we rewrite the Cholesky decomposition of $\Omega^{(\mathcal{T},l)}$ by

$$\Omega^{(\mathcal{T},l)} = \frac{\text{tr}(\Sigma^{(\mathcal{S},l)})}{q} (I - \beta^{(\mathcal{T},l)})^\top (\Phi^{(\mathcal{T},l)})^{-1} (I - \beta^{(\mathcal{T},l)}), \quad (9)$$

where $\Phi^{(\mathcal{T},l)} := \frac{\text{tr}(\Sigma^{(\mathcal{S},l)})}{q} (D^{(\mathcal{T},l)})^{-1}$.

In our working example, neural recordings are not guaranteed to be temporally aligned across sample groups due to response latencies to stimuli (Ventura, 2004). Hence we do not assume that $\Sigma^{(\mathcal{T},l)}$ is the same or even similar across sample groups $l \in [m]$. Instead, we impose a weaker bandable assumption on the modified Cholesky decomposition for each sample group. In physiological time-series signals, the dependence between time points naturally decays as the time lag increases, so a reasonable assumption is that $\beta_{st}^{(\mathcal{T},l)}$ approaches zero as $t - s \rightarrow \infty$. By applying bandable assumptions, we ignore weak dependencies between distant time points, achieving a bias-variance trade-off in the estimation of $\beta^{(\mathcal{T},l)}$.

We estimate $\beta^{(\mathcal{T},l)}$ following the procedure in Liu and Ren (2020). Specifically, we treat the observed data $X^{(k,l)}$ as q vector-variate ‘‘column samples’’, $X_{\cdot,1}^{(k,l)}, \dots, X_{\cdot,q}^{(k,l)}$ rather than as p vector-variate ‘‘row samples’’ as in Section 3.1 for spatial covariance matrix estimation, and fit the following linear regression model at each time point t :

$$\hat{\beta}_{\cdot,t}^{(\mathcal{T},l)} := \underset{b \in \mathbb{R}^p}{\text{argmin}} \frac{1}{2n_l q} \sum_{k=1}^{n_l} \|X_{t,\cdot}^{(k,l)} - X^{(k,l)\top} b\|_2^2 \quad (10)$$

with respect to $b_s = 0$ where $s < t - h_l$ or $s \geq t$, where the bandwidth hyperparameter h_l can be either user-specified or data-driven. Unlike the spatial case, the estimation of the temporal covariance matrix is performed individually for each sample group. Having the regression coefficients estimated, we estimate $\Phi^{(\mathcal{T},l)}$ by

$$\hat{\Phi}_{tt}^{(\mathcal{T},l)} := \frac{1}{n_l q} \sum_{k=1}^{n_l} \|X_{t,\cdot}^{(k,l)} - X^{(k,l)\top} \hat{\beta}_{\cdot,t}^{(\mathcal{T},l)}\|_2^2. \quad (11)$$

For technical issues, we truncate the eigenvalues of $I - \beta^{(\mathcal{T},l)}$ to ensure its invertibility, following the approach in Liu and Ren (2020). Given a cut-off hyperparameter $\eta > 0$, for a square matrix A , let $P_\eta(A) := U \max\{\min\{\Lambda, \eta\}, \eta^{-1}\} V^\top$, where A has a singular value decomposition $A = U\Lambda V^\top$, and the min and max above are element-wise operations. Let $\bar{\Omega}^{(\mathcal{T},l)}$ be the precursor estimator of $\Omega^{(\mathcal{T},l)}$ given by

$$\bar{\Omega}^{(\mathcal{T},l)} := P_\eta (I - \hat{\beta}^{(\mathcal{T},l)})^\top (\hat{\Phi}^{(\mathcal{T},l)})^{-1} P_\eta (I - \hat{\beta}^{(\mathcal{T},l)}). \quad (12)$$

Conforming to the identifiability constraint $\text{tr}(\Sigma^{(\mathcal{T},l)}) = p$, we propose our estimators of $\Sigma^{(\mathcal{T},l)}$ and $\Omega^{(\mathcal{T},l)}$ as

$$\hat{\Sigma}^{(\mathcal{T},l)} := \frac{p}{\text{tr}(\bar{\Sigma}^{(\mathcal{T},l)})} \bar{\Sigma}^{(\mathcal{T},l)} \quad \text{and} \quad \hat{\Omega}^{(\mathcal{T},l)} := (\hat{\Sigma}^{(\mathcal{T},l)})^{-1} = \frac{\text{tr}(\bar{\Sigma}^{(\mathcal{T},l)})}{p} \bar{\Omega}^{(\mathcal{T},l)}, \quad (13)$$

where $\bar{\Sigma}^{(\mathcal{T},l)} := (\bar{\Omega}^{(\mathcal{T},l)})^{-1}$. The estimation error bounds of the Frobenius norm of $\Sigma^{(\mathcal{T},l)}$ are provided in Section C.2.

4 Theoretical Properties

We make the following assumptions on the multiple MGGM and the observed dataset \mathcal{D} .

Assumption 1. $\max_{l=1,\dots,m} \frac{n_l}{n_0} \leq \kappa_1$ for some positive constant κ_1 where $n_0 = \min_{l=1,\dots,m} n_l$.

Assumption 2. $\text{tr}(\Sigma^{(\mathcal{T},l)}) = p$, $\forall l = 1, \dots, m$.

Assumption 3. For each $l \in [m]$, let $\{\lambda_i^{(\mathcal{T},l)}\}_{i=1,\dots,p}$ be the eigenvalues of $\Sigma^{(\mathcal{T},l)}$ while $\frac{1}{\kappa_3} \leq \lambda_1^{(\mathcal{T},l)} \leq \lambda_2^{(\mathcal{T},l)} \leq \dots \leq \lambda_p^{(\mathcal{T},l)} \leq \kappa_3$ for some constant $\kappa_3 > 0$; define and assume $\{\lambda_i^{(\mathcal{S},l)}\}_{i=1,\dots,q}$ similarly for $\Sigma^{(\mathcal{S},l)}$.

Assumption 4. Let $d := \max_i \left| \left\{ j \in [q] \setminus \{i\} : \Omega_{ij}^{(\mathcal{S},l)} \neq 0 \text{ for some } l \in [m] \right\} \right|$ be the group-wise maximum node degree.

We assume group sparsity of the partial-correlation graph in spatial association by $d \cdot \frac{\max\{m, \log(mn_0pq)\}}{(mn_0p)^{1/2}} \rightarrow 0$ as $n_0 \rightarrow \infty$.

Assumption 5. We assume the temporal precision matrix $\Omega^{(\mathcal{T},l)}$ for each $l \in [m]$, has Cholesky decomposition as in Eq. (9) where $\beta^{(\mathcal{T},l)}$ satisfies $|\beta_{st}^{(\mathcal{T},l)}| < \kappa_5(t-s)^{-\alpha_l-1}$ for any t and s such that $s < t$ and some $\alpha_l > 0$. We further assume that, for $\alpha_0 = \min_{l=1,\dots,m} \alpha_l$, $\frac{\log(mn_0pq)}{(n_0q)^{1-1/(\alpha_0+1)}} \rightarrow 0$ as $n_0 \rightarrow \infty$.

Axiom 1 assumes that the sample sizes across sample groups are balanced, with n_0 representing this common level. Axiom 2 ensures identifiability. Axiom 3 is a standard assumption on eigenvalues commonly used in covariance estimation and graphical models (Cai et al., 2016b). Axiom 4 assumes that the spatial (column) precision matrices are sparse, and it imposes a constraint on the spatial dimension relative to the number of samples, the temporal dimension, and the number of graphs. In the special case of a single vector-variate graphical model with $m = 1, p = 1$, this assumption coincides with the necessary condition for root-consistent estimation of individual edges (Ren et al., 2015). Moreover, a larger temporal dimension p can further relax the required sample size. The first part of Axiom 5 is reasonable for neural time series, as these data are often modeled as a low-order autoregressive process, a common assumption in the literature (Bickel and Levina, 2008; Liu and Ren, 2020). The second part, similar to Axiom 4, restricts the temporal dimension. Likewise, increasing the spatial dimension q can further relax the sample size requirement.

In the following, $C(\dots)$ indicates a constant that depends on the other constants within the parentheses, with values that may change across lines. For universal constants without any dependency, we omit the parentheses and denote them simply by C .

4.1 Non-asymptotic error bound for the group Lasso estimate

We first provide a theoretical justification for our group Lasso procedure proposed in Section 3.1. Although with correlated rows, our results below demonstrate that the optimal convergence rates for the estimation error, defined as $\Delta_{\cdot,i}^{(S,l)} := \widehat{\beta}_{\cdot,i}^{(S,l)} - \beta_{\cdot,i}^{(S,l)}$, and prediction can be still obtained compared to the case with i.i.d. samples. The proof is provided in Section C.3.

Theorem 4.1. Suppose that γ_i satisfies $\frac{1}{C(\kappa_1, \kappa_3)} \sqrt{\frac{m+\log(mn_0pq)}{n_0p}} \leq \gamma_i \leq C(\kappa_1, \kappa_3) \sqrt{\frac{m+\log(mn_0pq)}{n_0p}}$ for some sufficiently large $C(\kappa_1, \kappa_3)$. Then, under ?? 1–5,

$$\mathbb{P} \left[\begin{array}{l} \max_i \sum_{j:j \neq i} \left\| \underline{\Delta}_{ji}^{(S,\cdot)} \right\|_2^2 \leq C(\kappa_1, \kappa_3) d \frac{m + \log(mn_0pq)}{n_0p}, \\ \max_i \sum_{j:j \neq i} \left\| \underline{\Delta}_{ji}^{(S,\cdot)} \right\|_2 \leq C(\kappa_1, \kappa_3) d \sqrt{\frac{m + \log(mn_0pq)}{n_0p}}, \\ \max_i \frac{1}{2n_0p} \sum_{l=1}^m \sum_{k=1}^{n_l} \left\| X^{(k,l)} \Delta_{\cdot,i}^{(S,l)} \right\|_2^2 \leq C(\kappa_1, \kappa_3) d \frac{m + \log(mn_0pq)}{n_0p} \end{array} \right] \geq 1 - C(mn_0pq)^{-1/2},$$

for a sufficiently large n_0 , where $\underline{\Delta}_j^{(S,l)} := \frac{\|X_{\cdot,j}^{(S,l)}\|_2}{\sqrt{n_l p}} \Delta_j^{(S,l)}$.

4.2 Theoretical justification for the simultaneous edge testing

We now present the theoretical results for the simultaneous test in Section 3.2. In the proof of Theorem 4.2, we show that the error in the partial correlation estimate $\widehat{\rho}_{ij}^{(S,l)}$ from Eq. (4) is driven by a leading term

$$\Theta_{ij}^{(S,l)} := \frac{\widetilde{\phi}_{ij}^{(S,l)}}{\sqrt{\Phi_{ii}^{(S,l)} \Phi_{jj}^{(S,l)}}} - \frac{\Phi_{ij}^{(S,l)} \widetilde{\phi}_{jj}^{(S,l)}}{2\Phi_{jj}^{(S,l)} \sqrt{\Phi_{ii}^{(S,l)} \Phi_{jj}^{(S,l)}}} - \frac{\Phi_{ij}^{(S,l)} \widetilde{\phi}_{ii}^{(S,l)}}{2\Phi_{ii}^{(S,l)} \sqrt{\Phi_{ii}^{(S,l)} \Phi_{jj}^{(S,l)}}}, \quad (14)$$

where $\widetilde{\phi}_{ij}^{(S,l)} := \widetilde{\Phi}_{ij}^{(S,l)} - \Phi_{ij}^{(S,l)} = \frac{1}{n_l p} \sum_{k=1}^{n_l} \epsilon_{\cdot,i}^{(S,k,l)\top} \epsilon_{\cdot,j}^{(S,k,l)} - \Phi_{ij}^{(S,l)}$. Since $\widetilde{\phi}_{ij}^{(S,l)}$ is an average over $t \in [p]$ and $k \in [n_l]$, the central limit theorem ensures that the partial correlation estimate $\widehat{\rho}_{ij}^{(S,l)}$ and the single-edge test statistic \widehat{T}_{ij} converge in distribution to Gaussian limits for each edge (i, j) .

The Gaussian approximation error for the multiple-edge test statistic $\|\widehat{T}_E\|_\infty$ is governed by Berry–Esseen bounds over hyper-rectangles. The seminal work of Chernozhukov et al. (2013) established these bounds in high-dimensional settings, where the dimension can exceed the sample size. Building on this, we use the near-optimal convergence rate for the Berry–Esseen bound from Chernozhukov et al. (2023) to derive a sharp Gaussian approximation error bound for $\|\widehat{T}_E\|_\infty$. The proof is provided in Section C.4.

Proposition 4.2. Let $Z \sim \mathcal{N}(0, S_{EE})$ where the elements of S_{EE} are given as in Eq. (7), and \widehat{T}_E is estimated based on γ_i 's given as in Theorem 4.1. Then under ?? 1–5,

$$\begin{aligned} & \sup_{x>0} \left| \mathbb{P}[\|\widehat{T}_E\|_\infty > x] - \mathbb{P}[\|T_E + Z\|_\infty > x] \right| \\ & \leq \frac{C(\kappa_1, \kappa_3)}{\sqrt{mn_0p}} \max \left\{ (\log|E|)^2 \log(mn_0p), (\log|E|)^{5/2}, d\sqrt{\log|E|}(m + \log(mn_0pq)) \right\}, \end{aligned}$$

for a sufficiently large n_0 .

The following theorem mirrors the previous proposition, with the key difference being that we replace the population covariance S_{EE} with its plug-in estimator \widehat{S}_{EE} . In essence, as long as S_{EE} is well-estimated under the $\|\cdot\|_\infty$ -norm, the Gaussian approximation results remain valid. Using the convergence rate of \widehat{S}_{EE} in the $\|\cdot\|_\infty$ -norm, we derive the following bootstrap theorem, based on the relationship between convergence rate and bootstrap error as given in Lemma 2.1 of Chernozhukov et al. (2023).

Theorem 4.3. Let $\widehat{Z} \sim \mathcal{N}(0, \widehat{S}_{EE})$ where the plug-in estimator \widehat{S}_{EE} and \widehat{T}_E are estimated based on γ_i 's given in Theorem 4.1. Then, under ?? 1–5,

$$\begin{aligned} & \sup_{x>0} \left| \mathbb{P}[\|\widehat{T}_E\|_\infty > x] - \mathbb{P}[\|T_E + \widehat{Z}\|_\infty > x | \mathcal{D}] \right| \\ & \leq C(\kappa_1, \kappa_3, \kappa_5) \max \left\{ \frac{(\log|E|)^2 \log(mn_0p)}{\sqrt{mn_0p}}, \frac{(\log|E|)^{5/2}}{\sqrt{mn_0p}}, d\sqrt{\log|E|} \frac{m + \log(mn_0pq)}{\sqrt{mn_0p}}, \right. \\ & \quad \left. \log|E| \log(n_0pq) \sqrt{\frac{\log(mn_0pq)}{(n_0q)^{1-\frac{1}{2(\alpha_0+1)}}} + \frac{m + \log(mn_0pq)}{mn_0p}} \right\} \end{aligned}$$

with probability at least $1 - C(mn_0pq)^{-1/2}$ for a sufficiently large n_0 .

The above theorem establishes the theoretical foundation for the simultaneous multiple edge testing procedure in Algorithm 1. Next, we formally state the validity of our testing procedure as well as a power analysis. The proof is given in Section C.6

Theorem 4.4. Suppose that n_0 increases at a faster rate than

$$\frac{1}{mp} \max \left\{ (\log|E|)^4 (\log(mn_0p))^2, (\log|E|)^5, d^2 \log|E| (m + \log(mn_0pq))^2, (\log|E| \log(n_0p))^2 (m + \log(mn_0pq)) \right\}$$

and $\frac{1}{q} ((\log|E| \log(n_0q))^2 \log(mn_0pq))^{1+1/(2\alpha_0+1)}$. Under the null $H_{0,E}$ and ?? 1–5, the confidence region $\mathcal{C}_E(1 - \alpha)$ estimated based on γ_i 's given in Theorem 4.1 satisfies $\mathbb{P}[\mathbf{0} \notin \mathcal{C}_E(1 - \alpha)] \xrightarrow{P} \alpha$. On the other hand, as an alternative, if

$$\|T_E\|_\infty \geq C(\kappa_1, \kappa_3, \kappa_5) \sqrt{(\log q + \log(1/\alpha)) \max_{(i,j) \in E} S_{(i,j),(i,j)}},$$

then under the same assumptions and γ_i 's, we have $\mathbb{P}[\mathbf{0} \notin \mathcal{C}_E(1 - \alpha)] \xrightarrow{P} 1$.

Remark 4.5. Theorem 4.4 implies that the test power converges to 1 as $n_0 \rightarrow \infty$, provided that $\sum_{l=1}^m \rho_{ij}^{(S,l)}$ exceeds the order of $\sqrt{m \log q / (n_0p)}$ for some $(i, j) \in E$. When the partial correlations $\rho_{ij}^{(S,l)}$ have the same sign and comparable magnitude across sample groups, this condition simplifies to $\max_{(i,j) \in E} |\rho_{ij}^{(S,l)}|$ being larger than $\sqrt{\log q / (mn_0p)}$. In contrast, without aggregating multiple graphs, the corresponding detection boundary is $\sqrt{\log q / (n_0p)}$. Hence, by pooling information across m sample groups, the detectable signal strength is reduced by a factor of \sqrt{m} , thereby improving detection power.

Moreover, when the temporal covariance matrices satisfy $\Sigma^{(\mathcal{T},l)} = I$ for all $l \in [m]$, the model simplifies to the multiple vector-variate Gaussian graphical model studied in Ren et al. (2019), with an effective sample size of n_0p . According to their Theorem 2.3, the optimal separating rate for detecting a single edge, measured in terms of the sum of partial correlations, is $\sqrt{m / (n_0p)}$. This comparison indicates that our test achieves nearly optimal performance in terms of the testable region boundary. We further conjecture that the extra $\sqrt{\log q}$ factor is intrinsic when the edge set size $|E|$ grows at a polynomial rate in q .

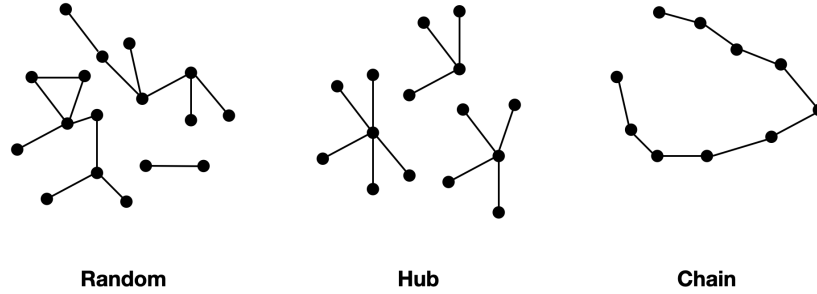


Figure 1: Simulated spatial graphs.

5 Numerical Studies

In Section 5.1, we present simulation studies to validate our theoretical results of Section 4 and evaluate the performance of our inference procedure for multiple matrix-variate graphical models in comparison to several baseline approaches. In Section 5.2, we apply our method to neural recordings from two Utah arrays implanted in the monkey brains during a spatial working memory task. The implementation of our proposed method is available in the `mmge` R package, along with vignettes for reproducing our results, accessible at github.com/HeejongBong/mmge.

5.1 Simulation Studies

We evaluated the performance of our method under three spatial graph structures, illustrated in Figure 1: (1) a random graph, where edges between nodes were generated with probability $\sqrt{\frac{3}{q}}$ for each pair (i, j) ; (2) a hub graph, where the nodes were divided into $\lceil \frac{q}{20} \rceil$ hub groups; and (3) a chain graph. Given each spatial graph structure, we generated the spatial precision matrix by sampling the non-zero entries from $\text{Unif}(0, \frac{0.3}{2^{i-1}})$, independently across sample groups $l \in [m]$. For the temporal precision matrix, we generated $\Sigma^{(\mathcal{T}, l)}$ using Eq. (9). Following Axiom 5, we set $\beta_{st}^{(\mathcal{T}, l)} = \kappa_5(t-s)^{-\alpha_l-1}$ for $1 \leq s < t \leq p$, with $\kappa_5 = 0.2$ and $\alpha_l = 1$. For $\Phi^{(\mathcal{T}, l)}$, we used the $p \times p$ identity matrix for all $l \in [m]$.

In Section 5.1.1, we compare our method’s performance with existing methods in terms of edge detection and precision matrix estimation. In Section 5.1.2, we assess the coverage of the proposed bootstrap confidence region for T_E .

5.1.1 Edge-wise Estimation Comparison

We compared our method (M0) with the following Gaussian graphical model estimation procedures:

- (M1): matrix-variate Gaussian multi-graph estimation method by Zhu and Li (2018)
- (M2): regression-based Gaussian graph estimation method by Ren et al. (2019)
- (M3 & M4): optimization based Gaussian graph estimation methods by Cai et al. (2016a) and Lee and Liu (2015), respectively

Methods (M0) and (M1) are based on the matrix-variate Gaussian graphical model, while the others are designed for the vector-variate model. Since the vector-variate model does not account for temporal correlation, methods (M2), (M3), and (M4) are at a disadvantage when applied to spatiotemporal data. To ensure a fair comparison, we used the `whiten` function from the `whitening` R package to whiten the simulated data before applying the vector-variate methods.

The edge detection performance of the methods was evaluated using receiver operating characteristic (ROC) curves. An ROC curve plots the true positive rate (TPR) against the false positive rate (FPR) as the detection threshold is varied by adjusting specific hyperparameters. For Methods (M0) and (M2), which detect non-zero spatial edges based on rejecting edge-wise null hypotheses (Eq. (5)), we generated ROC curves by varying the p -value threshold while keeping other hyperparameters fixed. For the sparsity hyperparameter of Method (M0), we fixed $\gamma_i = 1e-4$ for all i . For the other methods, ROC curves were plotted by varying the sparsity hyperparameter, with other hyperparameters held constant.

The results with $m = 5$, $n = 5$, and four different pairs of (p, q) are shown in Fig. 2. The ROC curves indicate that our method consistently outperformed the other methods, thanks to the efficient use of spatial observations across sample

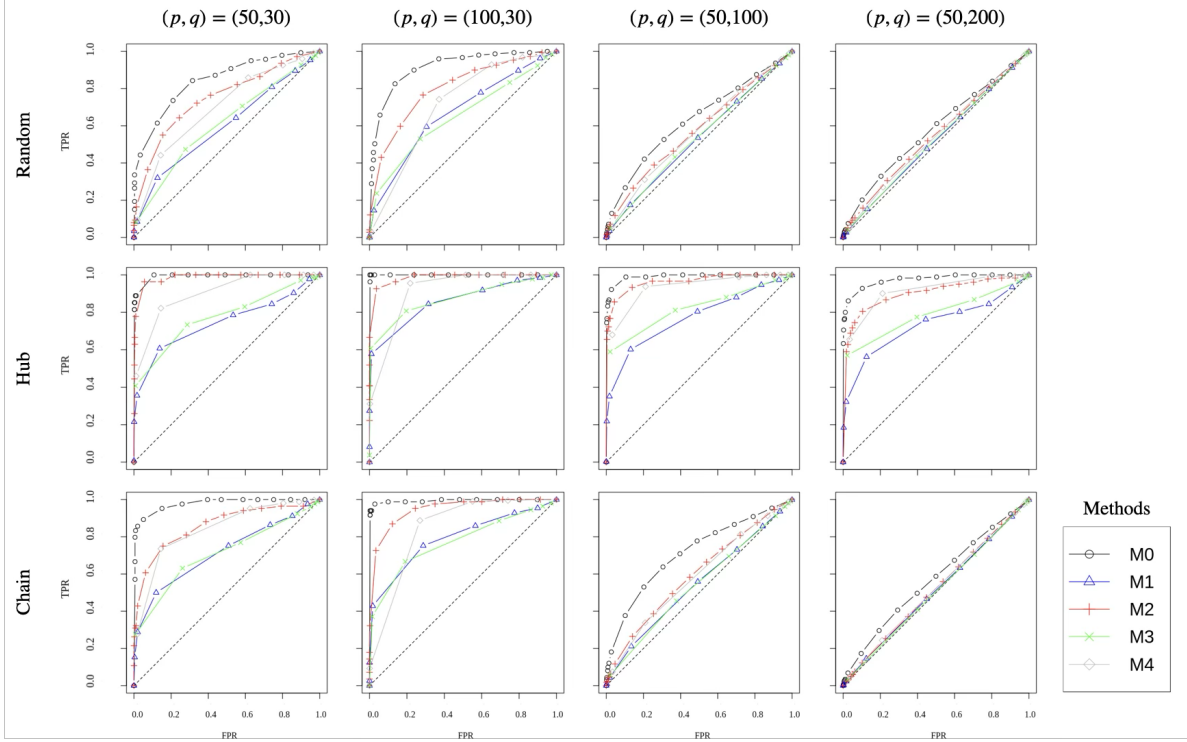


Figure 2: Simulation results are shown for different graph configurations and temporal dimensions with $n = 5$ and $m = 5$. Rows represent different graph types, while columns correspond to varying spatial and temporal dimensions. Curves represent our method (M0) and the other baseline methods.

Table 1: Empirical coverage of the confidence region when $m = 5, p = 50, q = 30$.

n	Nominal Coverage	Random		Hub		Chain	
		E_{off}	E_{zero}	E_{off}	E_{zero}	E_{off}	E_{zero}
5	0.925	0.906(0.009)	0.900(0.009)	0.901(0.006)	0.904(0.006)	0.886(0.008)	0.888(0.007)
	0.95	0.935(0.006)	0.938(0.006)	0.932(0.006)	0.934(0.007)	0.922(0.007)	0.923(0.008)
	0.975	0.971(0.004)	0.962(0.005)	0.962(0.004)	0.963(0.004)	0.959(0.005)	0.959(0.005)
10	0.925	0.908(0.006)	0.913(0.005)	0.931(0.005)	0.928(0.006)	0.931(0.006)	0.928(0.007)
	0.95	0.934(0.004)	0.937(0.004)	0.951(0.003)	0.950(0.003)	0.953(0.004)	0.953(0.005)
	0.975	0.961(0.004)	0.961(0.003)	0.971(0.003)	0.971(0.003)	0.974(0.003)	0.975(0.003)
20	0.925	0.917(0.007)	0.920(0.004)	0.934(0.004)	0.930(0.006)	0.931(0.006)	0.928(0.007)
	0.95	0.947(0.006)	0.948(0.005)	0.959(0.004)	0.955(0.004)	0.953(0.004)	0.953(0.005)
	0.975	0.978(0.002)	0.975(0.004)	0.985(0.002)	0.984(0.002)	0.974(0.003)	0.975(0.002)

groups. In an additional simulation study with varying γ_i values, our method demonstrated moderate sensitivity to the choice of the group Lasso hyperparameter, while it consistently outperformed the baseline methods across the range of tuning parameters considered, particularly in settings with high temporal and spatial dimensions.

5.1.2 Simultaneous Test

In this section, we evaluate the coverage of the proposed bootstrap confidence interval (Eq. (8)) using simulated data. The simulations were conducted with m sample groups of n i.i.d. matrix-variate data, with temporal dimension $p = 50$ and spatial dimension $q = 30$. We generated 3000 bootstrap samples to construct confidence intervals for $\|T_E\|_\infty$ over two edge sets: $E_{\text{off}} = \{(i, j) : i \neq j\}$ and $E_{\text{zero}} = \{(i, j) : \Omega_{ij}^{(S,l)} = 0, \forall l = 1, \dots, m\}$.

We repeated this procedure over 1000 datasets generated from the multiple matrix-variate Gaussian graphical models for each of the three spatial partial-correlation graphs (random, hub, and chain). For each graph, we computed the empirical coverage of the bootstrap confidence intervals. Table 1 presents the mean and standard deviation of the empirical coverage across the 1000 repetitions for each spatial graph and nominal coverage level. We observe that the empirical coverages are close to the nominal values and converge further as the sample size n increases. This result demonstrates the coverage of the bootstrap confidence region shown in Theorem 4.3.

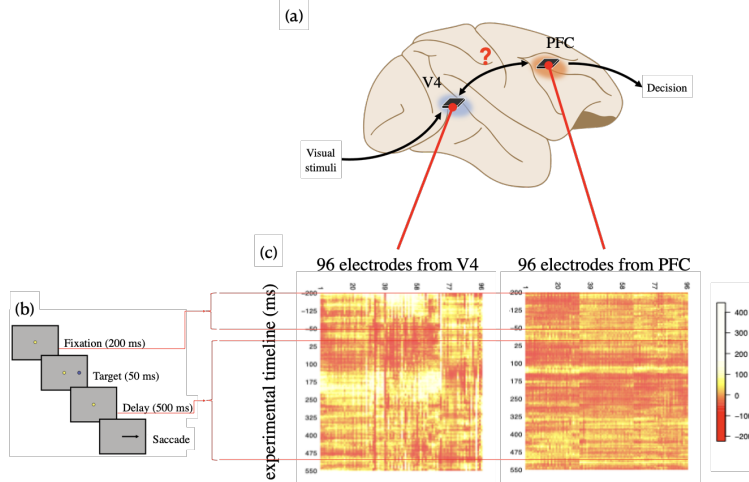


Figure 3: (a) The positions of the analyzed cortical areas, V4 and PFC in a primate brain. The neuroelectrical activity in each area was recorded by a 96-electrode Utah array. (b) The timeline of one experimental trial. (c) LFP recordings for one experimental trial. Each x-axis indicates 96 electrodes in each brain area, and the y-axis is time in ms. Time $t = 0$ was aligned at the start of the delay period.

5.2 Experimental Data Analysis

We analyzed local field potential recordings (LFPs) from two Utah arrays implanted in the prefrontal cortex (PFC) and visual area V4 of an experimental subject (a Macaque monkey, Fig. 3(a)). Each Utah array had 96 electrodes, and the neuroelectrical activity in the two areas were simultaneously recorded during a memory-guided saccade task. One experimental trial of the task consisted of the following stages (see Fig. 3(b)):

1. The subject fixated at the center of the screen for 200 ms.
2. A circular target appeared at a randomly chosen location out of the forty possible spots on the screen (8 directions and 5 amplitudes) and turned off after 50 ms.
3. The subject had to remember the target location during a delay period of 500 ms while maintaining fixation.
4. After the delay period, the fixation point turned off, and the subject had to make a saccade to the remembered target location.

See Khanna et al. (2020) for the details of the experiment and data collection. Previous studies in similar tasks have shown that area V4 encodes higher order visual features such as color and shape and is modulated by visual attention (Orban, 2008; Fries et al., 2001), while the prefrontal cortex (PFC) plays a central role in cognitive control and working memory (Miller and Cohen, 2001). Despite their anatomical separation and distinct functional roles, coordinated activity between V4 and PFC has been reported during visual memory retention (Sarnthein et al., 1998; Liebe et al., 2012). Building on these findings, our objective is to examine how the spatial correlation structure within and between these regions evolves across four experimental stages: fixation (200 ms), target presentation (50 ms), early delay (the first 250 ms of the delay period), and late delay (the last 250 ms of the delay period).

The dataset was collected across $m = 5$ experimental sessions indexed by l , containing $n_l = 2000, 2995, 3000, 3000,$ and 3000 successful trials, respectively. For each trial, we observed matrix-variate data with temporal dimension $p = 750$, corresponding to 750 ms recorded at a sampling rate of 1 kHz, and spatial dimension $q = 192$, corresponding to 2×96 electrodes. An example trial is shown in Fig. 3(c), where the heatmap color indicates the intensity of the local field potential signal. Although the strength of partial correlations may vary across experimental sessions due to session-specific variability, we expect the underlying sparsity pattern of the connectivity graph to be largely shared across sessions within each experimental stage. To exploit this structure, we applied the proposed method in Section 3 separately to each stage, jointly fitting multiple matrix-variate graphs across sessions by treating trials within each session as a single sample group. This joint modeling strategy allows us to borrow information across sessions, thereby improving statistical power for detecting common connectivity patterns while accommodating heterogeneity in correlation magnitudes.

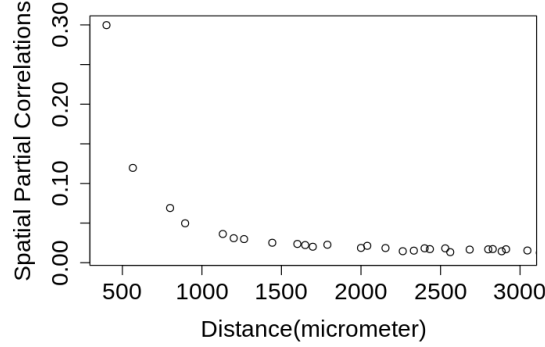


Figure 4: The averaged $\hat{\rho}_{ij}^{(S)}$ within a group of spatially equidistant within-area edges during the late delay stage in V4.

5.2.1 Correlated neural connectivity vs. Physical distance

As an initial sanity check, we examined the relationship between neural connectivity and physical distance. Previous studies have shown that LFP signals from neighboring electrodes in monkey brains tend to exhibit strong correlations and that the correlation decays sharply as the distance between electrodes increases (Leopold and Logothetis, 2003). To quantify this effect, we applied our method to the raw LFP signals from each brain region at each experimental stage. For each electrode pair (i, j) , we aggregated the spatial partial correlation estimates across sessions by calculating $\hat{\rho}_{ij}^{(S)} := \frac{1}{\sum_{l=1}^m \sqrt{n_l}} \sum_{l=1}^m \sqrt{n_l} \hat{\rho}_{ij}^{(S,l)}$, where the weight $\sqrt{n_l}$ accounts for the varying number of trials across sessions. We then grouped electrode pairs by spatial distance and calculated the average of $\hat{\rho}_{ij}^{(S)}$ within each distance group. Fig. 4 shows the average spatial partial correlations within each equidistant group in area V4 during the late delay stage, plotted against physical distance. The results demonstrate a clear monotonic decrease in average $\hat{\rho}_{ij}^{(S)}$ with increasing distance, consistent with prior findings. We observed similar trends in other stages and in the PFC.

5.2.2 Within-area Inference

Next, we examined how within-region connectivity changes across the experimental stages. Using the same output from our method applied to each brain region at each stage, we quantified the within-region average connectivity of each electrode i by computing $\sum_j |\hat{\rho}_{ij}^{(S)}|$, where \sum_j denotes summation over all other electrodes within the same region as i .

Fig. 5 presents the smoothed distributions of within-area connectivity across the four experimental stages in both brain regions. We observed that V4 exhibited higher within-area connectivity than PFC. In V4, connectivity was strongest during the fixation and cue stages, then declined during the delay stages. In contrast, the level of connectivity in PFC remained relatively stable across experimental stages.

5.2.3 Cross-area Inference

We applied our method to the recordings from both areas and identified significant cross-area connectivity. To reduce computation time and collinearity, we subsampled the electrodes in each area by taking every other node along the spatial dimension, reducing the spatial dimension q from 192 to 50 in total. This reduced the number of cross-area edges to 625. Also, because beta oscillations are often associated with communication across the two brain areas (Klein et al., 2020; Miller et al., 2018), we first band-pass filtered the LFP recordings at the beta band 15 – 30 Hz and downsampled the filtered data to 200 Hz. Fig. 6 shows the cross-area edges, color-coded by the estimated spatial partial correlations $\hat{\rho}_{ij}^{(S)}$ between electrode i in V4 and electrode j in PFC. We find that cross-area connectivity between V4 and PFC is markedly heterogeneous across electrode pairs and varies substantially across experimental stages. In particular, edges involving electrode e_1 (shown in red in Fig. 6) are consistently strong across stages and further strengthen during the late delay period, when working memory demands are highest. This pattern suggests that connectivity through electrode e_1 may reflect attentional signals directed by PFC during visual memory retention. In contrast, other cross-area edges are strongest during the target presentation stage, which may reflect transient top-down signaling from V4 to PFC associated with stimulus processing. These observations are broadly consistent with prior findings that V4–PFC interactions are engaged during attention tasks (Squire et al., 2013; Snyder et al., 2021), and that long-range corticocortical connections

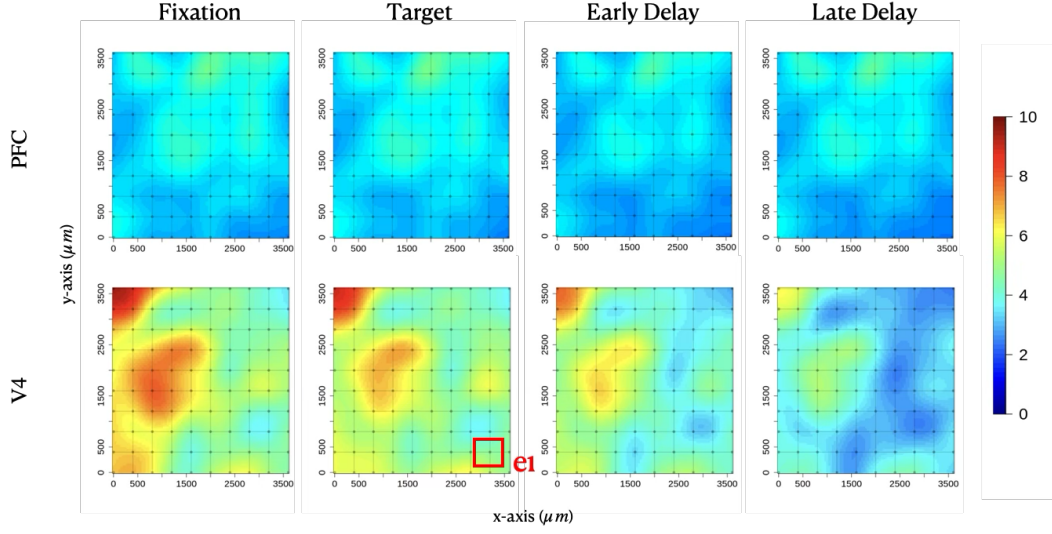


Figure 5: Spatially smoothed within-area connectivity strength distribution over the spatial electrode array for PFC and V4 over the experimental stages. The connectivity within V4 decayed over the stages, while the level of within-connectivity in PFC was stable.

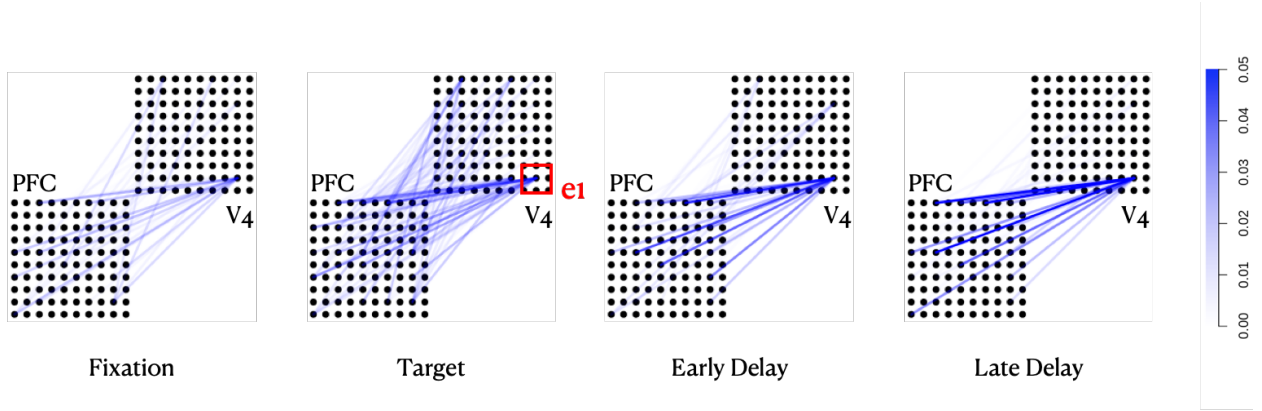


Figure 6: Estimated cross-area connectivity between PFC and V4, shown as edges color-coded by partial correlations $\hat{\rho}_{ij}^{(S)}$ between electrode i in V4 and electrode j in PFC over the four experimental stages. The x- and y-axes are spatial coordinates of the electrodes on each array. The plot shows a spatial distinction in the evolution of the cross-area connection.

are sparse and exhibit substantial variability in strength depending on anatomical distance and functional properties (Ts’o et al., 1986; El-Shamayleh et al., 2013; Smith and Kohn, 2008).

Based on this observation, we further analyzed the cross-area connectivity in two distinct edge sets: (i) edges incident to e_1 and (ii) edges excluding e_1 . Cross-area connectivity was quantified by the maximal partial correlations within each edge set across the four experimental stages. For statistical inference, we constructed 95%-confidence intervals for the maximal partial correlation in each edge set and stage, as defined in Eq. (8), using 100,000 Gaussian bootstrap samples, i.e., $\|\hat{T}_E + \hat{Z}\|_\infty$ where $\hat{Z} \sim N(0, \hat{S}_{EE})$.

Fig. 7 presents these confidence intervals, with points indicating the median values of the bootstrap samples $\|\hat{T}_E + \hat{Z}\|_\infty$ for the two edge sets across experimental stages. For edges excluding e_1 , we reaffirm that cross-area connectivity was strongest during target presentation. In contrast, edges incident to e_1 exhibited increased connectivity during the delay stage, when the animal processed the visual signal and prepared for the subsequent decision.

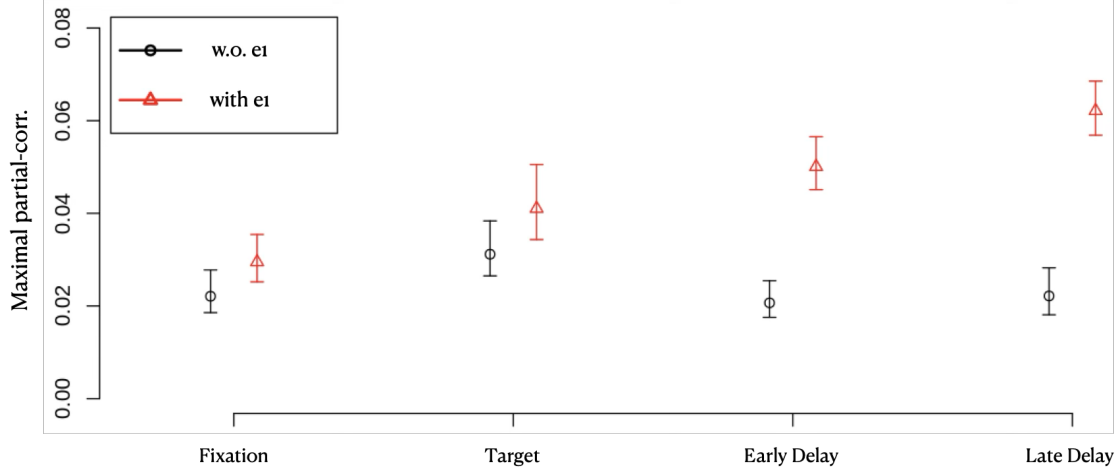


Figure 7: Inference on the maximal partial correlations over the two edge sets: (triangle) the cross-area edges with electrode e_1 , marked in Fig. 6 and (circle) the other cross-area edges. The points are the median values of the bootstrap samples obtained by Algorithm 1 with 100,000 bootstrap samples, and the error bars are the 95 % bootstrap confidence intervals.

We tested the monotonic trend in cross-area connectivity for edges incident to e_1 using a linear trend test. In this test, we regressed connectivity levels at the four stages against the respective time points on the experimental timeline. A positive slope indicated increasing connectivity, while a negative slope indicated decreasing connectivity. The uncertainty in the slope estimate was assessed by repeating the linear trend test over the Gaussian bootstrap samples $\|\hat{T}_E + \hat{Z}\|_\infty$. The 95%-confidence interval of the slope was $(5.03e-5, 8.17e-5) \text{ ms}^{-1}$, indicating that connectivity in edges incident to e_1 increased significantly over time.

A similar trend was observed when using the average partial correlation, rather than the maximal partial correlations, over the edge set (Fig. B.1). This contrasts with the decline in within-area connectivity in V4 during the delay stages, as shown in Fig. 5. When we applied the same trend test to averaged partial correlations within V4, we found that within-area connectivity in V4 decreased significantly (Fig. B.2).

In summary, (a) there is strong within-area functional connectivity (based on partial correlations) for V4 that diminishes across the four stages, while there is much weaker within-area connectivity for PFC that remains stable across the stages (Fig. 5); (b) the cross-area connectivity is relatively sparse in V4 compared with PFC, except during target illumination; the signal from electrode e_1 which, across all four stages, has the largest partial correlation (among those in V4) with those from PFC, during the final stage (late delay) has very much stronger connectivity with PFC than the signals from other electrodes in V4; also its connectivity strengthens across the stages, while connectivity of the other electrodes with PFC stays roughly the same (Figs. 6 and 7); and (c) the signal from electrode e_1 does not have especially strong connectivity within V4.

6 Conclusion

We proposed a method for jointly estimating multiple matrix-variate graphical models that leverages shared sparsity structures across sample groups, together with a unified framework for high-dimensional inference on graph edges. Estimation is carried out using group Lasso to exploit the shared sparsity structures, while inference is designed for high-dimensional settings via state-of-the-art central limit theorems for the supremum of weighted sums. The proposed approach accommodates settings in which the spatial and temporal dimensions, as well as the number of graphs, may all diverge and potentially exceed the available sample size.

Both our model and our assumptions are motivated by practical concerns in neural data analysis. In real data, we observed that the within-area connectivity and cross-area connectivity change as the animal progresses through different experimental stages. From a scientific perspective, the data analysis suggests the intriguing possibility that there is some degree of localization in the memory task-relevant neural signals connecting V4 with PFC. However, justification for a strong scientific conclusion would require additional experimental work. The findings are most interesting as illustrations of the way changing connectivity structure, across multiple stages of a task, can be determined from high-dimensional electrode recordings.

Our method represents the first attempt to address the simultaneous testing problem in multiple matrix-variate Gaussian graphs. An interesting future direction would be to extend this approach to other commonly used non-Gaussian graph types, such as Poisson networks. Additionally, our current implementation uses group Lasso for the regression model, which requires one tuning parameter. In the future, a tuning-free or scale-free approach, such as the self-tuned Dantzig selector or scaled Lasso, would be desirable to address issues of heterogeneity and correlation in regression with data from multiple matrix-variate Gaussian graphical models. These extensions, while beyond the scope of this work, offer promising directions for future research.

References

- Allen, G. I. and Tibshirani, R. (2010). Transposable regularized covariance models with an application to missing data imputation. *The Annals of Applied Statistics*, 4(2):764–790.
- Bickel, P. J. and Levina, E. (2008). Regularized estimation of large covariance matrices. *The Annals of Statistics*, 36(1):199–227.
- Bong, H. and Kuchibhotla, A. K. (2023). Tight concentration inequality for sub-Weibull random variables with generalized Bernstein Orlicz norm. *arXiv preprint*.
- Bong, H., Ventura, V., Yttri, E. A., Smith, M. A., and Kass, R. E. (2021). Cross-population amplitude coupling in high-dimensional oscillatory neural time series. *arXiv preprint arXiv:2105.03508*.
- Cai, T. T., Li, H., Liu, W., and Xie, J. (2016a). Joint estimation of multiple high-dimensional precision matrices. *Statistica Sinica*, 26(2):445–464.
- Cai, T. T., Ren, Z., and Zhou, H. H. (2016b). Estimating structured high-dimensional covariance and precision matrices: Optimal rates and adaptive estimation. *Electronic Journal of Statistics*, 10(1):1–59.
- Chang, J., Qiu, Y., Yao, Q., and Zou, T. (2018). Confidence regions for entries of a large precision matrix. *Journal of Econometrics*, 206(1):57–82.
- Chen, X. and Liu, W. (2018). Graph estimation for matrix-variate Gaussian data. *Statistica Sinica*, 29:479–504.
- Chernozhukov, V., Chetverikov, D., and Kato, K. (2013). Gaussian approximations and multiplier bootstrap for maxima of sums of high-dimensional random vectors. *The Annals of Statistics*, 41(6):2786–2819.
- Chernozhukov, V., Chetverikov, D., and Kato, K. (2015). Comparison and anti-concentration bounds for maxima of Gaussian random vectors. *Probability Theory and Related Fields*, 162(1):47–70.
- Chernozhukov, V., Chetverikov, D., and Koike, Y. (2023). Nearly optimal central limit theorem and bootstrap approximations in high dimensions. *The Annals of Applied Probability*, 33(3):2374–2425.
- Danaher, P., Wang, P., and Witten, D. M. (2014). The joint graphical lasso for inverse covariance estimation across multiple classes. *Journal of the Royal Statistical Society Series B: Statistical Methodology*, 76(2):373–397.
- Dawid, A. P. (1981). Some matrix-variate distribution theory: notational considerations and a Bayesian application. *Biometrika*, 68(1):265–274.
- El-Shamayleh, Y., Kumbhani, R. D., Dhruv, N. T., and Movshon, J. A. (2013). Visual response properties of V1 neurons projecting to V2 in macaque. *Journal of Neuroscience*, 33(42):16594–16605.
- Friedman, J., Hastie, T., and Tibshirani, R. (2008). Sparse inverse covariance estimation with the graphical lasso. *Biostatistics*, 9(3):432–441.
- Fries, P., Reynolds, J. H., Rorie, A. E., and Desimone, R. (2001). Modulation of oscillatory neuronal synchronization by selective visual attention. *Science*, 291(5508):1560–1563.
- Jankova, J. and van de Geer, S. (2015). Confidence intervals for high-dimensional inverse covariance estimation. *Electronic Journal of Statistics*, 9(1):1205–1229.
- Kass, R. E., Bong, H., Olanrinre, M., Xin, Q., and Urban, K. N. (2023). Identification of interacting neural populations: methods and statistical considerations. *Journal of Neurophysiology*, 130(3):475–496.
- Khanna, S. B., Scott, J. A., and Smith, M. A. (2020). Dynamic shifts of visual and saccadic signals in prefrontal cortical regions 8Ar and FEF. *Journal of Neurophysiology*, 124(6):1774–1791.
- Klein, N., Orellana, J., Brincat, S. L., Miller, E. K., Kass, R. E., et al. (2020). Torus graphs for multivariate phase coupling analysis. *The Annals of Applied Statistics*, 14(2):635–660.
- Kuchibhotla, A. K. and Chakraborty, A. (2022). Moving beyond sub-gaussianity in high-dimensional statistics: Applications in covariance estimation and linear regression. *Information and Inference: A Journal of the IMA*, 11(4):1389–1456.

- Lee, W. and Liu, Y. (2015). Joint estimation of multiple precision matrices with common structures. *Journal of Machine Learning Research*, 16:1035–1062.
- Leng, C. and Tang, C. Y. (2012). Sparse matrix graphical models. *Journal of the American Statistical Association*, 107(499):1187–1200.
- Leopold, D. A. and Logothetis, N. K. (2003). Spatial patterns of spontaneous local field activity in the monkey visual cortex. *Reviews in the Neurosciences*, 14(1-2):195–205.
- Liebe, S., Hoerzer, G. M., Logothetis, N. K., and Rainer, G. (2012). Theta coupling between V4 and prefrontal cortex predicts visual short-term memory performance. *Nature Neuroscience*, 15:456.
- Liu, W. (2013). Gaussian graphical model estimation with false discovery rate control. *The Annals of Statistics*, 41(6):2948–2978.
- Liu, Y. and Ren, Z. (2020). Minimax estimation of large precision matrices with bandable Cholesky factor. *The Annals of Statistics*, 48(4):2428–2454.
- Miller, E. K. and Cohen, J. D. (2001). An integrative theory of prefrontal cortex function. *Annual Review of Neuroscience*, 24:167–202.
- Miller, E. K., Lundqvist, M., and Bastos, A. M. (2018). Working memory 2.0. *Neuron*, 100(2):463–475.
- Orban, G. A. (2008). Higher order visual processing in macaque extrastriate cortex. *Physiological Reviews*, 88(1):59–89.
- Peterson, C., Stingo, F. C., and Vannucci, M. (2015). Bayesian inference of multiple gaussian graphical models. *Journal of the American Statistical Association*, 110(509):159–174. PMID: 26078481.
- Qiu, Y. and Zhou, X.-H. (2020). Estimating c -level partial correlation graphs with application to brain imaging. *Biostatistics*, 21(4):641–658.
- Ren, Z., Kang, Y., Fan, Y., and Lv, J. (2019). Tuning-free heterogeneous inference in massive networks. *Journal of the American Statistical Association*, 114(528):1908–1925.
- Ren, Z., Sun, T., Zhang, C.-H., and Zhou, H. H. (2015). Asymptotic normality and optimalities in estimation of large gaussian graphical models. *The Annals of Statistics*, 43(3):991–1026.
- Sarnthein, J., Petsche, H., Rappelsberger, P., Shaw, G., and Von Stein, A. (1998). Synchronization between prefrontal and posterior association cortex during human working memory. *Proceedings of the National Academy of Sciences*, 95:7092–7096.
- Smith, M. A. and Kohn, A. (2008). Spatial and temporal scales of neuronal correlation in primary visual cortex. *Journal of Neuroscience*, 28(48):12591–12603.
- Snyder, A. C., Yu, B. M., and Smith, M. A. (2021). A stable population code for attention in prefrontal cortex leads a dynamic attention code in visual cortex. *Journal of Neuroscience*, 41(44):9163–9176.
- Squire, R. F., Noudoost, B., Schafer, R. J., and Moore, T. (2013). Prefrontal contributions to visual selective attention. *Annual Review of Neuroscience*, 36:451–466.
- Ts’o, D. Y., Gilbert, C. D., and Wiesel, T. N. (1986). Relationships between horizontal interactions and functional architecture in cat striate cortex as revealed by cross-correlation analysis. *Journal of Neuroscience*, 6(4):1160–1170.
- Ventura, V. (2004). Testing for and estimating latency effects for Poisson and non-Poisson spike trains. *Neural Computation*, 16(11):2323–2349.
- Vershynin, R. (2018). *High-dimensional probability: An introduction with applications in data science*, volume 47. Cambridge university press.
- Wainwright, M. J. (2019). *High-dimensional statistics: A non-asymptotic viewpoint*, volume 48. Cambridge University Press.
- Ye, Y., Xia, Y., and Li, L. (2021). Paired test of matrix graphs and brain connectivity analysis. *Biostatistics*, 22(2):402–420.
- Yin, J. and Li, H. (2012). Model selection and estimation in the matrix normal graphical model. *Journal of Multivariate Analysis*, 107:119–140.
- Yuan, M. and Lin, Y. (2006). Model selection and estimation in regression with grouped variables. *Journal of the Royal Statistical Society Series B: Statistical Methodology*, 68(1):49–67.
- Zhou, S. (2014). Gemini: Graph estimation with matrix variate normal instances. *The Annals of Statistics*, 42(2):532–562.
- Zhu, Y. and Li, L. (2018). Multiple matrix Gaussian graphs estimation. *Journal of the Royal Statistical Society Series B: Statistical Methodology*, 80(5):927–950.

A Supplementary results for simulation study

Table A.1 presents the average empirical coverages under the same simulation setting as in Section 5.1.2 with the number of sessions fixed at $m = 3$.

Table A.1: Average of empirical coverages and their standard deviations for $m = 3, p = 50, q = 30$.

n	Quantile	Random		Hub		Band	
		E_{off}	E_{zero}	E_{off}	E_{zero}	E_{off}	E_{zero}
5	0.925	0.897(0.012)	0.898(0.009)	0.908(0.010)	0.908(0.009)	0.903(0.009)	0.907(0.010)
	0.95	0.935(0.006)	0.932(0.010)	0.939(0.007)	0.939(0.007)	0.934(0.008)	0.939(0.007)
	0.975	0.962(0.006)	0.969(0.002)	0.970(0.004)	0.971(0.004)	0.971(0.004)	0.971(0.003)
10	0.925	0.926(0.005)	0.924(0.006)	0.923(0.005)	0.923(0.006)	0.929(0.005)	0.927(0.006)
	0.95	0.944(0.003)	0.949(0.004)	0.945(0.004)	0.945(0.005)	0.953(0.005)	0.950(0.005)
	0.975	0.967(0.004)	0.970(0.002)	0.978(0.003)	0.977(0.005)	0.980(0.003)	0.977(0.003)
20	0.925	0.926(0.005)	0.921(0.004)	0.926(0.005)	0.926(0.006)	0.928(0.004)	0.925(0.005)
	0.95	0.954(0.005)	0.944(0.003)	0.948(0.004)	0.948(0.004)	0.951(0.005)	0.943(0.005)
	0.975	0.978(0.001)	0.975(0.004)	0.977(0.005)	0.975(0.004)	0.978(0.003)	0.975(0.003)

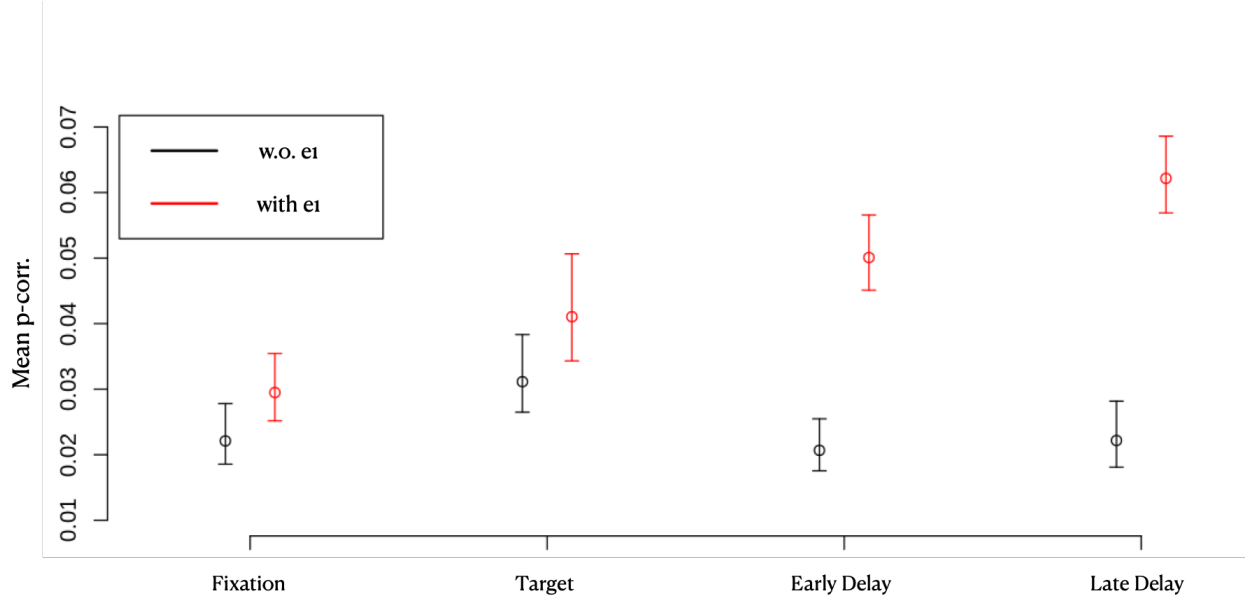


Figure B.1: Inference on the mean partial correlations over the two edge sets: (red) the cross-areas edges with electrode e_1 , marked in Fig. 6 and (black) the other cross-areas edges. The points are the median values of the bootstrap samples obtained by Algorithm 1 with 100,000 bootstrap samples, and the error bars are the 95 % bootstrap confidence intervals.

B Supplementary results for experimental data analysis

Figure B.1 presents the confidence intervals for the mean partial correlations over the two edge sets in the four experimental stages. The mean spatial partial correlation over the edges with electrode e_1 was shown to be significantly monotonic increasing by the linear trend test ($p < 1e-6$).

Figure B.2 presents the confidence intervals for the mean partial correlations within region V4 in the four experimental stages. The mean spatial partial correlation within V4 was shown to be significantly monotonic decreasing by the linear trend test ($p < 1e-6$).

The cross-area connectivity trend was further evidenced by the c -level testing. Our simultaneous testing approach of multiple edges can also be extended to c -level tests (Qiu and Zhou, 2020). By testing if $\|\rho_{E_2}\|_\infty$ exceeds threshold level c , i.e.,

$$H_{0,c} : \|\rho_{E_2}\|_\infty \leq c$$

we compared the cross-area connectivity strengths in the four stages. Table B.1 shows the test results at four levels $c = 0, 0.02, 0.03, 0.04$. At $c = 0$, the cross-area connectivity in E_1 was significant with $\alpha = 0.05$ at all experimental stages. As the level increased, the tests at the early stages began unrejected. At $c = 0.04$, the test was significant only at the late delay stage. These results are consistent with our finding in Fig. 7 and the subsequent linear trend test.

Table B.1: The c -level test results for $\|\hat{\rho}_{E_2}\|_\infty$ at c -levels $\{0, 0.02, 0.03, 0.04\}$. Entries with * represent the significance at $\alpha = 0.05$.

c -level	Fixation	Cue	Early Delay	Late Delay
0	*	*	*	*
0.02		*	*	*
0.03			*	*
0.04				*

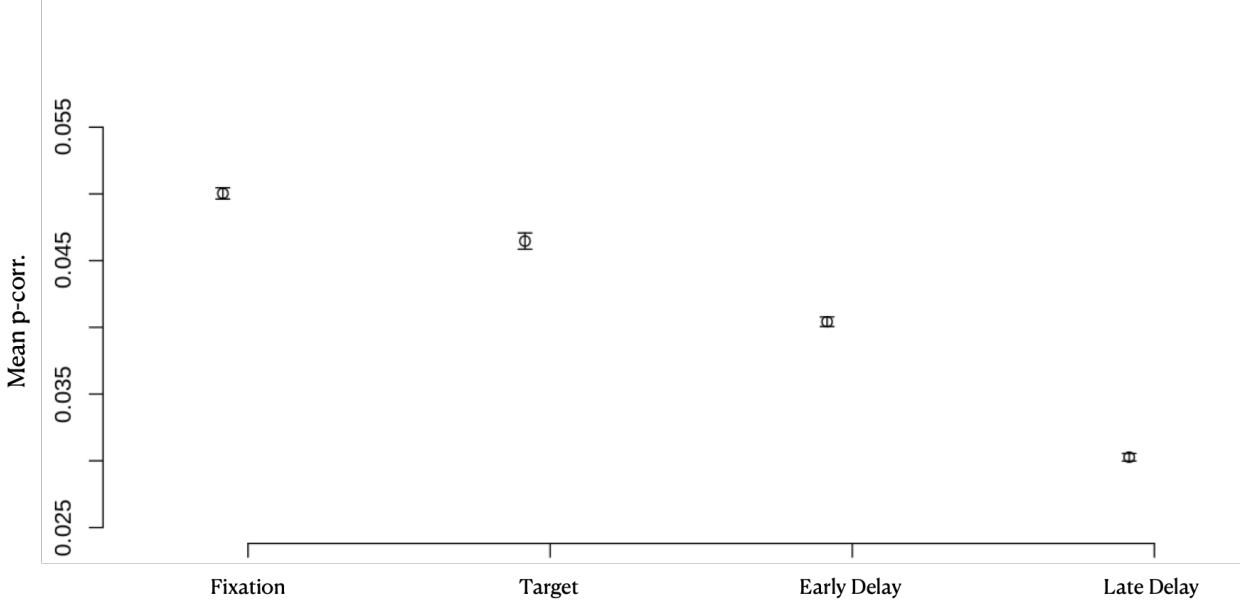


Figure B.2: Inference on the mean partial correlations within V4. The points are the median values of the bootstrap samples obtained by Algorithm 1 with 100,000 bootstrap samples, and the error bars are the 95 % bootstrap confidence intervals.

C Proofs

Throughout the following theoretical arguments, we use $X^{(S,l)}$ (or $X^{(T,l)}$) to notate stacked spatial (or temporal) observation over temporal (or spatial) components and samples within session l :

$$X^{(S,l)} = \left[X^{(1,l)\top}, \dots, X^{(n_l,l)\top} \right]^\top \in \mathbb{R}^{n_l p \times q}$$

$$X^{(T,l)} = \left[X^{(1,l)}, \dots, X^{(n_l,l)} \right]^\top \in \mathbb{R}^{n_l q \times p}.$$

These notations help us with connecting matrix-variate Gaussian graphical models to node-wise regression models:

$$X_{ti}^{(S,l)} = X_{t,\cdot}^{(S,l)} \beta_{\cdot,i}^{(S,l)} + \epsilon_{ti}^{(S,l)}$$

for $t = 1, \dots, n_l p$ where $X_t^{(S,l)}$ are now dependent and not identically distributed due to the temporal association, unlike the usual regression regime. Also, for any vector $b^{(\cdot)} := \{b^{(l)} \in \mathbb{R}^p\}_{l=1, \dots, m}$, we use $\underline{b}^{(\cdot)}$ to denote the collection of standardized elements, i.e.,

$$\underline{b}_j^{(\cdot)} := \left\{ \frac{\|X_{\cdot,j}^{(S,l)}\|_2}{\sqrt{n_l p}} b_j^{(l)} \right\}_{l=1, \dots, m}$$

so that Eq. (2) is expressed in a more canonical form:

$$\hat{\beta}_{\cdot,i}^{(S,\cdot)} := \operatorname{argmin}_{\{b^{(l)}\}_{l=1, \dots, m}} \left\{ \frac{1}{2n_0 p} \sum_{l=1}^m \|X_{\cdot,i}^{(S,l)} - X^{(S,l)} b^{(l)}\|_2^2 + \gamma_i \sum_{j:j \neq i} \|\underline{b}_j^{(\cdot)}\|_2 \right\}, \quad (15)$$

with respect to $b_i^{(l)} = 0$ for all l . In the following proofs, for a real matrix M , we use $\|M\|_{\text{op}}$ and $\|M\|_2$ interchangeably to denote the matrix 2-norm, also known as the operator norm.

C.1 Preliminary Lemmas

Here we introduce several lemmas that will help us prove propositions and theorems later. To apply the classical techniques and results in penalized regression analyses, we need to address the dependency among $X_t^{(S,l)}$'s. To do so,

we use the fact that, for $k = 1, \dots, n_l$,

$$\sum_{t=1}^p X_t^{(k,l)} X_t^{(k,l)\top} = \sum_{t=1}^p \lambda_t^{(\mathcal{T},l)} W_t^{(k,l)} W_t^{(k,l)\top} \quad (16)$$

where $W_t^{(k,l)} \stackrel{\text{i.i.d.}}{\sim} N(0, \Sigma^{(S,l)})$ for all $t = 1, \dots, p$. We further let $\xi_{ti}^{(k,l)} = W_{ti}^{(k,l)} - W_{t,\cdot}^{(k,l)} \beta_{\cdot,i}^{(S,l)}$ so that

$$\begin{aligned} \sum_{t=1}^p \epsilon_t^{(S,k,l)} X_t^{(k,l)\top} &= \sum_{t=1}^p \lambda_t^{(\mathcal{T},l)} \xi_t^{(k,l)} W_t^{(k,l)\top}, \\ \sum_{t=1}^p \epsilon_t^{(S,k,l)} \epsilon_t^{(S,k,l)\top} &= \sum_{t=1}^p \lambda_t^{(\mathcal{T},l)} \xi_t^{(k,l)} \xi_t^{(k,l)\top}, \end{aligned} \quad (17)$$

and $\xi_t^{(k,l)} \stackrel{\text{i.i.d.}}{\sim} N(0, \Phi^{(S,l)})$ across $t = 1, \dots, p$ and $k = 1, \dots, n_l$.

The subsequent lemmas follow the application to the above equations of sub-exponential concentration inequalities, which could be found in mathematical statistics literature such as Vershynin (2018). The proofs for the lemmas are given in Sections D.1 to D.4.

Lemma C.1.

$$\mathbb{P} \left[\left\| \frac{1}{n_l p} X^{(S,l)\top} X^{(S,l)} - \Sigma^{(S,l)} \right\|_{\infty} \geq C(\kappa_3) \sqrt{\frac{\nu}{n_l p}} \right] \leq q e^{-\nu}$$

for $0 \leq \frac{\nu}{n_l p} \leq C(\kappa_3)$.

Lemma C.2.

$$\mathbb{P} \left[\frac{1}{n_0 p} \left[\sum_{l=1}^m \left(\frac{\sqrt{n_l p}}{\|X_{\cdot,j}^{(S,l)}\|_2} \epsilon_{\cdot,i}^{(S,l)\top} X_{\cdot,j}^{(S,l)} \right)^2 \right]^{1/2} \geq C(\kappa_1, \kappa_3) \sqrt{\frac{m+\nu}{n_0 p}} \right] \leq e^{-\nu}.$$

and

$$\mathbb{P} \left[\frac{1}{n_0 p} \left[\sum_{l=1}^m \left(\frac{\sqrt{n_l p}}{\|X_{\cdot,i}^{(S,l)}\|_2} \epsilon_{\cdot,i}^{(S,l)\top} X^{(S,l)} \beta_{\cdot,i}^{(S,l)} \right)^2 \right]^{1/2} \geq C(\kappa_1, \kappa_3) \sqrt{\frac{m+\nu}{n_0 p}} \right] \leq e^{-\nu}.$$

Lemma C.3.

$$\mathbb{P} \left[\max_{i,j:j \neq i} \left| \frac{1}{n_l p} \epsilon_{\cdot,i}^{(S,l)\top} X_{\cdot,j}^{(S,l)} \right| \geq C(\kappa_3) \sqrt{\frac{\nu}{n_l p}} \right] \leq q e^{-\nu},$$

and

$$\mathbb{P} \left[\max_{i=1,\dots,q} \left| \frac{1}{n_l p} \epsilon_{\cdot,i}^{(S,l)\top} X^{(S,l)} \beta_{\cdot,i}^{(S,l)} \right| \geq C(\kappa_3) \sqrt{\frac{\nu}{n_l p}} \right] \leq q e^{-\nu}$$

for $0 \leq \frac{\nu}{n_0 p} \leq C(\kappa_3)$.

Lemma C.4.

$$\mathbb{P} \left[\left\| \frac{1}{n_l p} \epsilon^{(S,l)\top} \epsilon^{(S,l)} - \Phi^{(S,l)} \right\|_{\infty} \geq C(\kappa_3) \sqrt{\frac{\nu}{n_l p}} \right] \leq q e^{-\nu}$$

for $0 \leq \frac{\nu}{n_0 p} \leq C(\kappa_3)$.

C.2 Non-asymptotic error bound for the temporal covariance matrix estimate

In this section, we present the estimation error bounds for the session-specific temporal covariance and precision matrices obtained in Section 3.3. While results for i.i.d. samples are available in Liu and Ren (2020), no such results exist for the correlated samples considered in our model. Therefore, we provide a self-contained analysis, which may be of independent interest. The proof is detailed in Section C.8.

Proposition C.5. *Suppose that $h_l = \lfloor (n_l q)^{1/(1+\alpha_0)} \rfloor$. Then, following the procedure defined in Section 3.3,*

$$\begin{aligned} \mathbb{P} \left[\max_l \max_{1 \leq t \leq p} \|\widehat{\beta}_{\cdot,t}^{(\mathcal{T},l)} - \beta_{\cdot,t}^{(\mathcal{T},l)}\|_2 \geq C(\kappa_1, \kappa_3, \kappa_5) \sqrt{\frac{\log(mn_0 p q)}{(n_0 q)^{1-1/(2\alpha_0+2)}}} \right] &\leq C(mn_0 p q)^{-1/2}, \\ \mathbb{P} \left[\max_l \max_{1 \leq t \leq p} \left| \widehat{\Phi}_{tt}^{(\mathcal{T},l)} - \frac{\text{tr}(\Sigma^{(S,l)})}{q} \Phi_{tt}^{(\mathcal{T},l)} \right| \geq C(\kappa_1, \kappa_3, \kappa_5) \sqrt{\frac{\log(mn_0 p q)}{(n_0 q)^{1-1/(2\alpha_0+2)}}} \right] &\leq C(mn_0 p q)^{-1/2}. \end{aligned}$$

Theorem C.6. Suppose that $h_l = \lfloor (n_l q)^{1/(1+\alpha_0)} \rfloor$ and $\eta = C(\kappa_3)$ satisfies $\eta \leq \lambda_1(I - \beta^{(\mathcal{T}, l)})$ for $l = 1, \dots, m$, where $\lambda_1(I - \beta^{(\mathcal{T}, l)})$ is the smallest eigenvalue of $I - \beta^{(\mathcal{T}, l)}$. Then,

$$\mathbb{P} \left[\begin{array}{l} \max_l \frac{1}{p} \left\| \bar{\Sigma}^{(\mathcal{T}, l)} - \frac{\text{tr}(\Sigma^{(S, l)})}{q} \Sigma^{(\mathcal{T}, l)} \right\|_F^2 \geq C(\kappa_1, \kappa_3, \kappa_5) \frac{\log(mn_0pq)}{(n_0q)^{1-1/(2\alpha_0+2)}}, \\ \max_l \frac{1}{p} \left\| \bar{\Omega}^{(\mathcal{T}, l)} - \frac{q}{\text{tr}(\Sigma^{(S, l)})} \Omega^{(\mathcal{T}, l)} \right\|_F^2 \geq C(\kappa_1, \kappa_3, \kappa_5) \frac{\log(mn_0pq)}{(n_0q)^{1-1/(2\alpha_0+2)}} \end{array} \right] \leq C(mn_0pq)^{-1/2}.$$

Consequently, the Frobenius norms of $\Sigma^{(\mathcal{T}, l)}$ can be consistently estimated, which is sufficient for our main result Theorem 4.3. The proof is given in Section C.9.

Corollary C.7. Suppose that $h_l = \lfloor (n_l q)^{1/(1+\alpha_0)} \rfloor$ and $\eta = C(\kappa_3)$ satisfies $\eta \leq \lambda_1(I - \beta^{(\mathcal{T}, l)})$ for $l = 1, \dots, m$. Then,

$$\mathbb{P} \left[\max_l \left| \frac{\|\widehat{\Sigma}^{(\mathcal{T}, l)}\|_F^2 - \|\Sigma^{(\mathcal{T}, l)}\|_F^2}{p} \right| \geq C(\kappa_1, \kappa_3, \kappa_5) \frac{\log(mn_0pq)}{(n_0q)^{1-1/(2\alpha_0+2)}} \right] \leq C(mn_0pq)^{-1/2}$$

for sufficiently large n_0 .

C.3 Proof of Theorem 4.1

Based on the optimality of the group Lasso estimate in Eq. (15), we have the following basic inequality:

$$\begin{aligned} & \frac{1}{2n_0p} \sum_{l=1}^m \left(\|X_{\cdot, i}^{(S, l)} - X^{(S, l)} \widehat{\beta}_{\cdot, i}^{(S, l)}\|_2^2 - \|X_{\cdot, i}^{(S, l)} - X^{(S, l)} \beta_{\cdot, i}^{(S, l)}\|_2^2 \right) \\ & \leq \gamma_i \sum_{j: j \neq i} \left(\left\| \underline{\beta}_{\cdot, j}^{(S, \cdot)} \right\|_2 - \left\| \widehat{\underline{\beta}}_{\cdot, j}^{(S, \cdot)} \right\|_2 \right) \end{aligned} \quad (18)$$

for every $i = 1, \dots, q$. For the left hand side, by decomposing $\widehat{\beta}_{\cdot, i}^{(S, l)} = \Delta_{\cdot, i}^{(S, l)} + \beta_{\cdot, i}^{(S, l)}$,

$$\begin{aligned} & \frac{1}{2n_0p} \sum_{l=1}^m \left(\|X_{\cdot, i}^{(S, l)} - X^{(S, l)} \widehat{\beta}_{\cdot, i}^{(S, l)}\|_2^2 - \|X_{\cdot, i}^{(S, l)} - X^{(S, l)} \beta_{\cdot, i}^{(S, l)}\|_2^2 \right) \\ & = \frac{1}{2n_0p} \sum_{l=1}^m \left(\|X^{(S, l)} \Delta_{\cdot, i}^{(S, l)}\|_2^2 - 2(X^{(S, l)} \Delta_{\cdot, i}^{(S, l)})^\top \epsilon_{\cdot, i}^{(S, l)} \right). \end{aligned} \quad (19)$$

For the first term,

$$\begin{aligned} & \frac{1}{2n_0p} \sum_{l=1}^m \|X^{(S, l)} \Delta_{\cdot, i}^{(S, l)}\|_2^2 \\ & = \frac{1}{2n_0p} \sum_{l=1}^m \Delta_{\cdot, i}^{(S, l)\top} X^{(S, l)\top} X^{(S, l)} \Delta_{\cdot, i}^{(S, l)} \\ & = \sum_{l=1}^m \frac{2n_l p}{2n_0 p} \left[\Delta_{\cdot, i}^{(S, l)\top} \Sigma^{(S, l)} \Delta_{\cdot, i}^{(S, l)} + \Delta_{\cdot, i}^{(S, l)\top} \left\{ \frac{X^{(S, l)\top} X^{(S, l)}}{2n_l p} - \Sigma^{(S, l)} \right\} \Delta_{\cdot, i}^{(S, l)} \right] \\ & \geq \frac{1}{\kappa_3} \sum_{l=1}^m \|\Delta_{\cdot, i}^{(S, l)}\|_2^2 - \frac{\kappa_1}{\kappa_3} \sum_{l=1}^m \Delta_{\cdot, i}^{(S, l)\top} \left\{ \frac{X^{(S, l)\top} X^{(S, l)}}{2n_l p} - \Sigma^{(S, l)} \right\} \Delta_{\cdot, i}^{(S, l)} \end{aligned}$$

where the last inequality resorts to ?? 1?? 3. To provide a further lower-bound, we use the fact based on Theorem C.1 that

$$\frac{1}{\kappa_3} \sum_{l=1}^m \|\Delta_{\cdot, i}^{(S, l)}\|_2^2 \geq C(\kappa_3) \sum_{j: j \neq i} \|\Delta_{\cdot, j}^{(S, \cdot)}\|_2^2$$

and

$$\begin{aligned}
& \sum_{l=1}^m \Delta_{\cdot,i}^{(S,l)\top} \left\{ \frac{X^{(S,l)\top} X^{(S,l)}}{2n_l p} - \Sigma^{(S,l)} \right\} \Delta_{\cdot,i}^{(S,l)} \\
& \leq \sum_{l=1}^m \sum_{j_1, j_2} \Delta_{j_1 i}^{(S,l)} \left\{ \frac{X_{\cdot, j_1}^{(S,l)\top} X_{\cdot, j_2}^{(S,l)}}{2n_l p} - \Sigma_{j_1 j_2}^{(S,l)} \right\} \Delta_{j_2 i}^{(S,l)} \\
& \leq \sum_{j_1, j_2} \left\| \Delta_{j_1 i}^{(S,\cdot)} \right\|_2 \max_l \left| \frac{X_{\cdot, j_1}^{(S,l)\top} X_{\cdot, j_2}^{(S,l)}}{2n_l p} - \Sigma_{j_1 j_2}^{(S,l)} \right| \left\| \Delta_{j_2 i}^{(S,\cdot)} \right\|_2 \\
& \leq \max_l \left| \frac{X_{\cdot, j_1}^{(S,l)\top} X_{\cdot, j_2}^{(S,l)}}{2n_l p} - \Sigma_{j_1 j_2}^{(S,l)} \right| \left(\sum_j \left\| \Delta_{j i}^{(S,\cdot)} \right\|_2 \right)^2 \\
& \leq C(\kappa_3) \sqrt{\frac{\log(mn_0 p q)}{n_l p}} \left(\sum_{j:j \neq i} \left\| \Delta_{j i}^{(S,\cdot)} \right\|_2 \right)^2
\end{aligned} \tag{20}$$

uniformly over $i = 1, \dots, q$ with probability at least $1 - (mn_0 p q)^{-1/2}$. For the second term,

$$\begin{aligned}
& \frac{1}{n_0 p} \left| \sum_{l=1}^m (X^{(S,l)} \Delta_{\cdot,i}^{(S,l)})^\top \epsilon_{\cdot,i}^{(S,l)} \right| = \frac{1}{n_0 p} \sum_{j:j \neq i} \left| \sum_{l=1}^m (\epsilon_{\cdot,i}^{(S,l)\top} X_{\cdot,j}^{(S,l)}) \Delta_{j i}^{(S,l)} \right| \\
& \leq \frac{1}{n_0 p} \sum_{j:j \neq i} \left\| \left\{ \frac{\sqrt{n_l p}}{\|X_{\cdot,j}^{(S,l)}\|_2} \epsilon_{\cdot,i}^{(S,l)\top} X_{\cdot,j}^{(S,l)} \right\}_{l=1,\dots,m} \right\|_2 \left\| \Delta_{j i}^{(S,\cdot)} \right\|_2 \\
& \leq \frac{1}{n_0 p} \max_{j:j \neq i} \left\| \left\{ \frac{\sqrt{n_l p}}{\|X_{\cdot,j}^{(S,l)}\|_2} \epsilon_{\cdot,i}^{(S,l)\top} X_{\cdot,j}^{(S,l)} \right\}_{l=1,\dots,m} \right\|_2 \sum_{j:j \neq i} \left\| \Delta_{j i}^{(S,\cdot)} \right\|_2 \\
& \leq C(\kappa_1, \kappa_3) \sqrt{\frac{m + \log(mn_0 p q)}{n_0 p}} \sum_{j:j \neq i} \left\| \Delta_{j i}^{(S,\cdot)} \right\|_2
\end{aligned} \tag{21}$$

uniformly over $i = 1, \dots, q$ with probability at least $1 - (mn_0 p q)^{-1/2}$ where the first inequality is due to the Cauchy-Schwarz inequality, and the last inequality is due Theorem C.2. Suppose that $\gamma_i \asymp \sqrt{\frac{m + \log(mn_0 p q)}{n_0 p}}$ satisfies

$$\frac{1}{n_0 p} \left| \sum_{l=1}^m (X^{(S,l)} \Delta_{\cdot,i}^{(S,l)})^\top \epsilon_{\cdot,i}^{(S,l)} \right| \leq \frac{\gamma_i}{2} \sum_{j:j \neq i} \left\| \Delta_{j i}^{(S,\cdot)} \right\|_2.$$

For the right-hand side of Eq. (18),

$$\gamma_i \sum_{j:j \neq i} \left(\left\| \underline{\beta}_{j i}^{(S,\cdot)} \right\|_2 - \left\| \widehat{\beta}_{j i}^{(S,\cdot)} \right\|_2 \right) \leq \gamma_i \left(\sum_{j:\beta_{j i}^{(S,l)} \neq 0} \left\| \Delta_{j i}^{(S,\cdot)} \right\|_2 - \sum_{j:\beta_{j i}^{(S,l)} = 0} \left\| \Delta_{j i}^{(S,\cdot)} \right\|_2 \right). \tag{22}$$

On the one hand, because $\frac{1}{2n_0 p} \sum_{l=1}^m \|X^{(S,l)} \Delta_{\cdot,i}^{(S,l)}\|_2^2 \geq 0$ a.s.,

$$\begin{aligned}
& -\frac{\gamma_i}{2} \sum_{j:j \neq i} \left\| \Delta_{j i}^{(S,\cdot)} \right\|_2 \stackrel{(21)}{\leq} -\frac{1}{n_0 p} \left| \sum_{l=1}^m (X^{(S,l)} \Delta_{\cdot,i}^{(S,l)})^\top \epsilon_{\cdot,i}^{(S,l)} \right| \\
& \leq \frac{1}{2n_0 p} \sum_{l=1}^m \left(\|X^{(S,l)} \Delta_{\cdot,i}^{(S,l)}\|_2^2 - 2(X^{(S,l)} \Delta_{\cdot,i}^{(S,l)})^\top \epsilon_{\cdot,i}^{(S,l)} \right) \\
& \stackrel{(19)}{=} \frac{1}{2n_0 p} \sum_{l=1}^m \left(\|X_{\cdot,i}^{(S,l)} - X^{(S,l)} \widehat{\beta}_{\cdot,i}^{(S,l)}\|_2^2 - \|X_{\cdot,i}^{(S,l)} - X^{(S,l)} \beta_{\cdot,i}^{(S,l)}\|_2^2 \right) \\
& \stackrel{(18)}{\leq} \gamma_i \sum_{j:j \neq i} \left(\left\| \underline{\beta}_{j i}^{(S,\cdot)} \right\|_2 - \left\| \widehat{\beta}_{j i}^{(S,\cdot)} \right\|_2 \right) \stackrel{(22)}{\leq} \gamma_i \left(\sum_{j:\beta_{j i}^{(S,l)} \neq 0} \left\| \Delta_{j i}^{(S,\cdot)} \right\|_2 - \sum_{j:\beta_{j i}^{(S,l)} = 0} \left\| \Delta_{j i}^{(S,\cdot)} \right\|_2 \right)
\end{aligned} \tag{23}$$

uniformly over $i = 1, \dots, q$ with probability at least $1 - 2(mn_0pq)^{-1/2}$. Therefore

$$\sum_{j:\beta_{ji}^{(S,l)}=0} \left\| \underline{\Delta}_{ji}^{(S,\cdot)} \right\|_2 \leq 2 \sum_{j:\beta_{ji}^{(S,l)} \neq 0} \left\| \underline{\Delta}_{ji}^{(S,\cdot)} \right\|_2 \quad (24)$$

uniformly over $i = 1, \dots, q$ with the same probability. On the other hand, Eqs. (19) to (22) earn

$$\begin{aligned} & \gamma_i \left(\sum_{j:\beta_{ji}^{(S,l)} \neq 0} \left\| \underline{\Delta}_{ji}^{(S,\cdot)} \right\|_2 - \sum_{j:\beta_{ji}^{(S,l)}=0} \left\| \underline{\Delta}_{ji}^{(S,\cdot)} \right\|_2 \right) \\ & \stackrel{(22)}{\geq} \gamma_i \sum_{j:j \neq i} \left(\left\| \underline{\beta}_{-ji}^{(S,\cdot)} \right\|_2 - \left\| \widehat{\underline{\beta}}_{-ji}^{(S,\cdot)} \right\|_2 \right) \\ & \stackrel{(18)}{\geq} \frac{1}{2n_0p} \sum_{l=1}^m \left(\|X_{\cdot,i}^{(S,l)} - X^{(S,l)} \widehat{\beta}_{\cdot,i}^{(S,l)}\|_2^2 - \|X_{\cdot,i}^{(S,l)} - X^{(S,l)} \beta_{\cdot,i}^{(S,l)}\|_2^2 \right) \\ & \stackrel{(19)}{=} \frac{1}{2n_0p} \sum_{l=1}^m \left(\|X^{(S,l)} \underline{\Delta}_{\cdot,i}^{(S,l)}\|_2^2 - 2(X^{(S,l)} \underline{\Delta}_{\cdot,i}^{(S,l)})^\top \epsilon_{\cdot,i}^{(S,l)} \right) \\ & \stackrel{(20),(21)}{\geq} C(\kappa_3) \sum_{j:j \neq i} \left\| \underline{\Delta}_{ji}^{(S,\cdot)} \right\|_2^2 - C(\kappa_1, \kappa_3) \sqrt{\frac{\log(mn_0pq)}{n_0p}} \left(\sum_{j:j \neq i} \left\| \underline{\Delta}_{ji}^{(S,\cdot)} \right\|_2 \right)^2 \\ & \quad - \gamma_i \left\| \underline{\Delta}_{ji}^{(S,\cdot)} \right\|_2 \end{aligned} \quad (25)$$

uniformly over $i = 1, \dots, d$ with probability at least $1 - 2(mn_0pq)^{-1/2}$. Because

$$\left(\sum_{j:j \neq i} \left\| \underline{\Delta}_{ji}^{(S,\cdot)} \right\|_2 \right)^2 \stackrel{(24)}{\leq} 2 \left(\sum_{j:\beta_{ji}^{(S,l)} \neq 0} \left\| \underline{\Delta}_{ji}^{(S,\cdot)} \right\|_2 \right)^2 \leq 2d \sum_{j:\beta_{ji}^{(S,l)} \neq 0} \left\| \underline{\Delta}_{ji}^{(S,\cdot)} \right\|_2^2$$

with probability at least $1 - 2(mn_0pq)^{-1/2}$, Eq. (25) implies that

$$\begin{aligned} & \gamma_i \left(\sum_{j:\beta_{ji}^{(S,l)} \neq 0} \left\| \underline{\Delta}_{ji}^{(S,\cdot)} \right\|_2 - \sum_{j:\beta_{ji}^{(S,l)}=0} \left\| \underline{\Delta}_{ji}^{(S,\cdot)} \right\|_2 \right) \\ & \geq \left(C(\kappa_3) - C(\kappa_1, \kappa_3) d \sqrt{\frac{\log(mn_0pq)}{n_0p}} \right) \sum_{j:j \neq i} \left\| \underline{\Delta}_{ji}^{(S,\cdot)} \right\|_2^2 - \gamma_i \left\| \underline{\Delta}_{ji}^{(S,\cdot)} \right\|_2 \end{aligned}$$

uniformly over $i = 1, \dots, d$ with the same probability. As a result, with a sufficiently large n_0 and the same probability, because $d \sqrt{\frac{\log(mn_0pq)}{n_0p}} \rightarrow 0$ as $n_0 \rightarrow \infty$ due to Axiom 4,

$$\begin{aligned} & C(\kappa_3) \sum_{j:j \neq i} \left\| \underline{\Delta}_{ji}^{(S,\cdot)} \right\|_2^2 \\ & \leq \gamma_i \left(\sum_{j:\beta_{ji}^{(S,l)} \neq 0} \left\| \underline{\Delta}_{ji}^{(S,\cdot)} \right\|_2 - \sum_{j:\beta_{ji}^{(S,l)}=0} \left\| \underline{\Delta}_{ji}^{(S,\cdot)} \right\|_2 \right) + \gamma_i \sum_{j:j \neq i} \left\| \underline{\Delta}_{ji}^{(S,\cdot)} \right\|_2 \\ & \leq C(\kappa_1, \kappa_3) \sqrt{\frac{m + \log(mn_0pq)}{n_0p}} \sum_{j:j \neq i} \left\| \underline{\Delta}_{ji}^{(S,\cdot)} \right\|_2 \\ & \leq C(\kappa_1, \kappa_3) \sqrt{d \frac{m + \log(mn_0pq)}{n_0p}} \sqrt{\sum_{j:j \neq i} \left\| \underline{\Delta}_{ji}^{(S,\cdot)} \right\|_2^2}, \end{aligned}$$

uniformly over $i = 1, \dots, d$, and

$$\max_i \sum_{j:j \neq i} \left\| \underline{\Delta}_{ji}^{(S,\cdot)} \right\|_2^2 \leq C(\kappa_1, \kappa_3) d \frac{m + \log(mn_0pq)}{n_0p}.$$

In addition, due to Eq. (24), under the same event,

$$\begin{aligned} \max_i \sum_{j:j \neq i} \left\| \underline{\Delta}_{ji}^{(S,\cdot)} \right\|_2 &\leq C \max_i \sum_{j:\beta_{ji} \neq 0} \left\| \underline{\Delta}_{ji}^{(S,\cdot)} \right\|_2 \\ &\leq C\sqrt{d} \max_i \sqrt{\sum_{j:j \neq i} \left\| \underline{\Delta}_{ji}^{(S,\cdot)} \right\|_2^2} \leq C(\kappa_1, \kappa_3) d \sqrt{\frac{m + \log(mn_0pq)}{n_0p}}. \end{aligned}$$

Last, it follows Eqs. (18) and (19) that

$$\begin{aligned} &\max_i \frac{1}{2n_0p} \sum_{l=1}^m \left\| X^{(S,l)} \underline{\Delta}_{\cdot,i}^{(S,l)} \right\|_2^2 \\ &\leq \max_i \left[\gamma_i \sum_{j:j \neq i} \left(\left\| \underline{\beta}_{ji}^{(S,\cdot)} \right\|_2 - \left\| \widehat{\underline{\beta}}_{ji}^{(S,\cdot)} \right\|_2 \right) + \frac{1}{n_0p} \sum_{l=1}^m (X^{(S,l)} \underline{\Delta}_{\cdot,i}^{(S,l)})^\top \epsilon_{\cdot,i}^{(S,l)} \right] \\ &\leq \max_i \left[\gamma_i \sum_{j:j \neq i} \left\| \underline{\Delta}_{ji}^{(S,\cdot)} \right\|_2 + C(\kappa_1, \kappa_3) \sqrt{\frac{m + \log(mn_0pq)}{n_0p}} \sum_{j:j \neq i} \left\| \underline{\Delta}_{ji}^{(S,\cdot)} \right\|_2 \right] \\ &\leq C(\kappa_1, \kappa_3) d \frac{m + \log(mn_0pq)}{n_0p} \end{aligned}$$

under the same event.

C.4 Proof of Proposition 4.2

Let $O_{ij}^{(S,l)}$ be the error of $\widehat{\rho}_{ij}^{(S,l)}$ not governed by $\Theta_{ij}^{(S,l)}$. That is, $O_{ij}^{(S,l)} := \widehat{\rho}_{ij}^{(S,l)} - \rho_{ij}^{(S,l)} - \Theta_{ij}^{(S,l)}$. In the following lemma, we prove that $O_{ij}^{(S,l)}$ vanishes asymptotically. We provide the proof in Section D.5.

Lemma C.8. *Suppose that $\widehat{\rho}^{(S,l)}$ is estimated based on γ_i 's given as in Theorem 4.1. Then, under ?? 1–5,*

$$\mathbb{P} \left[\max_{i,j:i \neq j} \sum_{l=1}^m \left| O_{ij}^{(S,l)} \right| \geq C(\kappa_1, \kappa_3) d \frac{m + \log(mn_0pq)}{n_0p} \right] \leq C(mn_0pq)^{-1/2},$$

for a sufficiently large n_0 .

Let $\Theta_E = \frac{1}{\sqrt{m}} \sum_{l=1}^m \sqrt{n_l p} \Theta_E^{(S,l)}$, and $O_E = \frac{1}{\sqrt{m}} \sum_{l=1}^m \sqrt{n_l p} O_E^{(S,l)}$, where $\Theta_E^{(S,l)}$ and $O_E^{(S,l)}$ are the collections of $\Theta_{ij}^{(S,l)}$ and $O_{ij}^{(S,l)}$ for $(i, j) \in E$, respectively. For any $x > 0$ and $\delta > 0$,

$$\begin{aligned} \mathbb{P}[\|\widehat{T}_E - T_E\|_\infty > x] &\leq \mathbb{P}[\|\Theta_E\|_\infty > x - \delta] + \mathbb{P}[\|O_E\|_\infty > \delta] \\ &\leq \mathbb{P}[\|Z\|_\infty > x - \delta] + KS_\infty(\Theta_E, Z) + \mathbb{P}[\|O_E\|_\infty > \delta] \\ &= \mathbb{P}[\|Z\|_\infty > x] + \mathbb{P}[x \geq \|Z\|_\infty > x - \delta] + KS_\infty(\Theta_E, Z) + \mathbb{P}[\|O_E\|_\infty > \delta], \end{aligned}$$

where $KS_\infty(\Theta_E, Z) := \sup_{x>0} |\mathbb{P}[\|\Theta_E\|_\infty > x] - \mathbb{P}[\|Z\|_\infty > x]|$ is the Kolmogorov-Smirnov distance between $\|\Theta_E\|_\infty$ and $\|Z\|_\infty$. Similarly,

$$\begin{aligned} \mathbb{P}[\|\widehat{T}_E - T_E\|_\infty > x] &\geq \mathbb{P}[\|\Theta_E\|_\infty > x + \delta] - \mathbb{P}[\|O_E\|_\infty > \delta] \\ &\geq \mathbb{P}[\|Z\|_\infty > x + \delta] - KS_\infty(\Theta_E, Z) - \mathbb{P}[\|O_E\|_\infty > \delta] \\ &= \mathbb{P}[\|Z\|_\infty > x] - \mathbb{P}[x + \delta \geq \|Z\|_\infty > x] - KS_\infty(\Theta_E, Z) - \mathbb{P}[\|O_E\|_\infty > \delta]. \end{aligned}$$

Therefore we conclude that

$$\begin{aligned} &\sup_{x>0} \left| \mathbb{P}[\|\widehat{T}_E - T_E\|_\infty > x] - \mathbb{P}[\|Z\|_\infty > x] \right| \\ &\leq KS_\infty(\Theta_E, Z) + \sup_{x>0} \mathbb{P}[x + \delta \geq \|Z\|_\infty \geq x - \delta] + \mathbb{P}[\|O_E\|_\infty > \delta]. \end{aligned}$$

We use the anti-concentration inequality of the supremum norm of Gaussian random vectors with mean zero (Corollary 1, Chernozhukov et al., 2015) and the fact that

$$S_{(i,j),(i,j)} = \frac{1}{m} \sum_{l=1}^m \frac{\|\Sigma^{(\mathcal{T},l)}\|_F^2}{p} (1 - \rho_{ij}^{(S,l)2})^2 \geq C(\kappa_3)$$

to control the second term:

$$\sup_{x>0} \mathbb{P}[x + \delta \geq \|Z\|_\infty \geq x - \delta] \leq C(\kappa_3) \delta \sqrt{\log|E|}. \quad (26)$$

Setting $\delta = C(\kappa_1, \kappa_3) d \frac{m+\log(qmnp)}{\sqrt{mnp}}$, which converges to 0 as $n \rightarrow \infty$ due to Axiom 4, Theorem C.8 provides an upperbound over the size of the last term.

Now it suffices to derive a probabilistic upperbound for $KS_\infty(\Theta_E, Z)$. We recall that each element of Θ_E is

$$\begin{aligned} \Theta_{ij} &= \frac{1}{\sqrt{m}} \sum_{l=1}^m \sqrt{n_l p} \Theta_{ij}^{(S,l)} \\ &= \frac{1}{\sqrt{m}} \sum_{l=1}^m \sqrt{n_l p} \left(\frac{\tilde{\phi}_{ij}^{(S,l)}}{\sqrt{\Phi_{ii}^{(S,l)} \Phi_{jj}^{(S,l)}}} - \frac{\Phi_{ij}^{(S,l)} \tilde{\phi}_{jj}^{(S,l)}}{2\Phi_{jj}^{(S,l)} \sqrt{\Phi_{ii}^{(S,l)} \Phi_{jj}^{(S,l)}}} - \frac{\Phi_{ij}^{(S,l)} \tilde{\phi}_{ii}^{(S,l)}}{2\Phi_{ii}^{(S,l)} \sqrt{\Phi_{ii}^{(S,l)} \Phi_{jj}^{(S,l)}}} \right), \end{aligned}$$

where $\tilde{\phi}_{ij}^{(S,l)} := \frac{1}{n_l p} \sum_{k=1}^{n_l} \sum_{t=1}^p \epsilon_{ti}^{(S,k,l)\top} \epsilon_{tj}^{(S,k,l)} - \Phi_{ij}^{(S,l)}$. We notice that $\epsilon_{ti}^{(S,k,l)}, \epsilon_{tj}^{(S,k,l)}$ are not independent across $t = 1, \dots, p$ due to the temporal association, while the state-of-the-art theory of high-dimensional CLT elaborates only over independent random vectors yet. We use Eq. (17) to convert $\phi^{(S,l)}$ into a summation of independent random variables:

$$\tilde{\phi}_{ij}^{(S,l)} = \frac{1}{n_l p} \sum_{k=1}^{n_l} \sum_{t=1}^p \lambda_t^{(\mathcal{T},l)} \xi_{ti}^{(k,l)} \xi_{tj}^{(k,l)} - \Phi_{ij}^{(S,l)} = \frac{1}{n_l p} \sum_{k=1}^{n_l} \sum_{t=1}^p \lambda_t^{(\mathcal{T},l)} \left(\xi_{ti}^{(k,l)} \xi_{tj}^{(k,l)} - \Phi_{ij}^{(S,l)} \right),$$

where $\xi_t^{(k,l)} \stackrel{\text{i.i.d.}}{\sim} \mathcal{N}(0, \Phi^{(S,l)})$, and the last equation holds based on $\text{tr}(\Sigma^{(\mathcal{T},l)}) = 1$. Then, we rewrite

$$\Theta_{ij} = \frac{1}{\sqrt{Np}} \sum_{l=1}^m \sum_{k=1}^{n_l} \sum_{t=1}^p \theta_{t,ij}^{(k,l)},$$

where $N = \sum_{l=1}^m n_l$, and

$$\theta_{t,ij}^{(k,l)} := \lambda_t^{(\mathcal{T},l)} \sqrt{\frac{N}{n_l m}} \left(\frac{\xi_{t,i}^{(k,l)} \xi_{t,j}^{(k,l)} - \Phi_{ij}^{(S,l)}}{\sqrt{\Phi_{ii}^{(S,l)} \Phi_{jj}^{(S,l)}}} - \frac{\Phi_{ij}^{(S,l)} (\xi_{t,j}^{(k,l)2} - \Phi_{jj}^{(S,l)})}{2\Phi_{jj}^{(S,l)} \sqrt{\Phi_{ii}^{(S,l)} \Phi_{jj}^{(S,l)}}} - \frac{\Phi_{ij}^{(S,l)} (\xi_{t,i}^{(k,l)2} - \Phi_{ii}^{(S,l)})}{2\Phi_{ii}^{(S,l)} \sqrt{\Phi_{ii}^{(S,l)} \Phi_{jj}^{(S,l)}}} \right).$$

For fixed i and j , because $\xi_{ti}^{(k,l)}$ and $\xi_{tj}^{(k,l)}$ are Gaussian random variables independent across l, k , and t , $\theta_{t,ij}^{(k,l)}$'s are independent sub-exponential random variable across l, k , and t . Due to Axiom 3, $\theta_{t,ij}^{(k,l)}$'s has uniformly bounded ψ_1 -Orlicz norms (see Section D.7 for the definition of the Orlicz norm). That is,

$$\max_{k,l,t,(i,j) \in E} \left\| \frac{\theta_{t,ij}^{(k,l)}}{\sqrt{\text{Var}[\theta_{t,ij}^{(k,l)}]}} \right\|_{\psi_1} \leq C(\kappa_1, \kappa_3).$$

This automatically satisfies Condition (M) in Chernozhukov et al. (2023). Although Condition (E.2), requiring bounded ψ_2 -Orlicz norm, is not satisfied, the proof of Corollary 2.1 under Conditions (M) and (E.2) is easily modified under bounded ψ_2 -Orlicz norms. Based on the facts that

$$\begin{aligned} &\left(\mathbb{E} \left[\max_{k,l,t,(i,j) \in E} \left| \frac{\theta_{t,ij}^{(k,l)}}{\sqrt{\text{Var}[\theta_{t,ij}^{(k,l)}]}} \right|^4 \right] \right)^{1/4} \leq C(\kappa_1, \kappa_3) \log(|E| m n_0 p), \\ &\mathbb{P} \left[\max_{(i,j) \in E} \left\| \frac{\theta_{t,ij}^{(k,l)}}{\sqrt{\text{Var}[\theta_{t,ij}^{(k,l)}]}} \right\|_\infty > C B_n \log(dn) \right] \leq C, \end{aligned}$$

Theorem 2.2 in Chernozhukov et al. (2023) implies

$$KS_\infty(\Theta_E, Z) \leq \frac{C(\kappa_1, \kappa_3)}{\sqrt{mnp}} \max \left\{ (\log|E|)^2 \log(mnp), (\log|E|)^{5/2} \right\}.$$

Alongside the results in Theorem C.8 and Eq. (26), it obtains the desired result.

C.5 Proof of Theorem 4.3

We denote the conditional Kolmogorov-Smirnov distance between $\|\widehat{Z}\|_\infty$ and $\|Z\|_\infty$ given observed data \mathcal{D} by $KS_\infty(\widehat{Z}, Z|\mathcal{D})$.

$$KS_\infty(\widehat{Z}, Z|\mathcal{D}) := \sup_{x>0} |\mathbb{P}[\|\widehat{Z}\|_\infty > x|\mathcal{D}] - \mathbb{P}[\|Z\|_\infty > x]|.$$

The error of the probability estimate is upperbounded by

$$\begin{aligned} & \sup_{x>0} |\mathbb{P}[\|\widehat{T}_E\|_\infty > x] - \mathbb{P}[\|\widehat{Z}\|_\infty > x|\mathcal{D}]| \\ & \leq \sup_{x>0} |\mathbb{P}[\|\widehat{T}_E\|_\infty > x] - \mathbb{P}[\|Z\|_\infty > x]| + KS_\infty(\widehat{Z}, Z|\mathcal{D}). \end{aligned}$$

Theorem 4.2 provides an upperbound for the first term. Therefore, it suffices to derive an upperbound for $KS_\infty(\widehat{Z}, Z|\mathcal{D})$. According to Lemma 2.1 in Chernozhukov et al. (2023) and Axiom 3,

$$KS_\infty(\widehat{Z}, Z|\mathcal{D}) \leq C(\kappa_3) \|\widehat{S}_{EE} - S_{EE}\|_\infty \log|E|(1 \vee \|\log\|\widehat{S}_{EE} - S_{EE}\|_\infty). \quad (27)$$

Therefore, it suffices to upperbound the size of $\|\widehat{S}_{EE} - S_{EE}\|_\infty$. In Eq. (7), $S_{(i_1, j_1), (i_2, j_2)}$ is given by

$$\begin{aligned} & S_{(i_1, j_1), (i_2, j_2)} \\ & := \frac{1}{m} \sum_{l=1}^m \frac{\|\Sigma^{(\mathcal{T}, l)}\|_F^2}{p} \left[\begin{aligned} & \rho_{i_1 i_2}^{(S, l)} \rho_{j_1 j_2}^{(S, l)} + \rho_{i_1 j_2}^{(S, l)} \rho_{i_2 j_1}^{(S, l)} + \frac{1}{2} \rho_{i_1 j_1}^{(S, l)} \rho_{i_2 j_2}^{(S, l)} \left(\rho_{i_1 i_2}^{(S, l)2} + \rho_{j_1 j_2}^{(S, l)2} + \rho_{i_1 j_2}^{(S, l)2} + \rho_{i_2 j_1}^{(S, l)2} \right) \\ & - \rho_{i_1 i_2}^{(S, l)} \rho_{i_2 j_2}^{(S, l)} \rho_{i_2 j_1}^{(S, l)} - \rho_{i_1 i_2}^{(S, l)} \rho_{i_1 j_1}^{(S, l)} \rho_{i_1 j_2}^{(S, l)} - \rho_{j_1 j_2}^{(S, l)} \rho_{i_2 j_2}^{(S, l)} \rho_{i_1 j_2}^{(S, l)} - \rho_{j_1 j_2}^{(S, l)} \rho_{i_2 j_1}^{(S, l)} \rho_{i_1 j_1}^{(S, l)} \end{aligned} \right]. \quad (28) \end{aligned}$$

Theorem C.7 gives a bound on the error in $\|\widehat{\Sigma}^{(\mathcal{T}, l)}\|_F^2$:

$$\max_{l=1, \dots, m} \frac{\|\widehat{\Sigma}^{(\mathcal{T}, l)}\|_F^2 - \|\Sigma^{(\mathcal{T}, l)}\|_F^2}{p} \leq C(\kappa_1, \kappa_3) \frac{\log(mn_0pq)}{(qn_0)^{1 - \frac{1}{2(\alpha_0+1)}}}$$

with probability at least $1 - (mn_0pq)^{-1/2}$. On the other hand, Theorem C.8 implies that the error in $\widehat{\rho}_{ij}^{(S, l)}$ is mainly driven by $\Theta_{ij}^{(S, l)}$, where the size of $\Theta_{ij}^{(S, l)}$ is bounded by the Berry-Esseen bound for sub-exponential random variables (for example, see Kuchibhotla and Chakraborty, 2022):

$$\max_{i, j} \frac{1}{m} \sum_{l=1}^m |\Theta_{ij}^{(S, l)}| \leq C(\kappa_1, \kappa_3) \sqrt{\frac{m + \log(mn_0pq)}{mn_0p}}$$

with probability at least $1 - (mn_0pq)^{-1/2}$. (Notice that, because of Axiom 4, the above probabilistic bound is larger than $d \frac{m + \log(mn_0pq)}{n_0p}$, which is given as a probabilistic bound for $\max_{i, j} \sum_{l=1}^m |O_{ij}^{(S, l)}|$ in Theorem C.8.) Because Axiom 3 implies that both $\frac{\|\Sigma^{(\mathcal{T}, l)}\|_F^2}{p}$ and $\min_{i, j} \rho_{ij}^{(S, l)}$ are bounded away from both 0 and ∞ by some constants dependent to κ_3 ,

$$\begin{aligned} \|\widehat{S}_{EE} - S_{EE}\|_\infty & \leq C(\kappa_1, \kappa_3) \max \left\{ \max_{l=1, \dots, m} \left| \frac{\|\widehat{\Sigma}^{(\mathcal{T}, l)}\|_F^2 - \|\Sigma^{(\mathcal{T}, l)}\|_F^2}{p} \right|, \max_{i, j} \frac{1}{m} \sum_{l=1}^m |\Theta_{ij}^{(S, l)}| \right\} \\ & \leq C(\kappa_1, \kappa_3, \kappa_5) \max \left\{ \sqrt{\frac{\log(mn_0pq)}{(n_0q)^{1 - \frac{1}{2(\alpha_0+1)}}}}, \sqrt{\frac{m + \log(mn_0pq)}{mn_0p}} \right\} \end{aligned}$$

with probability at least $1 - C(mn_0pq)^{-1/2}$ for a sufficiently large n_0 . Plugging the result into Eq. (27), we obtain the conclusion of the theorem.

C.6 Proof of Theorem 4.4

Based on the definition of $\mathcal{C}_E(1 - \alpha)$ in Eq. (8),

$$\mathbf{0} \in \mathcal{C}_E(1 - \alpha) \iff \|\widehat{T}_E\|_\infty \leq \widehat{q}_{\|\widehat{Z}\|_\infty, 1 - \alpha}.$$

Under the null hypothesis, $T_E = \mathbf{0}$, and

$$\begin{aligned} \mathbb{P}[\mathbf{0} \in \mathcal{C}_E(1 - \alpha)] &= \mathbb{P}[\|\widehat{T}_E\|_\infty \leq \widehat{q}_{\|\widehat{Z}\|_\infty, 1-\alpha}] \\ &\leq \mathbb{P}[\|\widehat{Z}\|_\infty \leq \widehat{q}_{\|\widehat{Z}\|_\infty, 1-\alpha} | \mathcal{D}] + \sup_{x>0} |\mathbb{P}[\|\widehat{T}_E\|_\infty \leq x] - \mathbb{P}[\|\widehat{Z}\|_\infty \leq x | \mathcal{D}]| \\ &= 1 - \alpha + \sup_{x>0} |\mathbb{P}[\|\widehat{T}_E\|_\infty \leq x] - \mathbb{P}[\|\widehat{Z}\|_\infty \leq x | \mathcal{D}]| \end{aligned}$$

almost surely. Then, due to Theorem 4.3,

$$\mathbb{P}[\mathbf{0} \in \mathcal{C}_E(1 - \alpha)] \leq 1 - \alpha + \mathcal{M}$$

with probability at least $1 - C(mn_0pq)^{-1/2}$, where \mathcal{M} is the probabilistic upper bound for $\sup_{x>0} |\mathbb{P}[\|\widehat{T}_E\|_\infty \leq x] - \mathbb{P}[\|\widehat{Z}\|_\infty \leq x | \mathcal{D}]|$ in Theorem 4.3. Similarly,

$$\mathbb{P}[\mathbf{0} \in \mathcal{C}_E(1 - \alpha)] \geq 1 - \alpha - \mathcal{M}$$

with the same probability. Because the assumed sample complexity implies that $\mathcal{M} \rightarrow 0$, $\mathbb{P}[\mathbf{0} \notin \mathcal{C}_E(1 - \alpha)] \xrightarrow{P} \alpha$, which verifies the validity of the testing procedure.

For the second claim, we use existing results in the extreme value theory of Gaussian random vectors (e.g., see Exercise 5.10, Wainwright, 2019) that

$$\mathbb{P} \left[\|\widehat{Z}\|_\infty \geq \mathbb{E}[\|\widehat{Z}\|_\infty | \mathcal{D}] + \nu \mid \mathcal{D} \right] \leq \exp \left(- \frac{\nu^2}{2 \max_{(i,j) \in E} \widehat{S}_{(i,j),(i,j)}} \right).$$

and

$$\mathbb{E}[\|\widehat{Z}\|_\infty | \mathcal{D}] \leq C \sqrt{\log q} \max_{(i,j) \in E} \widehat{S}_{(i,j),(i,j)},$$

almost surely. With $\nu = \sqrt{-2 \log \alpha \max_{(i,j) \in E} \widehat{S}_{(i,j),(i,j)}}$,

$$\widehat{q}_{\|\widehat{Z}\|_\infty, 1-\alpha} \leq (C \sqrt{\log q} + \sqrt{-2 \log \alpha}) \max_{(i,j) \in E} \widehat{S}_{(i,j),(i,j)},$$

almost surely. As we saw in Section C.5,

$$\|\widehat{S}_{EE} - S_{EE}\|_\infty \leq C(\kappa_1, \kappa_3, \kappa_5) \max \left\{ \frac{\log(mn_0pq)}{(n_0q)^{1 - \frac{1}{2(\alpha_0+1)}}}, \sqrt{\frac{m + \log(mn_0pq)}{mn_0p}} \right\}$$

with probability at least $1 - C(mn_0pq)^{-1/2}$. Due to ?? 4?? 5, the right hand side converges to 0 as $n_0 \rightarrow \infty$, and therefore

$$\widehat{q}_{\|\widehat{Z}\|_\infty, 1-\alpha} \leq C(\kappa_1, \kappa_3, \kappa_5) (\sqrt{\log q} + \sqrt{-2 \log \alpha}) \max_{(i,j) \in E} S_{(i,j),(i,j)}$$

with the same probability for sufficiently large n_0 . Suppose that the assumed alternative hypothesis implies that

$$\|T_E\|_\infty \geq C(\kappa_1, \kappa_3, \kappa_5) \sqrt{\log q} \max_{(i,j) \in E} S_{(i,j),(i,j)} \geq \widehat{q}_{\|\widehat{Z}\|_\infty, 1-\alpha} + \widehat{q}_{\|\widehat{Z}\|_\infty, 1/q}.$$

Then,

$$\begin{aligned} \mathbb{P}[\mathbf{0} \in \mathcal{C}_E(1 - \alpha)] &= \mathbb{P}[\|\widehat{T}_E\|_\infty \leq \widehat{q}_{\|\widehat{Z}\|_\infty, 1-\alpha}] \\ &\leq \mathbb{P}[\|T_E\|_\infty - \|\widehat{T}_E - T_E\|_\infty \leq \widehat{q}_{\|\widehat{Z}\|_\infty, 1-\alpha}] \\ &= \mathbb{P}[\|\widehat{T}_E - T_E\|_\infty \geq \widehat{q}_{\|\widehat{Z}\|_\infty, 1/q}] \\ &\leq \mathbb{P}[\|\widehat{Z}\|_\infty \geq \widehat{q}_{\|\widehat{Z}\|_\infty, 1/q} | \mathcal{D}] + \sup_{x>0} |\mathbb{P}[\|\widehat{T}_E\|_\infty \leq x] - \mathbb{P}[\|\widehat{Z}\|_\infty \leq x | \mathcal{D}]| \\ &= 1/q + \sup_{x>0} |\mathbb{P}[\|\widehat{T}_E\|_\infty \leq x] - \mathbb{P}[\|\widehat{Z}\|_\infty \leq x | \mathcal{D}]|, \end{aligned}$$

which converges to 0 as $n_0 \rightarrow \infty$, due to the assumed sample complexity. It verifies the second conclusion about the power analysis.

C.7 Proof of Theorem C.5

Let $\tilde{\beta}^{(\mathcal{T},l)}$ be the projected parameter of $\beta^{(\mathcal{T},l)}$ onto the parameter space under the banded Cholesky factor assumption. That is, for $t = 1, \dots, p$,

$$\tilde{\beta}_{\cdot,t}^{(\mathcal{T},l)} := \operatorname{argmin}_{b \in \mathbb{R}^p} \mathbb{E} \left[\|X_{t,\cdot}^{(\mathcal{T},l)} - X^{(\mathcal{T},l)\top} b\|_2^2 \right]$$

w.r.t $b_s = 0$ where $s < t - h_l$ or $s \geq t$.

According to the regression theory, $\tilde{\beta}_{\cdot,t}^{(\mathcal{T},l)}$ can be rewritten in terms of $\Sigma^{(\mathcal{T},l)}$ only:

$$\tilde{\beta}_{t-h_l:t-1,t}^{(\mathcal{T},l)} = -\tilde{\Omega}_{t,h_l+1,1:h_l}^{(\mathcal{T},l)} / \tilde{\Omega}_{t,h_l+1,h_l+1}^{(\mathcal{T},l)}$$

where $\tilde{\Omega}_t^{(\mathcal{T},l)} = \left(\Sigma_{t-h_l:t,t-h_l:t}^{(\mathcal{T},l)} \right)^{-1} \in \mathbb{R}^{h_l+1 \times h_l+1}$. We denote the regression error by

$$\tilde{\epsilon}_{t,i}^{(\mathcal{T},l)} := X_{t,i}^{(\mathcal{T},l)} - X_{\cdot,i}^{(\mathcal{T},l)\top} \tilde{\beta}_{\cdot,t}^{(\mathcal{T},l)},$$

and $\tilde{\Phi}_{tt}^{(\mathcal{T},l)} := \frac{1}{n_l q} \mathbb{E} [\|\tilde{\epsilon}_{t,i}^{(\mathcal{T},l)}\|_2^2]$. Then,

$$\tilde{\Phi}_{tt}^{(\mathcal{T},l)} = \frac{\operatorname{tr}(\Sigma^{(\mathcal{S},l)})}{q} \frac{1}{\tilde{\Omega}_{t,h_l+1,h_l+1}^{(\mathcal{T},l)}}.$$

We notice that $\tilde{\Omega}_{t,h_l+1,1:h_l}^{(\mathcal{T},l)} / \tilde{\Omega}_{t,h_l+1,h_l+1}^{(\mathcal{T},l)}$ and $1 / \tilde{\Omega}_{t,h_l+1,h_l+1}^{(\mathcal{T},l)}$ are the projected parameter and prediction error of the $AR(h_l)$ regression on vector-variate observations, so the bias analyses in the existing literature (e.g., Liu and Ren (2020)) is useful here. For example, Lemma B.3 in Liu and Ren (2020) implies that under Axiom 5

$$\begin{aligned} \left\| \tilde{\beta}_{\cdot,t}^{(\mathcal{T},l)} - \beta_{\cdot,t}^{(\mathcal{T},l)} \right\|_2 &\leq C(\kappa_3, \kappa_5) (h_l - 1)^{-\alpha_l - 1/2}, \\ \left| \tilde{\Phi}_{tt}^{(\mathcal{T},l)} - \frac{\operatorname{tr}(\Sigma^{(\mathcal{S},l)})}{q} \Phi_{tt}^{(\mathcal{T},l)} \right| &\leq C(\kappa_3, \kappa_5) (h_l - 1)^{-\alpha_l - 1/2}. \end{aligned}$$

Now, it suffices to establish the probabilistic error bound of $\hat{\beta}^{(\mathcal{T},l)}$ and $\hat{\Phi}^{(\mathcal{T},l)}$ against $\tilde{\beta}^{(\mathcal{T},l)}$ and $\tilde{\Phi}^{(\mathcal{T},l)}$, respectively. We take a similar approach with the proof of Theorem 4.1. First, we notice that

$$\hat{\beta}_{t-h_l:t-1,t}^{(\mathcal{T},l)} = \left(X_{t-h_l:t-1,\cdot}^{(\mathcal{T},l)}, X_{t-h_l:t-1,\cdot}^{(\mathcal{T},l)\top} \right)^{-1} \left(X_{t-h_l:t-1,\cdot}^{(\mathcal{T},l)}, X_{t,\cdot}^{(\mathcal{T},l)\top} \right).$$

Then,

$$\begin{aligned} &\left(\frac{1}{n_l q} X_{t-h_l:t-1,\cdot}^{(\mathcal{T},l)}, X_{t-h_l:t-1,\cdot}^{(\mathcal{T},l)\top} \right) (\hat{\beta}_{\cdot,t}^{(\mathcal{T},l)} - \tilde{\beta}_{\cdot,t}^{(\mathcal{T},l)}) \\ &= \frac{1}{n_l q} X_{t-h_l:t-1,\cdot}^{(\mathcal{T},l)}, X_{t,\cdot}^{(\mathcal{T},l)\top} - \left(\frac{1}{n_l q} X_{t-h_l:t-1,\cdot}^{(\mathcal{T},l)}, X_{t-h_l:t-1,\cdot}^{(\mathcal{T},l)\top} \right) \tilde{\beta}_{t-h_l:t-1,t}^{(\mathcal{T},l)} \\ &= \frac{1}{n_l q} X_{t-h_l:t-1,\cdot}^{(\mathcal{T},l)}, \tilde{\epsilon}_{t,\cdot}^{(\mathcal{T},l)\top}. \end{aligned}$$

By a similar argument with the proof of Theorem C.3,

$$\begin{aligned} &\mathbb{P} \left[\max_{l=1,\dots,m} \max_{t=1,\dots,p} \left\| \left(\frac{1}{n_l q} X_{t-h_l:t-1,\cdot}^{(\mathcal{T},l)}, X_{t-h_l:t-1,\cdot}^{(\mathcal{T},l)\top} \right) \tilde{\Delta}_{\cdot,t}^{(\mathcal{T},l)} \right\|_{\infty} \geq C(\kappa_1, \kappa_3) \sqrt{\frac{\log(mn_0pq)}{n_0q}} \right] \\ &= \mathbb{P} \left[\max_{l=1,\dots,m} \max_{t=1,\dots,p} \left\| \frac{1}{n_l q} X_{t-h_l:t-1,\cdot}^{(\mathcal{T},l)}, \tilde{\epsilon}_{t,\cdot}^{(\mathcal{T},l)\top} \right\|_{\infty} \geq C(\kappa_1, \kappa_3) \sqrt{\frac{\log(mn_0pq)}{n_0q}} \right] \\ &\leq C(mn_0pq)^{-1/2} \end{aligned}$$

for some positive constants $C(\kappa_3)$ and C , where $\tilde{\Delta}^{(\mathcal{T},l)} := \hat{\beta}^{(\mathcal{T},l)} - \tilde{\beta}^{(\mathcal{T},l)}$. Under the event,

$$\begin{aligned} \left| \tilde{\Delta}_{\cdot,t}^{(\mathcal{T},l)\top} \left(\frac{1}{n_l q} X_{t-h_l:t-1,\cdot}^{(\mathcal{T},l)}, X_{t-h_l:t-1,\cdot}^{(\mathcal{T},l)\top} \right) \tilde{\Delta}_{\cdot,t}^{(\mathcal{T},l)} \right| &\leq \left\| \left(\frac{1}{n_l q} X_{t-h_l:t-1,\cdot}^{(\mathcal{T},l)}, X_{t-h_l:t-1,\cdot}^{(\mathcal{T},l)\top} \right) \tilde{\Delta}_{\cdot,t}^{(\mathcal{T},l)} \right\|_{\infty} \|\tilde{\Delta}_{\cdot,t}^{(\mathcal{T},l)}\|_1 \\ &\leq C(\kappa_1, \kappa_3) \sqrt{\frac{\log(mn_0pq)}{n_0q}} \|\tilde{\Delta}_{\cdot,t}^{(\mathcal{T},l)}\|_1 \\ &\leq C(\kappa_1, \kappa_3) \sqrt{h_l \frac{\log(mn_0pq)}{n_0q}} \|\tilde{\Delta}_{\cdot,t}^{(\mathcal{T},l)}\|_2, \end{aligned} \tag{29}$$

for any $t = 1, \dots, T$ and $l = 1, \dots, m$. On the other hand, by a similar argument with the proof of Theorem C.1,

$$\begin{aligned} & \mathbb{P} \left[\max_{l=1, \dots, m} \max_{s, t} \left| \frac{1}{n_l q} X_{s, \cdot}^{(\mathcal{T}, l)} X_{t, \cdot}^{(\mathcal{T}, l)\top} - \frac{\text{tr}(\Sigma^{(\mathcal{S}, l)})}{q} \Sigma_{st}^{(\mathcal{T}, l)} \right| \geq C(\kappa_1, \kappa_3) \sqrt{\frac{\log(mn_0 p q)}{n_0 q}} \right] \\ & \leq C(mn_0 p q)^{-1/2} \end{aligned}$$

for some positive constants $C(\kappa_3)$ and C . Under the event,

$$\begin{aligned} & \left| \tilde{\Delta}_{\cdot, t}^{(\mathcal{T}, l)\top} \left(\frac{1}{n_l q} X_{t-h_l:t-1, \cdot}^{(\mathcal{T}, l)} X_{t-h_l:t-1, \cdot}^{(\mathcal{T}, l)\top} - \frac{\text{tr}(\Sigma^{(\mathcal{S}, l)})}{q} \Sigma_{t-h_l:t-1, t-h_l:t-1}^{(\mathcal{T}, l)} \right) \tilde{\Delta}_{\cdot, t}^{(\mathcal{T}, l)} \right| \\ & \leq \left\| \frac{1}{n_l q} X_{t-h_l:t-1, \cdot}^{(\mathcal{T}, l)} X_{t-h_l:t-1, \cdot}^{(\mathcal{T}, l)\top} - \frac{\text{tr}(\Sigma^{(\mathcal{S}, l)})}{q} \Sigma_{t-h_l:t-1, t-h_l:t-1}^{(\mathcal{T}, l)} \right\|_{\infty} \|\tilde{\Delta}_{\cdot, t}^{(\mathcal{T}, l)}\|_1^2 \\ & \leq C(\kappa_1, \kappa_3) \sqrt{\frac{\log(mn_0 p q)}{n_0 q}} \|\tilde{\Delta}_{\cdot, t}^{(\mathcal{T}, l)}\|_1^2 \leq C(\kappa_1, \kappa_3) h_l \sqrt{\frac{\log(mn_0 p q)}{n_0 q}} \|\tilde{\Delta}_{\cdot, t}^{(\mathcal{T}, l)}\|_2^2 \\ & \leq \frac{1}{2\kappa_3} \|\tilde{\Delta}_{\cdot, t}^{(\mathcal{T}, l)}\|_2^2, \end{aligned} \tag{30}$$

for any $t = 1, \dots, T, l = 1, \dots, m$, and a sufficiently large n_0 due to Axiom 5. Moreover with Axiom 3,

$$\left| \tilde{\Delta}_{\cdot, t}^{(\mathcal{T}, l)\top} \left(\frac{1}{n_l q} X_{t-h_l:t-1, \cdot}^{(\mathcal{T}, l)} X_{t-h_l:t-1, \cdot}^{(\mathcal{T}, l)\top} \right) \tilde{\Delta}_{\cdot, t}^{(\mathcal{T}, l)} \right| \geq \frac{1}{2\kappa_3} \|\tilde{\Delta}_{\cdot, t}^{(\mathcal{T}, l)}\|_2^2 \tag{31}$$

with probability at least $1 - C(mn_0 p q)^{-1/2}$. Eqs. (29) and (31) imply

$$\frac{1}{2\kappa_3} \|\tilde{\Delta}_{\cdot, t}^{(\mathcal{T}, l)}\|_2^2 \leq C(\kappa_1, \kappa_3) \sqrt{h_l \frac{\log(mn_0 p q)}{n_0 q}} \|\tilde{\Delta}_{\cdot, t}^{(\mathcal{T}, l)}\|_2,$$

and

$$\|\tilde{\Delta}_{\cdot, t}^{(\mathcal{T}, l)}\|_2 \leq C(\kappa_1, \kappa_3) \sqrt{h_l \frac{\log(mn_0 p q)}{n_0 q}} \quad \text{and} \quad \|\tilde{\Delta}_{\cdot, t}^{(\mathcal{T}, l)}\|_1 \leq C(\kappa_1, \kappa_3) h_l \sqrt{\frac{\log(mn_0 p q)}{n_0 q}}. \tag{32}$$

for any $t = 1, \dots, T, l = 1, \dots, m$ and a sufficiently large n_0 , with probability at least $1 - C(mn_0 p q)^{-1/2}$. Integrating Section C.7 and Eq. (32), we obtain the first result that, with the same probability,

$$\begin{aligned} \|\hat{\beta}_{\cdot, t}^{(\mathcal{T}, l)} - \beta_{\cdot, t}^{(\mathcal{T}, l)}\|_2 & \leq C(\kappa_3, \kappa_5) (h_l - 1)^{-\alpha_l - 1/2} + C(\kappa_1, \kappa_3) h_l \sqrt{\frac{\log(mn_0 p q)}{n_0 q}} \\ & \leq C(\kappa_1, \kappa_3, \kappa_5) \sqrt{\frac{\log(mn_0 p q)}{(n_0 q)^{1-1/2(\alpha_0+1)}}, \end{aligned}$$

for any $t = 1, \dots, T, l = 1, \dots, m$ and a sufficiently large n_0 , given that $h_l = \lfloor (n_l q)^{1/2(\alpha_l+1)} \rfloor$.

For the second result, we observe that

$$\left| \hat{\Phi}_{tt}^{(\mathcal{T}, l)} - \tilde{\Phi}_{tt}^{(\mathcal{T}, l)} \right| \leq \frac{1}{n_l q} \left| \|\hat{\epsilon}_{t, \cdot}^{(\mathcal{T}, l)}\|_2^2 - \|\tilde{\epsilon}_{t, \cdot}^{(\mathcal{T}, l)}\|_2^2 \right| + \left| \frac{1}{n_l q} \|\hat{\epsilon}_{t, \cdot}^{(\mathcal{T}, l)}\|_2^2 - \tilde{\Phi}_{tt}^{(\mathcal{T}, l)} \right|.$$

For the first term,

$$\begin{aligned} & \frac{1}{n_l q} \left| \|\hat{\epsilon}_{t, \cdot}^{(\mathcal{T}, l)}\|_2^2 - \|\tilde{\epsilon}_{t, \cdot}^{(\mathcal{T}, l)}\|_2^2 \right| \\ & = \frac{2}{n_l q} \left| \tilde{\Delta}_{\cdot, t}^{(\mathcal{T}, l)\top} X_{t-h:t-1, \cdot}^{(\mathcal{T}, l)} \tilde{\epsilon}_{t, \cdot}^{(\mathcal{T}, l)\top} \right| + \frac{1}{n_l q} \left| \tilde{\Delta}_{\cdot, t}^{(\mathcal{T}, l)\top} X_{t-h:t-1}^{(\mathcal{T}, l)} X_{t-h:t-1}^{(\mathcal{T}, l)\top} \tilde{\Delta}_{\cdot, t}^{(\mathcal{T}, l)} \right| \\ & \leq \left\| \tilde{\Delta}_{\cdot, t}^{(\mathcal{T}, l)\top} \right\|_1 \left\| \frac{2}{n_l q} X_{t-h:t-1, \cdot}^{(\mathcal{T}, l)} \tilde{\epsilon}_{t, \cdot}^{(\mathcal{T}, l)\top} \right\|_{\infty} + \left\| \tilde{\Delta}_{\cdot, t}^{(\mathcal{T}, l)\top} \right\|_2^2 \left\| \frac{1}{n_l q} X_{t-h:t-1}^{(\mathcal{T}, l)} X_{t-h:t-1}^{(\mathcal{T}, l)\top} \right\|_2 \\ & \leq C(\kappa_1, \kappa_3) h \frac{\log p}{n_l q} \end{aligned}$$

for any $t = 1, \dots, T, l = 1, \dots, m$, and a sufficiently large n_0 , with probability at least $1 - C(mn_0pq)^{-1/2}$, based on Eqs. (29) and (30) and Axiom 3. For the second term, a similar argument with the proof of Theorem C.4 implies that

$$\begin{aligned} \mathbb{P} \left[\max_{l=1, \dots, m} \max_{s, t} \left| \frac{1}{n_l q} \tilde{\epsilon}_{s, \cdot}^{(\mathcal{T}, l)} \tilde{\epsilon}_{t, \cdot}^{(\mathcal{T}, l)\top} - \frac{\text{tr}(\Sigma^{(\mathcal{S}, l)})}{q} \tilde{\Phi}_{st}^{(\mathcal{T}, l)} \right| \geq C(\kappa_1, \kappa_3) \sqrt{\frac{\log(mn_0pq)}{n_l q}} \right] \\ \leq C(mn_0pq)^{-1/2}. \end{aligned}$$

In sum,

$$\left| \widehat{\Phi}_{tt}^{(\mathcal{T}, l)} - \tilde{\Phi}_{tt}^{(\mathcal{T}, l)} \right| \leq C(\kappa_1, \kappa_3) h \frac{\log p}{n_0 q} + C(\kappa_1, \kappa_3) \sqrt{\frac{\log(mn_0pq)}{n_l q}} \leq C(\kappa_1, \kappa_3) \sqrt{h \frac{\log p}{n_0 q}}$$

for any $t = 1, \dots, T, l = 1, \dots, m$ and a sufficiently large n_0 , with probability at least $1 - C(mn_0pq)^{-1/2}$, which implies the second conclusion where $h = \lfloor (n_l q)^{1/2(\alpha_l + 1)} \rfloor$.

C.8 Proof of Theorem C.6

We recall the Cholesky decomposition of the temporal precision matrix:

$$\begin{aligned} \Omega^{(\mathcal{T}, l)} &= \frac{\text{tr}(\Sigma^{(\mathcal{S}, l)})}{q} (I - \beta^{(\mathcal{T}, l)\top}) \Phi^{(\mathcal{T}, l)-1} (I - \beta^{(\mathcal{T}, l)}) \\ \Sigma^{(\mathcal{T}, l)} &= \frac{q}{\text{tr}(\Sigma^{(\mathcal{S}, l)})} (I - \beta^{(\mathcal{T}, l)\top})^{-1} \Phi^{(\mathcal{T}, l)} (I - \beta^{(\mathcal{T}, l)})^{-1} \end{aligned}$$

Our temporal covariance matrix estimate is based on the estimated Cholesky factor, $\widehat{\beta}^{(\mathcal{T}, l)}$, and noise variance, $\widehat{\Phi}^{(\mathcal{T}, l)}$, in Eqs. (10) and (11). In regard to their estimate errors, we use the following lemma as a corollary of Theorem C.5. See Section D.6 for the proof.

Lemma C.9. *Suppose that $h_l = \lfloor (n_l q)^{1/(1+\alpha)} \rfloor$ and $\eta = C(\kappa_3)$ satisfies $\eta \leq \lambda_1(I - \beta^{(\mathcal{T}, l)})$ for $l = 1, \dots, m$. Then, following the procedure defined in Section 3.3,*

$$\begin{aligned} \mathbb{P} \left[\begin{aligned} \max_l \frac{1}{p} \left\| \widehat{\Phi}^{(\mathcal{T}, l)} - \frac{\text{tr}(\Sigma^{(\mathcal{S}, l)})}{q} \Phi^{(\mathcal{T}, l)} \right\|_F^2 &\geq C(\kappa_1, \kappa_3, \kappa_5) \frac{\log(mn_0pq)}{(n_0q)^{1-1/(2\alpha_0+2)}}, \\ \max_l \frac{1}{p} \left\| \widehat{\Phi}^{(\mathcal{T}, l)-1} - \frac{q}{\text{tr}(\Sigma^{(\mathcal{S}, l)})} \Phi^{(\mathcal{T}, l)-1} \right\|_F^2 &\geq C(\kappa_1, \kappa_3, \kappa_5) \frac{\log(mn_0pq)}{(n_0q)^{1-1/(2\alpha_0+2)}} \end{aligned} \right] \\ \leq C(mn_0pq)^{-1/2}, \\ \mathbb{P} \left[\begin{aligned} \max_l \frac{1}{p} \|P_\eta(I - \widehat{\beta}^{(\mathcal{T}, l)}) - (I - \beta^{(\mathcal{T}, l)})\|_F^2 &\geq C(\kappa_1, \kappa_3, \kappa_5) \frac{\log(mn_0pq)}{(n_0q)^{1-1/(2\alpha_0+2)}}, \\ \max_l \frac{1}{p} \|P_\eta(I - \widehat{\beta}^{(\mathcal{T}, l)})^{-1} - (I - \beta^{(\mathcal{T}, l)})^{-1}\|_F^2 &\geq C(\kappa_1, \kappa_3, \kappa_5) \frac{\log(mn_0pq)}{(n_0q)^{1-1/(2\alpha_0+2)}} \end{aligned} \right] \\ \leq C(mn_0pq)^{-1/2}, \end{aligned}$$

for sufficiently large n_0 .

We note that Axiom 3 implies that the operator norms $I - \beta^{(\mathcal{T}, l)}$, $(I - \beta^{(\mathcal{T}, l)})^{-1}$, $\Phi^{(\mathcal{T}, l)}$, and $\Phi^{(\mathcal{T}, l)-1}$ are bounded; see Lemma B.2 in Liu and Ren (2020). The eigenvalue truncation in Eq. (12) implies the bounded operator norm for $P_\eta(I - \widehat{\beta}^{(\mathcal{T}, l)})$ and $P_\eta(I - \widehat{\beta}^{(\mathcal{T}, l)})^{-1}$. Finally, Theorem C.6 implies the bounded operator norm for $\widehat{\Phi}^{(\mathcal{T}, l)}$ and $\widehat{\Phi}^{(\mathcal{T}, l)-1}$. Namely,

$$\begin{aligned} \|I - \beta^{(\mathcal{T}, l)}\|_{\text{op}}, \|P_\eta(I - \widehat{\beta}^{(\mathcal{T}, l)})\|_{\text{op}} &\leq C(\kappa_3) \\ \|(I - \beta^{(\mathcal{T}, l)})^{-1}\|_{\text{op}}, \|P_\eta(I - \widehat{\beta}^{(\mathcal{T}, l)})^{-1}\|_{\text{op}} &\leq C(\kappa_3) \\ \|\Phi^{(\mathcal{T}, l)}\|_{\text{op}}, \left\| \frac{\text{tr}(\Sigma^{(\mathcal{S}, l)})}{q} \widehat{\Phi}^{(\mathcal{T}, l)} \right\|_{\text{op}} &\leq C(\kappa_3) \\ \|\Phi^{(\mathcal{T}, l)-1}\|_{\text{op}}, \left\| \frac{q}{\text{tr}(\Sigma^{(\mathcal{S}, l)})} \widehat{\Phi}^{(\mathcal{T}, l)-1} \right\|_{\text{op}} &\leq C(\kappa_3) \end{aligned}$$

for any $l = 1, \dots, m$ and a sufficiently large n_0 , with probability at least $1 - C(mn_0pq)^{-1/2}$.

Now, we move on to connect the error in the temporal covariance matrix estimate with the Frobenius norm bounds in Theorem C.9. We use a well known inequality about the Frobenius and operator norms:

$$\|AB\|_F \leq \|A\|_{\text{op}} \|B\|_F$$

for any compatible matrices A and B . For the temporal covariance matrix,

$$\begin{aligned} & \left\| \widehat{\Sigma}^{(\mathcal{T}, l)} - \frac{\text{tr}(\Sigma^{(\mathcal{S}, l)})}{q} \Sigma^{(\mathcal{T}, l)} \right\|_F \\ & \leq \|(I - \beta^{(\mathcal{T}, l)})^{-1}\|_{\text{op}} \left\| \frac{\text{tr}(\Sigma^{(\mathcal{S}, l)})}{q} \Phi^{(\mathcal{T}, l)} \right\|_{\text{op}} \|P_\eta(I - \widehat{\beta}^{(\mathcal{T}, l)})^{-1} - (I - \beta^{(\mathcal{T}, l)})^{-1}\|_F \\ & \quad + \|(I - \beta^{(\mathcal{T}, l)})^{-1}\|_{\text{op}} \left\| \widehat{\Phi}^{(\mathcal{T}, l)} - \frac{\text{tr}(\Sigma^{(\mathcal{S}, l)})}{q} \Phi^{(\mathcal{T}, l)} \right\|_F \|P_\eta(I - \widehat{\beta}^{(\mathcal{T}, l)})^{-1}\|_{\text{op}} \\ & \quad + \|P_\eta(I - \widehat{\beta}^{(\mathcal{T}, l)})^{-1} - (I - \beta^{(\mathcal{T}, l)})^{-1}\|_F \left\| \frac{\text{tr}(\Sigma^{(\mathcal{S}, l)})}{q} \Phi^{(\mathcal{T}, l)} \right\|_{\text{op}} \|P_\eta(I - \widehat{\beta}^{(\mathcal{T}, l)})^{-1}\|_{\text{op}} \end{aligned}$$

and hence, plugging in the previously obtained bounds,

$$\left\| \widehat{\Sigma}^{(\mathcal{T}, l)} - \frac{\text{tr}(\Sigma^{(\mathcal{S}, l)})}{q} \Sigma^{(\mathcal{T}, l)} \right\|_F \leq C(\kappa_1, \kappa_3, \kappa_5) \sqrt{p} \sqrt{\frac{\log(mn_0pq)}{(n_0q)^{1-1/(2\alpha_0+2)}}$$

for any $l = 1, \dots, m$ with probability at least $1 - C(mn_0pq)^{-1/2}$. The second conclusion about $\widehat{\Omega}^{(\mathcal{T}, l)}$ is similarly obtained.

C.9 Proof of Corollary C.7

The error in the Frobenius norm estimate can be upperbounded by a function of the error in the covariance matrix estimate:

$$\begin{aligned} & \frac{1}{p} \left| \|\widehat{\Sigma}^{(\mathcal{T}, l)}\|_F^2 - \|\Sigma^{(\mathcal{T}, l)}\|_F^2 \right| \\ & = \frac{1}{p} \left(\|\widehat{\Sigma}^{(\mathcal{T}, l)}\|_F + \|\Sigma^{(\mathcal{T}, l)}\|_F \right) \left| \|\widehat{\Sigma}^{(\mathcal{T}, l)}\|_F - \|\Sigma^{(\mathcal{T}, l)}\|_F \right| \\ & \leq \left(\frac{2}{\sqrt{p}} \|\Sigma^{(\mathcal{T}, l)}\|_F + \frac{1}{\sqrt{p}} \|\widehat{\Sigma}^{(\mathcal{T}, l)} - \Sigma^{(\mathcal{T}, l)}\|_F \right) \frac{1}{\sqrt{p}} \|\widehat{\Sigma}^{(\mathcal{T}, l)} - \Sigma^{(\mathcal{T}, l)}\|_F. \end{aligned}$$

Because $\frac{1}{\sqrt{p}} \|\Sigma^{(\mathcal{T}, l)}\|_F$ is bounded away from both 0 and ∞ , and Theorem C.6 implies that

$$\frac{1}{\sqrt{p}} \|\widehat{\Sigma}^{(\mathcal{T}, l)} - \Sigma^{(\mathcal{T}, l)}\|_F \leq C(\kappa_1, \kappa_3, \kappa_5) \sqrt{\frac{\log(mn_0pq)}{p(n_0q)^{1-1/(2\alpha_0+2)}}$$

with probability at least $1 - C(mn_0pq)^{-1/2}$,

$$\begin{aligned} \frac{1}{p} \left| \|\widehat{\Sigma}^{(\mathcal{T}, l)}\|_F^2 - \|\Sigma^{(\mathcal{T}, l)}\|_F^2 \right| & \leq C(\kappa_1, \kappa_3, \kappa_5) \frac{1}{\sqrt{p}} \|\widehat{\Sigma}^{(\mathcal{T}, l)} - \Sigma^{(\mathcal{T}, l)}\|_F \\ & \leq C(\kappa_1, \kappa_3, \kappa_5) \sqrt{\frac{\log(mn_0pq)}{p(n_0q)^{1-1/(2\alpha_0+2)}} \end{aligned}$$

with probability at least $1 - C(mn_0pq)^{-1/2}$ for sufficiently large n_0 .

D Proof of the Lemmas

D.1 Proof of Lemma C.1

In Eq. (16), $W_{ti}^{(\mathcal{S}, l)} W_{tj}^{(\mathcal{S}, l)}$ is a sub-exponential variable with

$$\mathbb{E} \left[\exp \left(\nu (W_{ti}^{(\mathcal{S}, l)} W_{tj}^{(\mathcal{S}, l)} - \Sigma_{tt}^{(\mathcal{T}, l)} \Sigma_{ij}^{(\mathcal{S}, l)}) \right) \right] \leq e^{C(\kappa_3) \nu^2},$$

for all ν : $|\nu| < C(\kappa_3)$ due to Axiom 3, and independent across $t = 1, \dots, n_l p$. According to Theorem 2.8.2 in Vershynin (2018) and ?? 1?? 2, our main claim is a result of maximal inequality on sub-exponential random variables.

D.2 Proof of Lemma C.2

In Eq. (17),

$$(\xi_{\cdot,i}^{(S,l)}, W_{\cdot,j}^{(S,l)}) \stackrel{\text{i.i.d.}}{\sim} N \left(0, I \otimes \text{diag} \left(\frac{1}{\Omega_{ii}^{(S,l)}}, \Sigma_{jj}^{(S,l)} \right) \right).$$

Because $W_{\cdot,i}^{(S,l)}$ is independent to $\xi_{\cdot,j}^{(S,l)}$,

$$\left\{ \xi_{\cdot,i}^{(S,l)} W_{\cdot,j}^{(S,l)\top} | W_{\cdot,j}^{(S,l)} \right\} \sim N \left(0, \frac{\|W_{\cdot,j}^{(S,l)}\|_2^2}{\Omega_{ii}^{(S,l)}} \right) \text{ a.s.},$$

and therefore

$$\begin{aligned} \left\{ \left(\frac{\sqrt{n_l p}}{\|X_{\cdot,j}^{(S,l)}\|_2} \epsilon_{\cdot,i}^{(S,l)\top} X_{\cdot,j}^{(S,l)} \right)^2 | X_{\cdot,j}^{(S,l)} \right\} &= \left\{ \left(\frac{\sqrt{n_l p}}{\|X_{\cdot,j}^{(S,l)}\|_2} \xi_{\cdot,i}^{(S,l)\top} W_{\cdot,j}^{(S,l)} \right)^2 | W_{\cdot,j}^{(S,l)} \right\} \\ &\sim n_l p \frac{\|W_{\cdot,j}^{(S,l)}\|_2^2}{\|X_{\cdot,j}^{(S,l)}\|_2^2} \chi^2(1) \text{ a.s.} \end{aligned}$$

Due to Axiom 3, $\frac{\|W_{\cdot,j}^{(S,l)}\|_2^2}{\|X_{\cdot,j}^{(S,l)}\|_2^2} \leq C(\kappa_3)$. Hence, the sub-exponential inequality in Theorem 2.8.2, Vershynin (2018) implies that, for any $\nu > 0$,

$$\begin{aligned} &\mathbb{P} \left[\sum_{l=1}^m \left(\frac{\sqrt{n_l p}}{\|X_{\cdot,j}^{(S,l)}\|_2} \epsilon_{\cdot,i}^{(S,l)\top} X_{\cdot,j}^{(S,l)} \right)^2 - \sum_{l=1}^m \mathbb{E} \left(\frac{\sqrt{n_l p}}{\|X_{\cdot,j}^{(S,l)}\|_2} \epsilon_{\cdot,i}^{(S,l)\top} X_{\cdot,j}^{(S,l)} \right)^2 \geq \eta \right] \\ &\leq \exp \left[-C(\kappa_3) \min \left\{ \left(\frac{\eta}{n_l p} \right)^2 \frac{1}{m}, \frac{\eta}{n_l p} \right\} \right]. \end{aligned}$$

Axiom 3 implies that $\sum_{l=1}^m \mathbb{E} \left(\frac{\sqrt{n_l p}}{\|X_{\cdot,j}^{(S,l)}\|_2} \epsilon_{\cdot,i}^{(S,l)\top} X_{\cdot,j}^{(S,l)} \right)^2 \leq C(\kappa_1, \kappa_3) m n_0 p$. Plugging-in $\eta = C(\kappa_1, \kappa_3) \cdot n_0 p \cdot \max \{ \sqrt{m\nu}, \nu \}$

$$\mathbb{P} \left[\frac{1}{n_0 p} \sum_{l=1}^m \left(\frac{\sqrt{n_l p}}{\|X_{\cdot,j}^{(S,l)}\|_2} \epsilon_{\cdot,i}^{(S,l)\top} X_{\cdot,j}^{(S,l)} \right)^2 \geq C(\kappa_1, \kappa_3) (m + \nu) \right] \leq e^{-\nu}.$$

The second conclusion follows a similar argument with

$$(\xi_{\cdot,i}^{(S,l)}, W^{(S,l)} \beta_{\cdot,j}^{(S,l)}) \stackrel{\text{i.i.d.}}{\sim} N \left(0, I \otimes \text{diag} \left(\frac{1}{\Omega_{ii}^{(S,l)}}, \frac{\Omega_{ii}^{(S,l)} \Sigma_{ii}^{(S,l)} - 1}{\Omega_{ii}^{(S,l)}} \right) \right).$$

D.3 Proof of Lemma C.3

In Eq. (17),

$$\begin{aligned} &(\xi_{\cdot,i}^{(S,l)}, W_{\cdot,j}^{(S,l)}) \stackrel{\text{i.i.d.}}{\sim} N \left(0, I \otimes \text{diag} \left(\frac{1}{\Omega_{ii}^{(S,l)}}, \Sigma_{jj}^{(S,l)} \right) \right), \\ &(\xi_{\cdot,i}^{(S,l)}, W^{(S,l)} \beta_{\cdot,j}^{(S,l)}) \stackrel{\text{i.i.d.}}{\sim} N \left(0, I \otimes \text{diag} \left(\frac{1}{\Omega_{ii}^{(S,l)}}, \frac{\Omega_{ii}^{(S,l)} \Sigma_{ii}^{(S,l)} - 1}{\Omega_{ii}^{(S,l)}} \right) \right). \end{aligned}$$

In other words, $\xi_{ti}^{(S,l)} W_{tj}^{(S,l)}$ and $\xi_{ti}^{(S,l)} W_{t\cdot}^{(S,l)} \beta_{\cdot,i}^{(S,l)}$ are sub-exponential random variables with mean zero and constant bounded by $C(\kappa_3)$:

$$\begin{aligned} \mathbb{E} \left[\exp \left(\nu \xi_{ti}^{(S,l)} W_{tj}^{(S,l)} \right) \right] &\leq e^{C(\kappa_3) \nu^2}, \\ \mathbb{E} \left[\exp \left(\nu \xi_{ti}^{(S,l)} W_{t\cdot}^{(S,l)} \beta_{\cdot,i}^{(S,l)} \right) \right] &\leq e^{C(\kappa_3) \nu^2}, \end{aligned}$$

for all $\nu : |\nu| < C(\kappa_3)$ due to Axiom 3, and independent across $t = 1, \dots, n_l p$. Then, similar arguments as in Theorem C.1 induce the desired conclusions.

D.4 Proof of Lemma C.4

In Eq. (17), $\xi_{ti}^{(S,l)} \xi_{tj}^{(S,l)}$ is a sub-exponential variable with

$$\mathbb{E} \left[\exp \left(\nu (\xi_{ti}^{(S,l)} \xi_{tj}^{(S,l)} - \Sigma_{tt}^{(T,l)} \Phi_{ij}^{(S,l)}) \right) \right] \leq e^{C(\kappa_3) \nu^2},$$

for all $\nu : |\nu| < C(\kappa_3)$ due to Axiom 3, and independent across $t = 1, \dots, n_l p$. Following the same proof as in Theorem C.1, we prove the claim.

D.5 Proof of Lemma C.8

For $i, j \in \{1, \dots, q\}$, let

$$\widehat{\phi}_{ij}^{(S,l)} := \frac{1}{n_l p} \left[\widehat{\epsilon}_{\cdot, i}^{(S,l) \top} \widehat{\epsilon}_{\cdot, j}^{(S,l)} - \epsilon_{\cdot, i}^{(S,l) \top} \epsilon_{\cdot, j}^{(S,l)} \right] + \frac{1}{n_l p} \left(\|\epsilon_{\cdot, i}^{(S,l)}\|_2^2 \Delta_{ij}^{(S,l)} + \|\epsilon_{\cdot, j}^{(S,l)}\|_2^2 \Delta_{ji}^{(S,l)} \right) \mathbb{I}(i \neq j)$$

and

$$\widetilde{\phi}_{ij}^{(S,l)} := \frac{1}{n_l p} \epsilon_{\cdot, i}^{(S,l) \top} \epsilon_{\cdot, j}^{(S,l)} - \Phi_{ij}^{(S,l)}.$$

Then, for $i = j$,

$$\widehat{\Phi}_{ii}^{(S,l)} - \Phi_{ii}^{(S,l)} = \frac{1}{n_l p} \widehat{\epsilon}_{\cdot, i}^{(S,l) \top} \widehat{\epsilon}_{\cdot, i}^{(S,l)} - \Phi_{ii}^{(S,l)} = \widehat{\phi}_{ii}^{(S,l)} + \widetilde{\phi}_{ii}^{(S,l)},$$

and, for $i \neq j$, because $\beta_{ij}^{(S,l)} = -\Phi_{ij}^{(S,l)}/\Phi_{ii}^{(S,l)}$,

$$\begin{aligned} \Phi_{ij}^{(S,l)} - \widehat{\Phi}_{ij}^{(S,l)} &= - \left(\Phi_{ij}^{(S,l)} + \Phi_{ii}^{(S,l)} \beta_{ij}^{(S,l)} + \Phi_{jj}^{(S,l)} \beta_{ji}^{(S,l)} \right) \\ &\quad + \frac{1}{n_l p} \left(\widehat{\epsilon}_{\cdot, i}^{(S,l) \top} \widehat{\epsilon}_{\cdot, j}^{(S,l)} + \|\widehat{\epsilon}_{\cdot, i}^{(S,l)}\|_2^2 \widehat{\beta}_{ij}^{(S,l)} + \|\widehat{\epsilon}_{\cdot, j}^{(S,l)}\|_2^2 \widehat{\beta}_{ji}^{(S,l)} \right) \\ &= \widehat{\phi}_{ij}^{(S,l)} + \widehat{\phi}_{ii}^{(S,l)} \beta_{ij}^{(S,l)} + \widehat{\phi}_{jj}^{(S,l)} \beta_{ji}^{(S,l)} \\ &\quad + \widetilde{\phi}_{ij}^{(S,l)} + \widetilde{\phi}_{ii}^{(S,l)} \beta_{ij}^{(S,l)} + \widetilde{\phi}_{jj}^{(S,l)} \beta_{ji}^{(S,l)} \end{aligned}$$

These error terms drive $\widehat{\rho}_{ij}^{(S,l)} - \rho_{ij}^{(S,l)}$ for $i, j : i \neq j$ by

$$\begin{aligned} \widehat{\rho}_{ij}^{(S,l)} - \rho_{ij}^{(S,l)} &= - \frac{\widehat{\Phi}_{ij}^{(S,l)}}{\sqrt{\widehat{\Phi}_{ii}^{(S,l)} \widehat{\Phi}_{jj}^{(S,l)}}} + \frac{\Phi_{ij}^{(S,l)}}{\sqrt{\Phi_{ii}^{(S,l)} \Phi_{jj}^{(S,l)}}} \\ &= \frac{\Phi_{ij}^{(S,l)} - \widehat{\Phi}_{ij}^{(S,l)}}{\sqrt{\widehat{\Phi}_{ii}^{(S,l)} \widehat{\Phi}_{jj}^{(S,l)}}} + \Phi_{ij}^{(S,l)} \left(\frac{1}{\sqrt{\Phi_{ii}^{(S,l)} \Phi_{jj}^{(S,l)}}} - \frac{1}{\sqrt{\widehat{\Phi}_{ii}^{(S,l)} \widehat{\Phi}_{jj}^{(S,l)}}} \right) \\ &= \frac{\widehat{\phi}_{ij}^{(S,l)} + \widehat{\phi}_{ii}^{(S,l)} \beta_{ij}^{(S,l)} + \widehat{\phi}_{jj}^{(S,l)} \beta_{ji}^{(S,l)} + \widetilde{\phi}_{ij}^{(S,l)} + \widetilde{\phi}_{ii}^{(S,l)} \beta_{ij}^{(S,l)} + \widetilde{\phi}_{jj}^{(S,l)} \beta_{ji}^{(S,l)}}{\sqrt{\widehat{\Phi}_{ii}^{(S,l)} \widehat{\Phi}_{jj}^{(S,l)}}} \\ &\quad + \Phi_{ij}^{(S,l)} \left(\frac{1}{\sqrt{\Phi_{ii}^{(S,l)} \Phi_{jj}^{(S,l)}}} - \frac{1}{\sqrt{\widehat{\Phi}_{ii}^{(S,l)} \widehat{\Phi}_{jj}^{(S,l)}}} \right) \end{aligned}$$

We notice that

$$\begin{aligned} \Theta_{ij}^{(S,l)} &= \frac{\widetilde{\phi}_{ij}^{(S,l)} + \widetilde{\phi}_{ii}^{(S,l)} \beta_{ij}^{(S,l)}/2 + \widetilde{\phi}_{jj}^{(S,l)} \beta_{ji}^{(S,l)}/2}{\sqrt{\Phi_{ii}^{(S,l)} \Phi_{jj}^{(S,l)}}} \\ &= \frac{\widetilde{\phi}_{ij}^{(S,l)} + \widetilde{\phi}_{ii}^{(S,l)} \beta_{ij}^{(S,l)} + \widetilde{\phi}_{jj}^{(S,l)} \beta_{ji}^{(S,l)}}{\sqrt{\Phi_{ii}^{(S,l)} \Phi_{jj}^{(S,l)}}} + \frac{\Phi_{ij}^{(S,l)} \left(\Phi_{ii}^{(S,l)} \widetilde{\phi}_{jj}^{(S,l)} + \Phi_{jj}^{(S,l)} \widetilde{\phi}_{ii}^{(S,l)} \right)}{2 \Phi_{ii}^{(S,l)} \Phi_{jj}^{(S,l)} \sqrt{\Phi_{ii}^{(S,l)} \Phi_{jj}^{(S,l)}}}, \end{aligned}$$

because $\beta_{ij}^{(S,l)} = -\widehat{\Phi}_{ij}^{(S,l)}/\widehat{\Phi}_{ii}^{(S,l)}$. Hence, the remainder term turns out to be

$$\begin{aligned} O_{ij}^{(S,l)} &= \left[\widehat{\Phi}_{ij}^{(S,l)} \left(\frac{1}{\sqrt{\widehat{\Phi}_{ii}^{(S,l)}\widehat{\Phi}_{jj}^{(S,l)}}} - \frac{1}{\sqrt{\widehat{\Phi}_{ii}^{(S,l)}\widehat{\Phi}_{jj}^{(S,l)}}} \right) - \frac{\widehat{\Phi}_{ij}^{(S,l)} \left(\widehat{\Phi}_{ii}^{(S,l)}\widetilde{\phi}_{jj}^{(S,l)} + \widehat{\Phi}_{jj}^{(S,l)}\widetilde{\phi}_{ii}^{(S,l)} \right)}{2\widehat{\Phi}_{ii}^{(S,l)}\widehat{\Phi}_{jj}^{(S,l)}\sqrt{\widehat{\Phi}_{ii}^{(S,l)}\widehat{\Phi}_{jj}^{(S,l)}}} \right] \\ &\quad + \left(\widetilde{\phi}_{ij}^{(S,l)} + \widetilde{\phi}_{ii}^{(S,l)}\beta_{ij}^{(S,l)} + \widetilde{\phi}_{jj}^{(S,l)}\beta_{ji}^{(S,l)} \right) \left(\frac{1}{\sqrt{\widehat{\Phi}_{ii}^{(S,l)}\widehat{\Phi}_{jj}^{(S,l)}}} - \frac{1}{\sqrt{\widehat{\Phi}_{ii}^{(S,l)}\widehat{\Phi}_{jj}^{(S,l)}}} \right) \\ &\quad + \frac{\widetilde{\phi}_{ij}^{(S,l)} + \widetilde{\phi}_{ii}^{(S,l)}\beta_{ij}^{(S,l)} + \widetilde{\phi}_{jj}^{(S,l)}\beta_{ji}^{(S,l)}}{\sqrt{\widehat{\Phi}_{ii}^{(S,l)}\widehat{\Phi}_{jj}^{(S,l)}}} \end{aligned}$$

For $\widehat{\phi}_{ii}^{(S,l)}$'s,

$$\begin{aligned} \max_i \sum_{l=1}^m |\widehat{\phi}_{ii}^{(S,l)}| &\leq \max_i \sum_{l=1}^m \left| \|\widehat{\epsilon}_{\cdot,i}^{(S,l)}\|_2^2 - \|\epsilon_{\cdot,i}^{(S,l)}\|_2^2 \right| \\ &\leq C(\kappa_3) \max_i \sum_{l=1}^m \frac{1}{2n_0p} \left\| \widehat{\epsilon}_{\cdot,i}^{(S,l)} - \epsilon_{\cdot,i}^{(S,l)} \right\|_2^2 \\ &\leq C(\kappa_1, \kappa_3) d \frac{m + \log(mn_0pq)}{n_0p} \end{aligned}$$

with probability at least $1 - C(mn_0pq)^{-1/2}$ for a sufficiently large n_0 , where the probability inequality at the last line is the result of Theorem 4.1. For $\widetilde{\phi}_{ii}^{(S,l)}$'s,

$$\max_i \max_l |\widetilde{\phi}_{ii}^{(S,l)}| \leq C(\kappa_1, \kappa_3) \sqrt{\frac{\log(mn_0pq)}{n_0p}}$$

with probability at least $1 - (mn_0pq)^{-1/2}$ as a result of Theorem C.4. Axiom 4 implies that $\max_i \widehat{\Phi}_{ii}^{(S,l)} \leq C(\kappa_1, \kappa_3)$, so both $\widehat{\phi}^{(S,l)}$ and $\widetilde{\phi}^{(S,l)}$ are bounded. As a result, it is easily seen that, with the same probability,

$$\left| \sum_{l=1}^m O_{ij}^{(S,l)} \right| \leq C(\kappa_1, \kappa_3) \max \left\{ \begin{aligned} &\left(\sum_l |\widehat{\phi}_{ii}^{(S,l)}|, \sum_l |\widehat{\phi}_{ij}^{(S,l)}|, \sum_l |\widehat{\phi}_{jj}^{(S,l)}|, \right. \\ &\left. \sum_l |\widetilde{\phi}_{ii}^{(S,l)2}|, \sum_l |\widetilde{\phi}_{ii}^{(S,l)}\widetilde{\phi}_{jj}^{(S,l)}|, \sum_l |\widetilde{\phi}_{jj}^{(S,l)2}|, \right. \\ &\left. \sum_l |\widetilde{\phi}_{ii}^{(S,l)}\widetilde{\phi}_{ij}^{(S,l)}|, \sum_l |\widetilde{\phi}_{jj}^{(S,l)}\widetilde{\phi}_{ij}^{(S,l)}| \right) \end{aligned} \right\} \quad (33)$$

For example, the Taylor's theorem gives

$$\begin{aligned} &\widehat{\Phi}_{ij}^{(S,l)} \left(\frac{1}{\sqrt{\widehat{\Phi}_{ii}^{(S,l)}\widehat{\Phi}_{jj}^{(S,l)}}} - \frac{1}{\sqrt{\widehat{\Phi}_{ii}^{(S,l)}\widehat{\Phi}_{jj}^{(S,l)}}} \right) - \frac{\widehat{\Phi}_{ij}^{(S,l)} \left(\widehat{\Phi}_{ii}^{(S,l)}\widetilde{\phi}_{jj}^{(S,l)} + \widehat{\Phi}_{jj}^{(S,l)}\widetilde{\phi}_{ii}^{(S,l)} \right)}{2\widehat{\Phi}_{ii}^{(S,l)}\widehat{\Phi}_{jj}^{(S,l)}\sqrt{\widehat{\Phi}_{ii}^{(S,l)}\widehat{\Phi}_{jj}^{(S,l)}}} \\ &= \frac{\widehat{\Phi}_{ij}^{(S,l)} \left(\widehat{\Phi}_{ii}^{(S,l)}\widehat{\Phi}_{jj}^{(S,l)} - \widehat{\Phi}_{ii}^{(S,l)}\widehat{\Phi}_{jj}^{(S,l)} - \widehat{\Phi}_{ii}^{(S,l)}\widetilde{\phi}_{jj}^{(S,l)} - \widehat{\Phi}_{jj}^{(S,l)}\widetilde{\phi}_{ii}^{(S,l)} \right)}{2\widehat{\Phi}_{ii}^{(S,l)}\widehat{\Phi}_{jj}^{(S,l)}\sqrt{\widehat{\Phi}_{ii}^{(S,l)}\widehat{\Phi}_{jj}^{(S,l)}}} \\ &\quad + \widehat{\Phi}_{ij}^{(S,l)} \int_{\widehat{\Phi}_{ii}^{(S,l)}\widehat{\Phi}_{jj}^{(S,l)}}^{\widehat{\Phi}_{ii}^{(S,l)}\widehat{\Phi}_{jj}^{(S,l)}} \frac{3}{4t^{5/2}} \left(\widehat{\Phi}_{ii}^{(S,l)}\widehat{\Phi}_{jj}^{(S,l)} - t \right)^2 dt \\ &\leq C(\kappa_1, \kappa_3, \kappa_4) \max \left\{ \begin{aligned} &\left(\widehat{\Phi}_{ii}^{(S,l)}\widehat{\Phi}_{jj}^{(S,l)} - \widehat{\Phi}_{ii}^{(S,l)}\widehat{\Phi}_{jj}^{(S,l)} - \widehat{\Phi}_{ii}^{(S,l)}\widetilde{\phi}_{jj}^{(S,l)} - \widehat{\Phi}_{jj}^{(S,l)}\widetilde{\phi}_{ii}^{(S,l)} \right), \\ &\left(\widehat{\Phi}_{ii}^{(S,l)}\widehat{\Phi}_{jj}^{(S,l)} - \widehat{\Phi}_{ii}^{(S,l)}\widehat{\Phi}_{jj}^{(S,l)} \right)^2 \end{aligned} \right\}, \end{aligned}$$

which is easily fit into Eq. (33).

For the second order terms of $\tilde{\phi}^{(S,l)}$ in Eq. (33), we recognize that they are random variables exhibiting a mixture of sub-Gaussian, sub-exponential, and sub-Weibull tail behaviors. The following lemma comes as a corollary of Theorem 4, (Bong and Kuchibhotla, 2023). See Section D.7 for the definition of sub-Weibull random variables and the proof.

Lemma D.1.

$$\mathbb{P} \left[\max_{i,j} \max \left\{ \sum_{l=1}^m |\tilde{\phi}_{ii}^{(S,l)} \tilde{\phi}_{jj}^{(S,l)}|, \sum_{l=1}^m |\tilde{\phi}_{ii}^{(S,l)} \tilde{\phi}_{ij}^{(S,l)}| \right\} \geq C(\kappa_1, \kappa_3) \frac{m + \log(mn_0pq)}{n_0p} \right] \leq (mn_0pq)^{-1/2}.$$

For the linear terms of $\hat{\phi}^{(S,l)}$, we use the following upperbound. See Section D.8 for the proof.

Lemma D.2.

$$\mathbb{P} \left[\max_{i,j} \sum_{l=1}^m |\hat{\phi}_{ij}^{(S,l)}| \geq C(\kappa_1, \kappa_3) d \frac{m + \log(qmn_0p)}{n_0p} \right] \leq C(qmn_0p)^{-1/2}.$$

The desired result is a straightforward result of the two above lemmas.

D.6 Proof of Lemma C.9

Because

$$\frac{1}{p} \left\| \hat{\Phi}^{(\mathcal{T},l)} - \frac{\text{tr}(\Sigma^{(S,l)})}{q} \Phi^{(\mathcal{T},l)} \right\|_F^2 = \frac{1}{p} \sum_{t=1}^p \left| \Phi_{tt}^{(\mathcal{T},l)} - \frac{\text{tr}(\Sigma^{(S,l)})}{q} \Phi_{tt}^{(\mathcal{T},l)} \right|^2,$$

Theorem C.5 implies that

$$\frac{1}{p} \left\| \hat{\Phi}^{(\mathcal{T},l)} - \frac{\text{tr}(\Sigma^{(S,l)})}{q} \Phi^{(\mathcal{T},l)} \right\|_F^2 \leq C(\kappa_3, \kappa_5) \frac{\nu + 1}{(n_l q)^{1-1/(2+2\alpha_l)}}$$

with probability at least $1 - Cph_l^2 e^{-\nu}$. Under the same event,

$$\begin{aligned} & \frac{1}{p} \left\| \hat{\Phi}^{(\mathcal{T},l)-1} - \frac{q}{\text{tr}(\Sigma^{(S,l)})} \Phi^{(\mathcal{T},l)-1} \right\|_F^2 \\ & \leq \frac{1}{p} \left\| \hat{\Phi}^{(\mathcal{T},l)} - \frac{\text{tr}(\Sigma^{(S,l)})}{q} \Phi^{(\mathcal{T},l)} \right\|_F^2 \left\| \frac{q}{\text{tr}(\Sigma^{(S,l)})} \Phi^{(\mathcal{T},l)-1} \right\|_{\text{op}}^2 \left\| \hat{\Phi}^{(\mathcal{T},l)-1} \right\|_{\text{op}}^2 \\ & \leq C(\kappa_3) \frac{1}{p} \left\| \hat{\Phi}^{(\mathcal{T},l)} - \frac{\text{tr}(\Sigma^{(S,l)})}{q} \Phi^{(\mathcal{T},l)} \right\|_F^2 \end{aligned}$$

due to Axiom 3. The first conclusion follows the second result of Theorem C.5. For $\hat{\beta}$, Theorem C.5 implies that

$$\begin{aligned} \frac{1}{p} \left\| (I - \hat{\beta}^{(\mathcal{T},l)}) - (I - \beta^{(\mathcal{T},l)}) \right\|_F^2 &= \frac{1}{p} \sum_{t=1}^p \left\| \hat{\beta}_{\cdot,t}^{(\mathcal{T},l)} - \beta_{\cdot,t}^{(\mathcal{T},l)} \right\|_2^2 \\ &\leq C(\kappa_3, \kappa_5) \frac{\nu + 1}{(n_l q)^{1-1/(2+2\alpha_l)}} \end{aligned}$$

with probability at least $1 - Cph_l^2 e^{-\nu}$. Because our estimator uses eigenvalue truncation, we use Lemma B.1 in Liu and Ren (2020) to guarantee the error bound for $P_\eta(I - \hat{\beta}^{(\mathcal{T},l)})$: given that $\eta \leq \lambda_1(I - \beta)$,

$$\begin{aligned} \frac{1}{p} \left\| P_\eta(I - \hat{\beta}^{(\mathcal{T},l)}) - (I - \beta^{(\mathcal{T},l)}) \right\|_F^2 &\leq \frac{C}{p} \left\| (I - \hat{\beta}^{(\mathcal{T},l)}) - (I - \beta^{(\mathcal{T},l)}) \right\|_F^2 \\ &\leq C(\kappa_3, \kappa_5) \frac{\nu + 1}{(n_l q)^{1-1/(2+2\alpha_l)}} \end{aligned}$$

with probability at least $1 - C(mn_0pq)^{-1/2}$. Then,

$$\begin{aligned} & \frac{1}{p} \left\| P_\eta(I - \hat{\beta}^{(\mathcal{T},l)-1}) - (I - \beta^{(\mathcal{T},l)-1}) \right\|_F^2 \\ & \leq \frac{1}{p} \left\| P_\eta(I - \hat{\beta}^{(\mathcal{T},l)}) - (I - \beta^{(\mathcal{T},l)}) \right\|_F^2 \left\| P_\eta(I - \hat{\beta}^{(\mathcal{T},l)-1}) \right\|_{\text{op}}^2 \left\| (I - \beta^{(\mathcal{T},l)-1}) \right\|_{\text{op}}^2 \\ & \leq C(\kappa_3) \frac{1}{p} \left\| P_\eta(I - \hat{\beta}^{(\mathcal{T},l)}) - (I - \beta^{(\mathcal{T},l)}) \right\|_F^2 \end{aligned}$$

due to Lemma B.2 in Liu and Ren (2020) and the bounded operator norm of $P_\eta(I - \widehat{\beta}^{(\mathcal{T}, l)})$. It verifies the second conclusion.

D.7 Proof of Lemma D.1

We first refer to the definitions of Orlicz norms and sub-Weibull random variables in Kuchibhotla and Chakraborty (2022).

Definition D.3. Let g be a non-decreasing non-negative function on $[0, \infty)$ with $g(0) = 0$. For a random variable X , the g -Orlicz norm is defined as

$$\|X\|_g := \inf\{\nu > 0 : \mathbb{E}[g(|X|/\nu)] \leq 1\}.$$

Definition D.4. A random variable X is sub-Weibull of order $\alpha > 0$, denoted by $X \sim \text{sub-Weibull}(\alpha)$, if

$$\|X\|_{\psi_\alpha} < \infty, \text{ where } \psi_\alpha(x) := \exp(x^\alpha) - 1 \text{ for } x \geq 0.$$

Two important examples of sub-Weibull random variables are sub-Gaussian and sub-exponential random variables, which are sub-Weibull(2) and sub-Weibull(1), respectively. Theorem 4 in Bong and Kuchibhotla (2023) induces, for any given $i, j \in [q]$, and $\nu > 0$,

$$\mathbb{P} \left[\sum_{l=1}^m |\widetilde{\phi}_{ii}^{(S,l)} \widetilde{\phi}_{jj}^{(S,l)}| \geq C(\kappa_1, \kappa_3) \left(\frac{m + \sqrt{m\nu} + \nu}{n_0 p} + \frac{\nu^2}{n_0^2 p^2} \right) \right] \leq e^{-\nu},$$

and by setting $\nu = C \log(mn_0 p q)$, due to Axiom 4,

$$\begin{aligned} \mathbb{P} \left[\sum_{l=1}^m |\widetilde{\phi}_{ii}^{(S,l)} \widetilde{\phi}_{jj}^{(S,l)}| \geq \sum_{l=1}^m \mathbb{E} |\widetilde{\phi}_{ii}^{(S,l)} \widetilde{\phi}_{jj}^{(S,l)}| + C(\kappa_1, \kappa_3) \frac{m + \log(mn_0 p q)}{n_0 p} \right] \\ \leq \frac{2}{q^2} (mn_0 p q)^{-1/2}, \end{aligned}$$

which similarly applies to $\widetilde{\phi}_{ii}^{(S,l)} \widetilde{\phi}_{ij}^{(S,l)}$. Thus, by the maximal inequality,

$$\begin{aligned} \mathbb{P} \left[\max_{i,j} \max \left\{ \sum_{l=1}^m |\widetilde{\phi}_{ii}^{(S,l)} \widetilde{\phi}_{jj}^{(S,l)}|, \sum_{l=1}^m |\widetilde{\phi}_{ii}^{(S,l)} \widetilde{\phi}_{ij}^{(S,l)}| \right\} \geq C(\kappa_1, \kappa_3) \left(\frac{m + \log(mn_0 p q)}{n_0 p} \right) \right] \\ \leq (mn_0 p q)^{-1/2}. \end{aligned}$$

D.8 Proof of Lemma D.2

Because $\widehat{\epsilon}_{\cdot, i}^{(S,l)} = X_{\cdot, i}^{(S,l)} - X^{(S,l)} \widehat{\beta}_{\cdot, i}^{(S,l)}$ and $\epsilon_{\cdot, i}^{(S,l)} = X_{\cdot, i}^{(S,l)} - X^{(S,l)} \beta_{\cdot, i}^{(S,l)}$,

$$\begin{aligned} & \sum_{l=1}^m |\widehat{\phi}_{ij}^{(S,l)}| \\ &= \sum_{l=1}^m \frac{1}{n_l p} \left| \widehat{\epsilon}_{\cdot, i}^{(S,l)\top} \widehat{\epsilon}_{\cdot, j}^{(S,l)} - \epsilon_{\cdot, i}^{(S,l)\top} \epsilon_{\cdot, j}^{(S,l)} + \left(\|\epsilon_{\cdot, i}^{(S,l)}\|_2^2 \Delta_{ij}^{(S,l)} + \|\epsilon_{\cdot, j}^{(S,l)}\|_2^2 \Delta_{ji}^{(S,l)} \right) \mathbb{I}(i \neq j) \right| \\ &= \sum_{l=1}^m \frac{1}{n_l p} \left| \Delta_{\cdot, i}^{(S,l)\top} X^{(S,l)\top} X^{(S,l)} \Delta_{\cdot, j}^{(S,l)} - \epsilon_{\cdot, j}^{(S,l)\top} X^{(S,l)} \Delta_{\cdot, i}^{(S,l)} - \epsilon_{\cdot, i}^{(S,l)\top} X^{(S,l)} \Delta_{\cdot, j}^{(S,l)} \right. \\ & \quad \left. + \left(\|\epsilon_{\cdot, i}^{(S,l)}\|_2^2 \Delta_{ij}^{(S,l)} + \|\epsilon_{\cdot, j}^{(S,l)}\|_2^2 \Delta_{ji}^{(S,l)} \right) \mathbb{I}(i \neq j) \right| \end{aligned} \quad (34)$$

For the first term, it follows Theorem 4.1 that

$$\sum_{l=1}^m \frac{1}{n_l p} \left| \Delta_{\cdot, i}^{(S,l)\top} X^{(S,l)\top} X^{(S,l)} \Delta_{\cdot, j}^{(S,l)} \right| \leq C(\kappa_1, \kappa_3) d \frac{m + \log(mn_0 p q)}{n_0 p} \quad (35)$$

uniformly over i and j , with probability at least $1 - 2(mn_0pq)^{-1/2}$. For the rest terms,

$$\begin{aligned} & \sum_{l=1}^m \frac{1}{n_l p} \left| \epsilon_{\cdot,j}^{(S,l)\top} X^{(S,l)} \Delta_{\cdot,i}^{(S,l)} - \|\epsilon_{\cdot,j}^{(S,l)}\|_2^2 \Delta_{ij}^{(S,l)} \mathbb{I}(i \neq j) \right| \\ &= \sum_{l=1}^m \frac{1}{n_l p} \left| \epsilon_{\cdot,j}^{(S,l)\top} X_{\cdot,j}^{(S,l)} \Delta_{ji}^{(S,l)} \mathbb{I}(i \neq j) - \|\epsilon_{\cdot,j}^{(S,l)}\|_2^2 \Delta_{ij}^{(S,l)} \mathbb{I}(i \neq j) + \sum_{k:k \neq i,j} \epsilon_{\cdot,j}^{(S,l)\top} X_{\cdot,k}^{(S,l)} \Delta_{ki}^{(S,l)} \right| \\ &\leq \sum_{l=1}^m \frac{1}{n_l p} \left(\left| \epsilon_{\cdot,j}^{(S,l)\top} X^{(S,l)} \beta_{\cdot,j}^{(S,l)} \Delta_{ji}^{(S,l)} \mathbb{I}(i \neq j) \right| + \sum_{k:k \neq i,j} \left| \epsilon_{\cdot,j}^{(S,l)\top} X_{\cdot,k}^{(S,l)} \Delta_{ki}^{(S,l)} \right| \right). \end{aligned}$$

We notice that Theorems C.2 and 4.1 implies that

$$\begin{aligned} & \sum_{l=1}^m \frac{1}{n_l p} \sum_{k:k \neq i,j} \left| \epsilon_{\cdot,j}^{(S,l)\top} X_{\cdot,k}^{(S,l)} \Delta_{ki}^{(S,l)} \right| \\ &\leq \sum_{k:k \neq i,j} \frac{1}{n_0 p} \left[\sum_{l=1}^m \left(\frac{\sqrt{n_l p}}{\|X_{\cdot,k}^{(S,l)}\|_2} \epsilon_{\cdot,i}^{(S,l)\top} X_{\cdot,k}^{(S,l)} \right)^2 \right]^{1/2} \|\Delta_{ki}^{(S,\cdot)}\|_2 \\ &\leq \left(\max_{k:k \neq i,j} \frac{1}{n_0 p} \left[\sum_{l=1}^m \left(\frac{\sqrt{n_l p}}{\|X_{\cdot,k}^{(S,l)}\|_2} \epsilon_{\cdot,i}^{(S,l)\top} X_{\cdot,k}^{(S,l)} \right)^2 \right]^{1/2} \right) \left(\sum_{k:k \neq i,j} \|\Delta_{ki}^{(S,\cdot)}\|_2 \right) \\ &\leq C(\kappa_1, \kappa_3) d \frac{m + \log(mn_0pq)}{n_0 p} \end{aligned}$$

and

$$\begin{aligned} & \sum_{l=1}^m \frac{1}{n_l p} \epsilon_{\cdot,j}^{(S,l)\top} X^{(S,l)} \beta_{\cdot,j}^{(S,l)} \Delta_{ji}^{(S,l)} \\ &\leq \frac{1}{n_0 p} \left[\sum_{l=1}^m \left(\frac{\sqrt{n_l p}}{\|X_{\cdot,j}^{(S,l)}\|_2} \epsilon_{\cdot,i}^{(S,l)\top} X^{(S,l)} \beta_{\cdot,j}^{(S,l)} \right)^2 \right]^{1/2} \|\Delta_{ji}^{(S,\cdot)}\|_2 \\ &\leq C(\kappa_1, \kappa_3) d \frac{m + \log(mn_0pq)}{n_0 p} \end{aligned}$$

satisfy simultaneously uniformly over i and j with probability at least $1 - C(mn_0pq)^{-1/2}$. We obtain the desired result by plugging the above probability bounds into Eq. (34).

E Derivation of the asymptotic covariance between the edge-wise test statistics

In this section, we derive the asymptotic covariance of $\widehat{T}_{i_1 j_1}$ and $\widehat{T}_{i_2 j_2}$ in Eq. (7):

$$\begin{aligned} & S_{(i_1, j_1), (i_2, j_2)} \\ &:= \frac{1}{m} \sum_{l=1}^m \frac{\|\Sigma(\mathcal{T}, l)\|_F^2}{p} \left[\begin{aligned} & \rho_{i_1 i_2}^{(S,l)} \rho_{j_1 j_2}^{(S,l)} + \rho_{i_1 j_2}^{(S,l)} \rho_{i_2 j_1}^{(S,l)} + \frac{1}{2} \rho_{i_1 j_1}^{(S,l)} \rho_{i_2 j_2}^{(S,l)} \left(\rho_{i_1 i_2}^{(S,l)2} + \rho_{j_1 j_2}^{(S,l)2} + \rho_{i_1 j_2}^{(S,l)2} + \rho_{i_2 j_1}^{(S,l)2} \right) \\ & - \rho_{i_1 i_2}^{(S,l)} \rho_{i_2 j_2}^{(S,l)} \rho_{i_2 j_1}^{(S,l)} - \rho_{i_1 i_2}^{(S,l)} \rho_{i_1 j_1}^{(S,l)} \rho_{i_1 j_2}^{(S,l)} - \rho_{j_1 j_2}^{(S,l)} \rho_{i_2 j_2}^{(S,l)} \rho_{i_1 j_2}^{(S,l)} - \rho_{j_1 j_2}^{(S,l)} \rho_{i_2 j_1}^{(S,l)} \rho_{i_1 j_1}^{(S,l)} \end{aligned} \right]. \end{aligned}$$

By Theorem C.8, $\widehat{\rho}_{ij}^{(S,l)} - \rho_{ij}^{(S,l)}$ has the leading term $\Theta_{ij}^{(S,l)}$. Hence, $\widehat{T}_{i_1 j_1}$ and $\widehat{T}_{i_2 j_2}$ have asymptotic covariance,

$$\begin{aligned} S_{(i_1, j_1), (i_2, j_2)} &= \mathbb{E} \left[\left(\frac{1}{\sqrt{m}} \sum_{l=1}^m \sqrt{n_l p} \Theta_{i_1 j_1}^{(S,l)} \right) \left(\frac{1}{\sqrt{m}} \sum_{l=1}^m \sqrt{n_l p} \Theta_{i_2 j_2}^{(S,l)} \right) \right] \\ &= \frac{1}{m} \sum_{l=1}^m n_l p \mathbb{E} \left[\Theta_{i_1 j_1}^{(S,l)} \Theta_{i_2 j_2}^{(S,l)} \right]. \end{aligned} \tag{36}$$

Based on Eq. (14), for each $l = 1, \dots, m$,

$$\begin{aligned} & \mathbb{E} \left[\Theta_{i_1 j_1}^{(S,l)} \Theta_{i_2 j_2}^{(S,l)} \right] \\ &= \mathbb{E} \left[\begin{aligned} & \left(\frac{\tilde{\delta}_{i_1 j_1}^{(S,l)}}{\sqrt{\Phi_{i_1 i_1}^{(S,l)} \Phi_{j_1 j_1}^{(S,l)}}} - \frac{\Phi_{i_1 j_1}^{(S,l)} \tilde{\delta}_{j_1 j_1}^{(S,l)}}{2\Phi_{j_1 j_1}^{(S,l)} \sqrt{\Phi_{i_1 i_1}^{(S,l)} \Phi_{j_1 j_1}^{(S,l)}}} - \frac{\Phi_{i_1 j_1}^{(S,l)} \tilde{\delta}_{i_1 i_1}^{(S,l)}}{2\Phi_{i_1 i_1}^{(S,l)} \sqrt{\Phi_{i_1 i_1}^{(S,l)} \Phi_{j_1 j_1}^{(S,l)}}} \right) \\ & \times \left(\frac{\tilde{\delta}_{i_2 j_2}^{(S,l)}}{\sqrt{\Phi_{i_2 i_2}^{(S,l)} \Phi_{j_2 j_2}^{(S,l)}}} - \frac{\Phi_{i_2 j_2}^{(S,l)} \tilde{\delta}_{j_2 j_2}^{(S,l)}}{2\Phi_{j_2 j_2}^{(S,l)} \sqrt{\Phi_{i_2 i_2}^{(S,l)} \Phi_{j_2 j_2}^{(S,l)}}} - \frac{\Phi_{i_2 j_2}^{(S,l)} \tilde{\delta}_{i_2 i_2}^{(S,l)}}{2\Phi_{i_2 i_2}^{(S,l)} \sqrt{\Phi_{i_2 i_2}^{(S,l)} \Phi_{j_2 j_2}^{(S,l)}}} \right) \end{aligned} \right], \end{aligned} \quad (37)$$

which is a summation of the second moments of $\tilde{\delta}^{(S,l)}$. For each second moment,

$$\begin{aligned} & \mathbb{E}[\tilde{\delta}_{i_1 j_1}^{(S,l)} \tilde{\delta}_{i_2 j_2}^{(S,l)}] \\ &= \mathbb{E} \left[\frac{1}{n_i^2 p^2} \sum_{k=1}^{n_i} \sum_{t=1}^p \left(\epsilon_{t i_1}^{(S,k,l)} \epsilon_{t j_1}^{(S,k,l)} - \Sigma_{tt}^{(\mathcal{T},l)} \Phi_{i_1 j_1}^{(S,l)} \right) \cdot \sum_{k=1}^{n_i} \sum_{t=1}^p \left(\epsilon_{t i_2}^{(S,k,l)} \epsilon_{t j_2}^{(S,k,l)} - \Sigma_{tt}^{(\mathcal{T},l)} \Phi_{i_2 j_2}^{(S,l)} \right) \right] \\ &= \frac{1}{n_i^2 p^2} \sum_{t=1}^p \lambda_t^{(\mathcal{T},l)} \cdot \mathbb{E} \left[\sum_{k=1}^{n_i} \left(\xi_{t i_1}^{(k,l)} \xi_{t j_1}^{(k,l)} - \Phi_{i_1 j_1}^{(S,l)} \right) \cdot \sum_{k=1}^{n_i} \left(\xi_{t i_2}^{(k,l)} \xi_{t j_2}^{(k,l)} - \Phi_{i_2 j_2}^{(S,l)} \right) \right] \\ &= \frac{\|\Sigma^{(\mathcal{T},l)}\|_F^2}{n_i p^2} \cdot \mathbb{E} \left[\left(\xi_{t i_1}^{(k,l)} \xi_{t j_1}^{(k,l)} - \Phi_{i_1 j_1}^{(S,l)} \right) \cdot \left(\xi_{t i_2}^{(k,l)} \xi_{t j_2}^{(k,l)} - \Phi_{i_2 j_2}^{(S,l)} \right) \right], \end{aligned} \quad (38)$$

where

$$\mathbb{E} \left[\left(\xi_{t i_1}^{(k,l)} \xi_{t j_1}^{(k,l)} - \Phi_{i_1 j_1}^{(S,l)} \right) \cdot \left(\xi_{t i_2}^{(k,l)} \xi_{t j_2}^{(k,l)} - \Phi_{i_2 j_2}^{(S,l)} \right) \right] = \Phi_{i_1 i_2}^{(S,l)} \Phi_{j_1 j_2}^{(S,l)} + \Phi_{i_1 j_1}^{(S,l)} \Phi_{i_2 j_2}^{(S,l)}. \quad (39)$$

Plugging it into Eq. (37),

$$\begin{aligned} & \mathbb{E} \left[\Theta_{i_1 j_1}^{(S,l)} \Theta_{i_2 j_2}^{(S,l)} \right] \\ &= \frac{\|\Sigma^{(\mathcal{T},l)}\|_F^2}{n_i p^2} \frac{1}{\sqrt{\Phi_{i_1 i_1}^{(S,l)} \Phi_{j_1 j_1}^{(S,l)} \Phi_{i_2 i_2}^{(S,l)} \Phi_{j_2 j_2}^{(S,l)}}} \\ & \quad \times \left[\begin{aligned} & \Phi_{i_1 i_2}^{(S,l)} \Phi_{j_1 j_2}^{(S,l)} + \Phi_{i_1 j_2}^{(S,l)} \Phi_{j_2 i_1}^{(S,l)} + \frac{\Phi_{i_1 j_1}^{(S,l)} \Phi_{i_2 j_2}^{(S,l)}}{2\Phi_{i_1 i_1}^{(S,l)} \Phi_{i_2 i_2}^{(S,l)}} (\Phi_{i_1 i_2}^{(S,l)2} + \Phi_{i_1 j_2}^{(S,l)2} + \Phi_{j_1 i_2}^{(S,l)2} + \Phi_{j_1 j_2}^{(S,l)2}) \\ & - \frac{\Phi_{i_2 j_2}^{(S,l)}}{\Phi_{i_2 i_2}^{(S,l)}} \Phi_{i_1 i_2}^{(S,l)} \Phi_{j_1 i_2}^{(S,l)} - \frac{\Phi_{i_2 j_2}^{(S,l)}}{\Phi_{j_2 j_2}^{(S,l)}} \Phi_{i_1 j_2}^{(S,l)} \Phi_{j_1 j_2}^{(S,l)} - \frac{\Phi_{i_1 j_1}^{(S,l)}}{\Phi_{i_1 i_1}^{(S,l)}} \Phi_{i_2 i_1}^{(S,l)} \Phi_{j_2 i_1}^{(S,l)} - \frac{\Phi_{i_1 j_1}^{(S,l)}}{\Phi_{j_1 j_1}^{(S,l)}} \Phi_{i_2 j_1}^{(S,l)} \Phi_{j_2 j_1}^{(S,l)} \end{aligned} \right] \\ &= \frac{\|\Sigma^{(\mathcal{T},l)}\|_F^2}{n_i p^2} \left[\begin{aligned} & \rho_{i_1 i_2}^{(S,l)} \rho_{j_1 j_2}^{(S,l)} + \rho_{i_1 j_2}^{(S,l)} \rho_{i_2 j_1}^{(S,l)} + \frac{1}{2} \rho_{i_1 j_1}^{(S,l)} \rho_{i_2 j_2}^{(S,l)} (\rho_{i_1 i_2}^{(S,l)2} + \rho_{j_1 j_2}^{(S,l)2} + \rho_{i_1 j_2}^{(S,l)2} + \rho_{i_2 j_1}^{(S,l)2}) \\ & - \rho_{i_1 i_2}^{(S,l)} \rho_{i_2 j_2}^{(S,l)} \rho_{i_2 j_1}^{(S,l)} - \rho_{i_1 i_2}^{(S,l)} \rho_{i_1 j_1}^{(S,l)} \rho_{i_1 j_2}^{(S,l)} - \rho_{j_1 j_2}^{(S,l)} \rho_{i_2 j_2}^{(S,l)} \rho_{i_2 j_1}^{(S,l)} - \rho_{j_1 j_2}^{(S,l)} \rho_{i_2 j_1}^{(S,l)} \rho_{i_1 j_1}^{(S,l)} \end{aligned} \right]. \end{aligned}$$

Plugging it into Eq. (36) retrieves the desired result.